UNCLASSIFIED

AD NUMBER

AD833215

NEW LIMITATION CHANGE

TO

Approved for public release, distribution unlimited

FROM

Distribution authorized to U.S. Gov't. agencies and their contractors; Critical Technology; 15 DEC 1954. Other requests shall be referred to Soace and Missile Systems Organiation, Los Angeles, CA.

AUTHORITY

SAMSO USAF ltr, 28 Feb 1972

THIS PAGE IS UNCLASSIFIED

A-Atlas-103

ZA-7-065

Curves of Shockwave, Expansion Wave and Skin Friction Data for Hypersonic Speeds

M. F. Romig

15 December 1954

20060314000

Curves of Shockwave, Expansion Wave and Skin Friction Data for Hypersonic Speeds

1.0 Summary

This report presents curves of shockwave, expansion wave and boundary layer data plotted for use at Mach numbers up to 20. Normal and oblique shockwave parameters, conical shock parameters, expansion wave parameters, some aerodynamic coefficients and compressible laminar and turbulent boundary layer skin friction formulas are given for Mach numbers up to at least 20. The use of these curves is briefly described in the text.

2.0 Symbols

C_D	-	wave drag coefficient $= \frac{\text{Wave Drag}}{qS}$	
C_f	-	local skin friction coefficient $= \frac{\tau}{q}$	
C_F	-	mean skin friction coefficient $= \frac{\text{Drag}}{qS}$	
C_N	-	normal force coefficient $= \frac{\text{Normal Force}}{qS}$	
C_p	-	coefficient of specific heat at constant pressure BTU/lb.°R	
C_X	-	axial drag coefficient $= \frac{\text{axial drag}}{qS}$	
g	-	acceleration due to gravity	ft./sec.^{2}
h	-	heat transfer coefficient	BTU/ft.^{2}hr.°R
H	-	total pressure	lbs./ft.^{2}
J	-	mechanical equivalent of heat	ft.-lb./BTU
k	-	thermal conductivity	BTU/ft. hr.°R
l	-	wetted length	ft.
l'	-	effective starting length	ft.
M	-	Mach number	
N	-	Nusselt number $= \frac{hl}{k}$	
p	-	static pressure	lb./ft.^{2}
P_r	-	Prandtl number $= \frac{\mu C_p}{k}$	

Q -	heat flux	BTU/hr. ft.^{2}
q -	dynamic pressure	lb./ft.^{2}
Re -	Reynolds number = $\frac{\rho u l}{\mu}$	
S -	reference area	ft.^{2}
T -	static temperature	°R
T' -	reference temperature	°R
T_i -	recovery or inherent temperature	°R
u -	velocity	ft./sec.
x -	axial length	ft.

Greek

α -	angle of attack	degrees
β -	shockwave angle	degrees
γ -	ratio of specific heat	
δ -	flow deflection angle, boundary layer thickness	degrees, ft.
θ -	boundary layer momentum thickness	ft.
θ_v -	cone semi-vertex angle	degrees
θ_w -	cone shockwave half angle	degrees
μ -	coefficient of viscosity	lb. sec./ft.^{2}
ν -	Prandtl-Meyer angle	degrees
ρ -	density	lb. sec.^{2}/ft.^{4}
τ -	shear stress	lbs./ft.^{2}

Subscripts

1 -	initial or free stream
2 -	after the shock
s -	surface of the cone
00 -	sea level

w - at the wall

∞ - local

i - incompressible or location index

3.0 Discussion and Results

The need for a combined collection of basic supersonic aerodynamic data has long been evident to Convair Aerodynamicists working with high velocity bodies. The existing charts and tables (Reference 1, 2, 3) are either limited in some phase of Mach number and flow deflection angle or the data are not presented graphically (Reference 4). It was believed also that some convenient reference should be provided for the skin friction and heat transfer formulas associated with the reference temperature method explained in Reference 9. This report fulfills these needs.

The sections following will deal with the separate types of curves presented.

3.1 Inviscid Flow Parameters

The curves in this section are separated into one, two and three dimensional flow. The flow parameters presented, all versus initial Mach number, are Mach number after the shock, static pressure ratio, static temperature ratio, density ratio, velocity ratio, dynamic pressure ratio, Reynolds number ratio, total head ratio and shockwave angle. All ratios are quantities after the wave divided by the value of the same quantity before the wave.

Three coefficients are given for both unyawed and yawed cones. C_N, $\frac{dC_N}{d\alpha}$ and C_X are given for cones in Newtonian flow (Reference 4, 5, 6).

The Reynolds numbers presented in Figure 1.6, 2.8 and 3.8 were found from

$$\frac{R_{e2}}{R_{e1}} = \frac{\rho_2}{\rho_1}\frac{u_2}{u_1}\left(\frac{T_1}{T_2}\right)^{0.7}$$

where an exponential viscosity - temperature relation

$$\frac{\mu_2}{\mu_1} = \left(\frac{T_2}{T_1}\right)^{0.7}$$

was assumed.

The data for these curves were obtained from Reference 1 through Reference 6 or were computed for high Mach number-deflection angle combinations when they were not tabulated.

3.2 Viscous Flow Parameters By The Reference Temperature Method

The curves presented in this section are primarily for use with the reference temperature method of calculating heat transfer and skin friction. Figures 4.1 - 4.7 include: local and mean incompressible flow skin friction coefficients for laminar, transition and turbulent flow vs. Reynolds number (Reference 7); reference temperature ratio T'/T vs. Mach number; and reference temperature $(T')^{1.7}$ vs. T'. For use in the heat balance equation the inherent (recovery) temperature rise ΔT_i is given versus velocity. The theoretical laminary boundary layer stability curve (Reference 8) is shown in Figure 4.5 to indicate the type of boundary layer flow which might be expected for various M, T_w/T and Re combinations. Figures 4.6 and 4.7 present the NACA-NBS variation of C_p with T and variation of μ with T as given by the Sutherland viscosity rule.

The reference temperature method and its associated equations will be presented below in outline form. A complete derivation of these equations may be found in Reference 9, which also contains a critical evaluation of the method. The concept of an "effective length", needed for the application of this method to bodies other than flat plates, is discussed by Sieff (Reference 10) and Romig (Reference 11). Therefore the following sections are primarily on the use of the method in obtaining the heat transfer and skin friction.

The reference temperature method is based on the assumption that the use of a characteristic temperature in the compressible equations for drag and heat transfer will eliminate their outward dependence on temperature and Mach number, i.e., convert them to the incompressible, constant-property equation. Under this assumption the T' method is thus described as: if all temperature-dependent properties in the incompressible equations for heat transfer and drag are based on the reference temperature T' then the incompressible equations will yield the compressible friction or heat transfer coefficients. Use of this method therefore obviates solving the compressible laminar and turbulent boundary layer equations. The equations for the reference temperature are

$$\boxed{\begin{aligned} T' &= T_\infty\left[0.42 + 0.032M_\infty^2 + 0.58\frac{T_w}{T_\infty}\right], \; M_\infty \le 5.5 \\ T' &= T_\infty\left[0.70 + 0.023M_\infty^2 + 0.58\frac{T_w}{T_\infty}\right], \; M_\infty \ge 5.5 \end{aligned}} \qquad (1)$$

where the ratio T'/T_∞ may be found in Figure 4.2 vs. Mach number for integral values of $1 \le T_w/T_\infty \le 4$. The eq. (1) are valid for both laminar and turbulent flow.

3.2.1 Basic Equations for Two-Dimensional Flow

The compressible skin friction may be obtained either as the ratio of compressible to incompressible, c_f / c_{f_i}, or explicitly as a function of the Reynolds number based on T'. For practical considerations explicit relationships will be developed first for the local and mean compressible friction.

Assume all air properties in the incompressible drag equations are based on T' so that according to the assumption stated in 3.2,

$$(\text{compressible})\ c_{f_\infty} q_\infty \equiv \tau \equiv (\text{incompressible})\ c_{f_i}' q'$$

where the primes denote that air properties are based on T'.

or

$$c_{f_\infty} = c_{f_i}' \frac{\rho'}{\rho_\infty}$$

Using the perfect gas equation at constant pressure,

$$\boxed{c_{f_\infty} = \frac{T_\infty}{T'} c_{f_i}'} \tag{2}$$

where c_{f_i}' is given either by the Blasius formula

$$\text{LAMINAR} \quad c_{f_i}' = \frac{0.664}{\sqrt{\frac{\rho' u \ell}{\mu'}}} \tag{3}$$

or the Karman equation

$$\text{TURBULENT} \quad \left(c_{f_i}'\right)^{-1/2} = 1.7 + 4.15 \log_{10} \frac{\rho' u \ell}{\mu'} c_{f_i}' \tag{4}$$

These laminar and turbulent incompressible friction coefficients (Eq. 3 & 4) are plotted in Figure 4.1 versus Reynolds number. The Reynolds number to be used with Eq. (3) & (4) and hence in evaluating Eq. (2) is a function of T'. The expression for $R_{e_{T'}}$ is given as

$$R_{e_{T'}} = \frac{\rho' u \ell}{\mu'}$$

or, using the power law for viscosity, $\mu \propto (T)^{0.7}$ and using ambient conditions as a reference,

$$\boxed{R_{e_{T'}} = \left(\frac{T_\infty}{T'}\right)^{1.7} R_{e_\infty}} \tag{5}$$

If the perfect gas law is used and sea level (T = 518.4°R) conditions are used in the power law,

$$\boxed{R_{e_{T'}} = 12.44 \times 10^{4} \frac{p_\infty u_\infty l}{(T')^{1.7}}} \tag{6}$$

Thus it is only necessary to enter Figure 4.1 with $R_{e_{T'}}$, computed by Eq. (5) or Eq. (6), locate the desired c_{f_i}' and compute c_{f_∞} by Eq. (2). For convenience in computing $R_{e_{T'}}$, the function $(T')^{1.7}$ is plotted versus T' in Figure 4.3.

The mean skin friction coefficients may be obtained in much the same way from the drag equation. For both laminar and turbulent flow

$$\boxed{C_{F_\infty} = \frac{T_\infty}{T'} C_{F_i}'} \tag{7}$$

where C_{F_i}' is given by the Blasius formula

$$\text{LAMINAR} \quad C_{F_i}' = \frac{1.328}{\sqrt{R_{e_{T'}}}} \tag{8}$$

and the Prandtl-Schlicting equation

$$\text{TURBULENT} \quad C_{F_i}' = \frac{0.455}{(\log_{10} R_{e_{T'}})^{2.58}} \tag{9}$$

Eqs. (8) and (9) are also plotted versus Reynolds number in Figure 4.1. The same procedure is used in evaluating the mean coefficient as was used for the local.

The compressible heat transfer rate can be obtained from the definition of the heat equation

$$\boxed{Q = h\,(T_i - T_w)} \tag{10}$$

where the heat transfer coefficient is defined as

$$h = \frac{Nu\, k}{l} \tag{11}$$

If the air properties in h are based on T' and the following incompressible relationships for Nusselt number are used,

$$\text{LAMINAR} \quad Nu_\infty = 0.332 \sqrt[3]{Pr'} \sqrt{Re_{T'}} \tag{12}$$

and

$$\text{TURBULENT} \quad Nu_\infty = 0.0296 \left(Re_{T'}\right)^{0.8} \tag{13}$$

then after considerable algebraic manipulation the following heat transfer equations are found

$$\boxed{\text{LAMINAR} \quad h = 0.0074 \left[\frac{\rho_\infty u_\infty}{l}\right]^{0.5}} \tag{14}$$

$$\boxed{\text{TURBULENT} \quad h = \frac{0.02498 \, (\rho_\infty u_\infty)^{0.8}}{l^{0.2} \, (T')^{0.51}}} \tag{15}$$

It was assumed in Eq. (14) and (15) that the air properties varied in the following way

$$\frac{\mu}{\mu_\infty} = \left(\frac{T}{T_\infty}\right)^{0.7}, \quad \frac{k}{k_\infty} = \left(\frac{T}{T_\infty}\right)^{0.85}, \quad Pr = 0.72 \ \ \& \ \ p = \rho R T \tag{15a}$$

The validity of Eq. (14) in particular and the exponents in the power laws were substantiated in the investigations of Reference (9). It was found that these heat transfer equations are correct as long as the boundary layer air is not dissociated.

Curves of $\Delta T_i = T_i - T_1$, where T_1 is the free stream static temperature, are plotted versus free stream velocity in Figure 4.4a - 4.4c for use in eq. (10).

Thus to compute the compressible laminar or turbulent heat, it is only necessary to find the reference temperature and solve eq. (14) or (15). These values of h are used along with the temperatures obtained from Figure 4.4a - 4.4c in eq. (10) to find the heat rate Q.

3.2.2 Two Dimensional Flow With Discontinuties

The equations (1) - (15) written above apply in strict sense only to flat plate flow. Any condition which would tend to make the external flow discontinuous at a point, such as transition from laminar to turbulent flow, or passing through a shockwave or expansion, renders the equations inapplicable.

In order to use eq. (1) - (15) it is necessary, therefore, to somehow refer the boundary layer characteristics at the point of discontinuity to a flat plate boundary layer with identical characteristics but with no flow discontinuties. This can be accomplished by forcing, as it were, the momentum loss of the boundary layer flow to remain constant across any discontinuity. This momentum-loss method will give an effective starting length for the boundary layer characteristics to the point of discontinuity.

The momentum loss equations are discussed at length in Reference (10) and (11) and only a brief outline of them are given here. If the momentum loss through the boundary layer is defined as

$$\int_0^{\delta} \rho u (u_\infty - u)\, dy$$

then across any point of discontinuity it is assumed that

$$\int_0^{\delta_1} \rho u (u_1 - u)\, dy = \int_0^{\delta_2} \rho u (u_2 - u)\, dy \tag{16}$$

This is equivalent to stating that.

$$\theta_1 q_1 = \theta_2 q_2 \tag{17}$$

where θ is the boundary layer momentum thickness and q the stream dynamic pressure. The laminar or turbulent equations for θ allow (17) to be solved for ℓ_2, the effective starting length. For convenience in nomenclature ℓ_2 is designated as ℓ' hereafter.

Therefore let

$$\theta_{LAM} = \frac{1.328}{\left(\frac{\rho_\infty u_0 \ell}{\mu_\infty}\right)^{1/2}} \left(\frac{C_F}{C_{Fi}}\right)_{LAM} \ell \tag{18}$$

and

$$\theta_{TURB} = \frac{0.072}{\left(\frac{\rho_\infty u_\infty \ell}{\mu_\infty}\right)^{0.2}} \left(\frac{C_F}{C_{Fi}}\right)_{TURB} \ell \tag{19}$$

where ℓ is the length along the body to the point of discontinuity. The turbulent expression for θ is based on the 1/7th power law for velocity. It is adequate for $5 \times 10^5 \leq R_\ell \leq 10^7$. The more exact solution (Eq. (9)) would not be amenable for computation of ℓ'. These equations giving θ can be simplified by making the same assumptions used in the heat equations (14) and (15) in the skin friction derivation to get

$$\left(\frac{C_F}{C_{Fi}}\right)_{LAM} = \left(\frac{T_\infty}{T'}\right)^{0.15} \quad \& \quad \left(\frac{C_F}{C_{Fi}}\right)_{TURB} = \left(\frac{T_\infty}{T'}\right)^{0.66} \tag{20}$$

Substitution of (20) into (18) and (19) and use of Eq. (15a) gives

$$\boxed{\theta_{LAM} = 0.003765 \left[\frac{p_\infty u_\infty}{(T_\infty)^{1.7}}\right]^{-0.5} \left(\frac{T_\infty}{T'}\right)^{0.15} \ell^{0.5}} \tag{21}$$

and

$$\boxed{\theta_{TURB} = 0.006892 \left[\frac{p_\infty u_\infty}{(T_\infty)^{1.7}}\right]^{-0.2} \left(\frac{T_\infty}{T'}\right)^{0.66} \ell^{0.8}} \tag{22}$$

These equations can then be used in (17) to obtain ℓ'.

Two types of flow discontinuities can be encountered in two dimensional flow. These are (a) transition from laminar to turbulent flow and (b) shockwave or an expansion. The equations for ℓ' for combinations of these cases are obtained from Eq. (17) - (22) and are summarized in the following table for flow on an infinite double-wedge airfoil, a typical two-dimensional body.

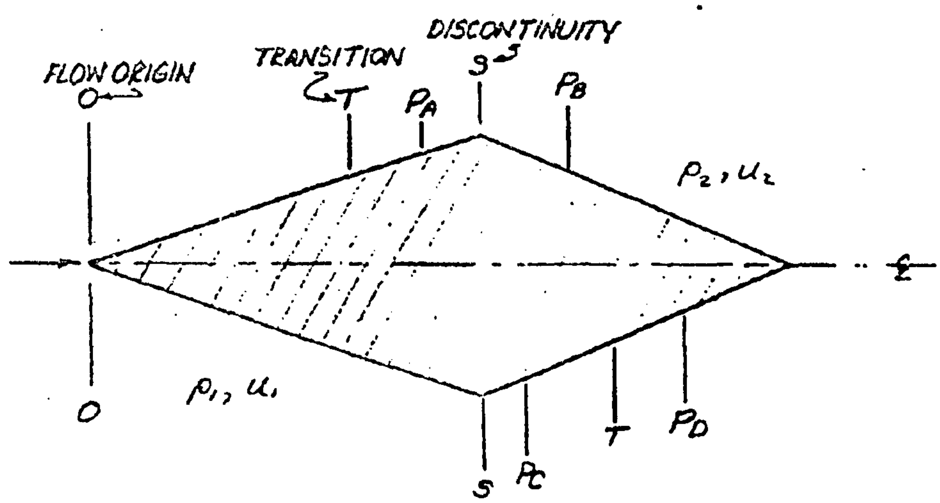

The following effective starting lengths are given to the points P of interest

TO P_A $$\ell_A' = \overline{TP_A} + 0.4696\left[\frac{p_1 u_1}{(T_1')^{1.7}}\right]^{-0.375}(\overline{OT})^{0.625} \tag{23}$$

TO P_B $$\ell_B' = \overline{SP_B} + (\overline{SP_A} + \ell_A')\frac{p_1}{p_2}\left(\frac{u_1}{u_2}\right)^{1.5}\left(\frac{T_2'}{T_1'}\right)^{0.825} \tag{24}$$

TO P_C $$\ell_C' = \overline{SP_C} + \overline{OS}\,\frac{p_1}{p_2}\left(\frac{u_1}{u_2}\right)^{3}\left(\frac{T_2'}{T_1'}\right)^{0.3} \tag{25}$$

TO P_D $$\ell_D' = \overline{TP_D} + (\ell_C' + \overline{P_C T})^{0.625}\cdot 0.4696\left[\frac{p_2 u_2}{(T_2')^{1.7}}\right]^{-0.375} \tag{26}$$

Eq. (23) - (26) may then be used to evaluate the ℓ', which in turn can be used in Eq. (2) - (15) along with local conditions to evaluate the desired coefficients. Since Eq. (1) is independent of length this method does not involve iteration.

3.2.3 Three Dimensional Flow

Since the boundary layer at any point on a cone is much thinner than the boundary layer of a flat plate which has otherwise the same boundary layer characteristics as the cone, the Eq. (2) - (15) do not apply to conical flow unless some correction is made in order to correlate the boundary layer thicknesses. This correction can be made by working directly with the three-dimensional boundary layer equations in the laminar case. Hantzsche and Wendt (Reference 12) found that the conical equations transformed directly into the two dimensional equations if the factor 1/3 were inserted in the cone length. Therefore, for laminar flow, if

$$\text{LAMINAR: } \ell_{CONE} = \frac{1}{3}\ell_{FLAT\ PLATE} \qquad (27)$$

then Eq. (2) - (15) (with slight modification in the mean friction coefficient) can be used. Van Driest (Reference 13) made the same type of investigation of the three-dimensional turbulent equations and found that the effective starting length for a cone in fully turbulent flow is

$$\text{TURBULENT } \ell_{CONE} = \frac{1}{2}\ell_{FLAT\ PLATE} \qquad (28)$$

Summarized below, for convenience, are eq. (2) - (15) for conical flow. The length used ~~in~~ is the actual cone wetted length.

laminar $$R_{e_{T'}} = 4.147\times10^{4}\frac{\rho_s u_s \ell}{(T'_v)^{1.7}} \qquad (29)$$

turbulent $$R_{e_{T'}} = 6.22\times10^{4}\frac{\rho_s u_s \ell}{(T')^{1.7}} \qquad (30)$$

Local skin friction (unchanged) $$c_{f_\infty} = \left(\frac{T_\infty}{T'}\right)c_{f_i}'$$

mean laminar $$C_{F_\infty} = 2/3 \cot\theta_v\left(\frac{T_s}{T'}\right)C_{F_i}' \qquad (31)$$

referred to base area of cone

mean turbulent $$C_{F_\infty} = 1.02\cot\theta_v\left(\frac{T_s}{T'}\right)C_{F_i}' \qquad (32)$$

referred to base area of cone
(using the 1/5 or 1/7 power law for gives identical results)

laminar $$h = \cancel{0.1281}\ 0.01281\left(\frac{\rho_s u_s}{\ell}\right)^{0.5} \qquad (33)$$

and turbulent $$h = \frac{0.02866\,(\rho_s u_s)^{0.8}}{(\ell)^{0.2}\,(T')^{0.51}} \tag{34}$$

Eq. (29) - (34) are then solved in the same manner as the equations (2) - (15) for two dimensional flow.

3.2.4 Three Dimensional Flow with Discontinuities

The constant momentum-loss method of section 3.2.2 can be applied to the case of three-dimensional flow. The only changes which need be made are in the equations for the momentum thickness where the factors 1/3 and 1/2 must be inserted in the laminar and turbulent θ, respectively. Making this change we have

$$\boxed{\text{LAMINAR} \quad \theta_{cone} = 0.002174\left(\frac{\rho_s u_s}{(T_s)^{1.7}}\right)^{-0.5}\left(\frac{T_s}{T'}\right)^{0.15}\ell^{0.5}} \tag{35}$$

$$\boxed{\text{TURBULENT} \quad \theta_{cone} = 0.003959\left(\frac{\rho_s u_s}{(T_s)^{1.7}}\right)^{-0.2}\left(\frac{T_s}{T'}\right)^{0.66}\ell^{0.8}} \tag{36}$$

These equations are used in Eq. (17) to find ℓ', the effective length, which is then used in Eq. (2) - (15) to obtain friction and heat transfer.

The types of discontinuities usually encountered in conical flow would be found, say, on a cone-cylinder. The equations for various starting lengths found from Eq. (17), (35) and (36) are summarized for that body in the following table:

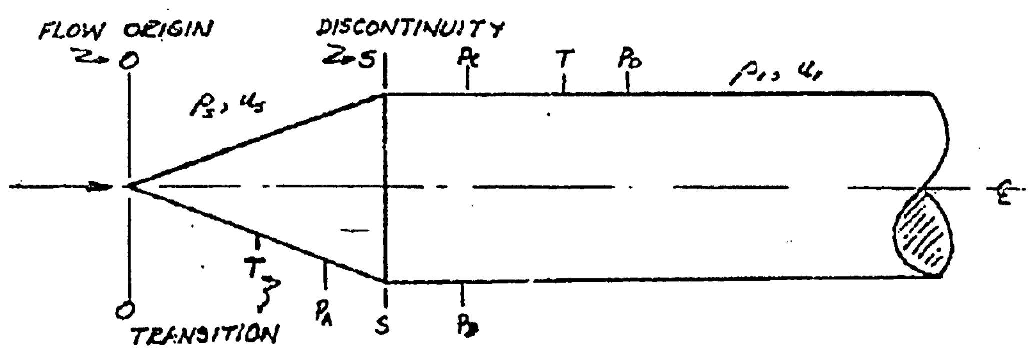

ASSUMED PRESSURE GRADIENT ON THE CYLINDER

AT P_A: $$\ell_A' = \frac{\overline{TP_A}}{2} + 0.4727(\overline{OT})^{0.625}\left[\frac{p_s u_s}{(T_s')^{1.7}}\right]^{-0.375} \qquad (37)$$

AT P_B: $$\ell_B' = \overline{SP_B} + 0.57435\left(\ell_A' + \frac{\overline{SP_A}}{2}\right)\frac{p_s}{p_1}\left(\frac{u_s}{u_1}\right)^{1.5}\left(\frac{T_1'}{T_s'}\right)^{0.825} \qquad (38)$$

AT P_C: $$\ell_C' = \overline{SP_C} + 0.57735\,\frac{\overline{OS}}{3}\,\frac{p_s}{p_1}\left(\frac{u_s}{u_1}\right)^{3}\left(\frac{T_1'}{T_s'}\right)^{0.3} \qquad (39)$$

AT P_D: $$\ell_D' = \overline{TP_D} + 0.4696\left[\ell_C' + \overline{TP_C}\right]^{0.625}\left[\frac{p_s u_s}{(T_s')^{1.7}}\right]^{-0.375} \qquad (40)$$

to be used in Eq. (2) - (15) to find the friction and heat transfer.

3.2.5 Flow With Streamwise Gradients

In section 3.2.4 the flow on the cylinder portion of the body investigated was assumed to be at constant pressure in order to obtain the simple equations (38), (39) and (40). For the case where a streamwise gradient is to be considered the body must be broken into small segments of constant flow properties. If this is done then the equations (17), (21) and (22) can be applied to each section and equivalent starting lengths can be found for any point on the body. For flow of such a type consider a semi-infinite biconvex airfoil broken into small segments of constant stream properties as shown below:

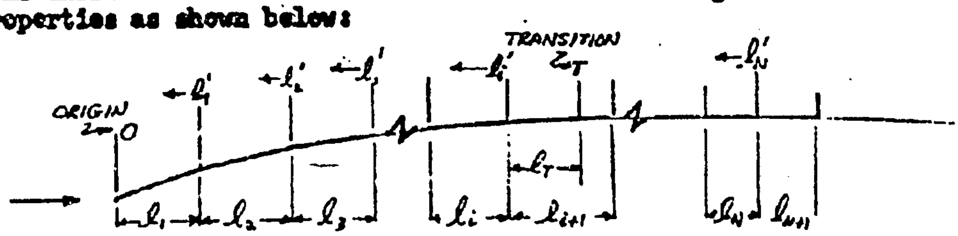

Each segment has the stream properties p_1, u_1; p_2, u_2; p_3, u_3; ...etc.

To derive the general equation for the effective length along the body at a point preceded by completely laminar flow, apply Eq. (21) and (22) to Eq. (17). For segment ℓ_1 ,

$$\theta_1 g_1 = \theta_2 g_2$$

So

$$0.003765\left[\frac{p_1 u_1}{(T_1)^{1.7}}\right]^{-0.5}\left(\frac{T_1}{T_1'}\right)^{0.15}\ell_1^{0.5}\, g_1 = 0.003765\left[\frac{p_2 u_2}{(T_2)^{1.7}}\right]^{-0.5}\left(\frac{T_2}{T_2'}\right)^{0.15}\left[\ell_1'\right]^{0.5} g_2$$

or

$$(\ell_1')^{0.5} = \ell_1^{0.5}\left(\frac{p_2 u_2}{p_1 u_1}\right)^{0.5}\left(\frac{T_1}{T_2}\right)^{0.85}\left(\frac{T_1}{T_2}\right)^{0.15}\left(\frac{T_2'}{T_1'}\right)^{0.15}\frac{g_1}{g_2}$$

$$\ell_1' = \ell_1\left(\frac{p_2 u_2}{p_1 u_1}\right)\left(\frac{T_1}{T_2}\right)^2\left(\frac{T_2'}{T_1'}\right)^{0.3}\left(\frac{g_1}{g_2}\right)^2$$

Apply the perfect gas law to the g ratio

$$\frac{g_1}{g_2} = \frac{\rho_1 u_1^2}{\rho_2 u_2^2} = \frac{p_1 u_1^2 T_2}{p_2 u_2^2 T_1}$$

and insert in the above equation to get

$$\ell_1' = \ell_1\left(\frac{p_1 u_1^2}{p_2 u_2^2}\right)^2\left(\frac{p_2 u_2}{p_1 u_1}\right)\left(\frac{T_2'}{T_1'}\right)^{0.3}\left(\frac{T_1}{T_2}\right)^2\left(\frac{T_2}{T_1}\right)^2.$$

or $$\ell_1' = \ell_1\,\frac{p_1}{p_2}\left(\frac{u_1}{u_2}\right)^3\left(\frac{T_2'}{T_1'}\right)^{0.3}$$

This procedure can be repeated for each segment, i.e.,

$$\ell_3' = \left(\ell_2 + \ell_1'\right)\frac{p_2}{p_3}\left(\frac{u_2}{u_3}\right)^3\left(\frac{T_3'}{T_2'}\right)^{0.3}$$

or

$$\ell_3' = \ell_2\frac{p_2}{p_3}\left(\frac{u_2}{u_3}\right)^3\left(\frac{T_3'}{T_2'}\right)^{0.3} + \ell_1\frac{p_1}{p_3}\left(\frac{u_1}{u_3}\right)^3\left(\frac{T_3'}{T_1'}\right)^{0.3}$$

and in general

$$\boxed{\ell_i' = \sum_{k=1}^{k=i}\ell_k\,\frac{p_k}{p_i}\left(\frac{u_k}{u_i}\right)^3\left(\frac{T_i'}{T_k'}\right)^{0.3}} \qquad (41)$$

Let transition occur at some point T in segment ℓ_{i+1} at some distance ℓ_T from the beginning of the segment. Then the effective length to T is

$$\boxed{\ell_T' = \left(\ell_T + \ell_i'\right)^{0.625} 0.4696\left[\frac{p_{i+1}\,u_{i+1}}{\left(T_{i+1}'\right)^{1.7}}\right]^{-0.375}} \qquad (42)$$

and for any general turbulent section thereafter

$$\boxed{\ell_N' = \sum_{k=i+2}^{k=N}\ell_k\,\frac{p_k}{p_N}\left(\frac{u_k}{u_N}\right)^{1.5}\left(\frac{T_N'}{T_k'}\right)^{0.825} + \left(\ell_T' + \ell_{i+1} - \ell_T\right)\frac{p_{i+1}}{p_N}\left(\frac{u_{i+1}}{u_N}\right)^{1.5}\left(\frac{T_N'}{T_{i+1}'}\right)^{0.825}} \qquad (43)$$

These generalized formulas for ℓ' may then be used along with local conditions to evaluate the friction and heat transfer at any point from Eq. (2) - (15).

4.0 Conclusions

A collection has been made of aerodynamic flow characteristics for one, two and three dimensional hypersonic flow. The Mach number range is from $0 \leq M \leq 20$. The flow parameters are shown as functions of initial Mach number and deflection angle in sections 1, 2, 3; Figures 1.0 through 3.16.

Equations for compressible skin friction and heat transfer using the reference temperature method were presented for two and three dimensional flow, flow with discontinuities and flow with streamwise gradient. Figures necessary in using the formulae are in section 4, Figure 4.1 - 4.7.

5.0 References

1. Dailey, C. C. and Wood, F. C. "Computation Curves for Compressible Fluid Problems". 1949.

2. "Notes and Tables For Use in the Analysis of Supersonic Flow". Staff of the 1 x 3 foot Supersonic Wind Tunnel Section, Ames Aeronautical Laboratory. NACA TN 1428, 1947.

3. "Charts and Tables for Analysis of Supersonic Flow". GALCIT Memo #4. Pasadena, 1951.

4. Kopal, Z., ed. Tables of Supersonic Flow Around Cones. MIT Technical Report No. 1, 1947.

5. Grimminger, G., et. al., "Lift on Inclined Bodies of Revolution in Hypersonic Flow". Journal of Aeronautical Sciences, November, 1950.

6. Young, G. B. W. and Siska, C. P., "Supersonic Flow Around Cones at Large Yaw". RAND Report P-198, March 1951.

7. Von Karman, T. "Turbulence and Skin Friction", Journal of Aeronautical Sciences, January 1934.

8. Van Driest, E. R. "Calculation of the Stability of the Laminar Boundary Layer in a Compressible Fluid on a Flat Plate With Heat Transfer", Journal of Aeronautical Sciences, December 1952.

9. Romig, M. F. "The Reference Temperature Method for Calculating Skin Friction and Heat Transfer in Compressible Flow". Convair Memo A-Atlas-151, 3 December 1954.

10. Sieff, A. "Examination of the Existing Data on the Heat Transfer of Turbulent Boundary Layers at Supersonic Speeds From the Point of View of Reynolds Analogy". NACA TN 3284, August 1954.

11. Romig, M. F. "Survey and Analysis of Experimental Data on Boundary Layer Transition in Hypersonic Flow". Convair Memo A-Atlas-142, 5 November 1954. (Confidential)

12. Mantzsche, W. and Wendt, H. "The Laminar Boundary Layer on a Cone in a Supersonic Air Stream at Zero Angle of Attack". Translation RAT-6, RAND Corporation, 1947.

13. Van Driest, E. R. "Turbulent Boundary Layer on a Cone in a Supersonic Flow at Zero Angle of Attack". Journal of Aeronautical Sciences, January 1952.

Prepared by: Mary F. Romig
M. F. Romig

Checked by : R. C. Huyett
R. C. Huyett

Approved by: William H. Dorrance
W. H. Dorrance

cc:
H. F. Dunholter
C. S. Ames
D. Folland
W. Schwidetzky
H. Friedrich
W. F. Radcliffe
L. Jirsa
D. Collins
H. Steele
B. Shorey
W. H. Dorrance
File
R. J. Kirby
R. C. Huyett
M. F. Romig
R. O. Morell
W. B. Mitchell
W. J. Gaudtner
H. Serbin
F. M. Perkins
C. H. Heaton
P. I. Dickey
P. E. Culbertson
J. Q. Wenzel
G. Noble
S. Remington
J. Farber
V. Kebely
D. Otis
K. Ehricke
MIT (Attn. Security Officer) Copy #31
P. S. Yip
J. Sherley
R. Wentink
J. Bowyer
H. U. Eckert
W. F. Radcliffe
R-W Library via M. Rosenbaum
Avco Mfg. Co. via M. Rosenbaum

Index to Figures

Section 1. One-Dimensional Flow Characteristics

Plotted versus Initial Mach Number

Figure No.	Page
1.1 - Mach number after shock	20
1.2 - Static pressure ratio	21
1.3 - Static temperature ratio	22
1.4 - Density ratio	23
1.5 - Velocity and dynamic pressure ratio	24
1.6 - Reynolds number ratio	25
1.7 - Total head ratio	26
1.8 - Area Ratio	27

Section 2. Two-Dimensional Flow Characteristics

A. Compression

Plotted versus Initial Mach Number with Wedge Angle a Parameter

Figure No.	Page
2.0 - Maximum cone, wedge angles for attached shock	28
2.1 - Mach number after shock	29
2.2 - Static pressure ratio	30
2.3 - Static temperature ratio	31
2.4 - Density ratio	32
2.5 - Shockwave angle	33
2.6 - Velocity ratio	34
2.7 - Dynamic pressure ratio	35
2.8 - Reynolds number ratio	36
2.9 - Total head ratio	37

B. Expansion

2.10a - Mach number versus Prandtl-Meyer angle	38
2.10b - Continued	39
2.11a - Static pressure to total head ratio versus	40 to
-2.11i Prandtl-Meyer angle	48

Section 3. Conical Flow

A. Flow Characteristics, Unyawed Cone

Plotted versus Free Stream Mach Number with Cone Semi-Vertex Angle a Parameter

Figure No. — Page

3.1 - Surface Mach number — 49
3.2 - Surface static pressure ratio — 51
3.3 - Surface static temperature ratio — 52
3.4 - Surface density ratio — 53
3.5 - Shock wave angle — 54
3.6 - Surface velocity ratio — 55
3.7 - Surface dynamic pressure ratio — 56
3.8 - Surface Reynolds Number ratio — 57
3.9 - Surface total head ratio — 58

B. Force Coefficients, Unyawed Cone

Figure No. — Page

3.10a - Wave drag coefficient versus — 59 to
-3.10d Cone half-angle — 62
3.11 - Initial Axial Force coefficient, $C_{X_{\alpha=0}} / \sin^2 \theta_v$ versus Mach number — 63
3.12 - Initial normal force coefficient slope, $(dC_N/d\alpha)_{\alpha=0} / \cos^2 \theta_v$, vs. Mach number — 64

C. Force Coefficients, Yawed Cone

Figure No. — Page

3.13 - Additional axial force coefficient due to angle of attack/α^2 versus Mach number — 65
3.14 - Normal force coefficient/$\cos^2 \theta_v$ versus angle of attack (Newtonian Flow) — 66
3.15 - Normal force coefficient slope/$\cos^2 \theta_v$ versus angle of attack (Newtonian Flow) — 67
3.16 - Axial force coefficient versus angle of attack (Newtonian Flow) — 68

Section 4. Viscous Flow Phenomena

Figure No. — Page

4.1 - Incompressible laminar and turbulent mean and local skin friction coefficients versus Reynolds number — 69
4.2 - T'/T versus Mach number — 70
4.3 - $(T')^{1.7}$ versus T' — 71
4.4A - 4.4c - Inherent temperature rise, ΔT_i, versus velocity — 72 - 74
4.5 - Specific heat of air versus temperature — 75
4.6 - Minimum critical Reynolds number for stability of the laminar boundary layer — 76
4.7 - Coefficient of viscosity versus temperature for the Sutherland Viscosity Law — 77

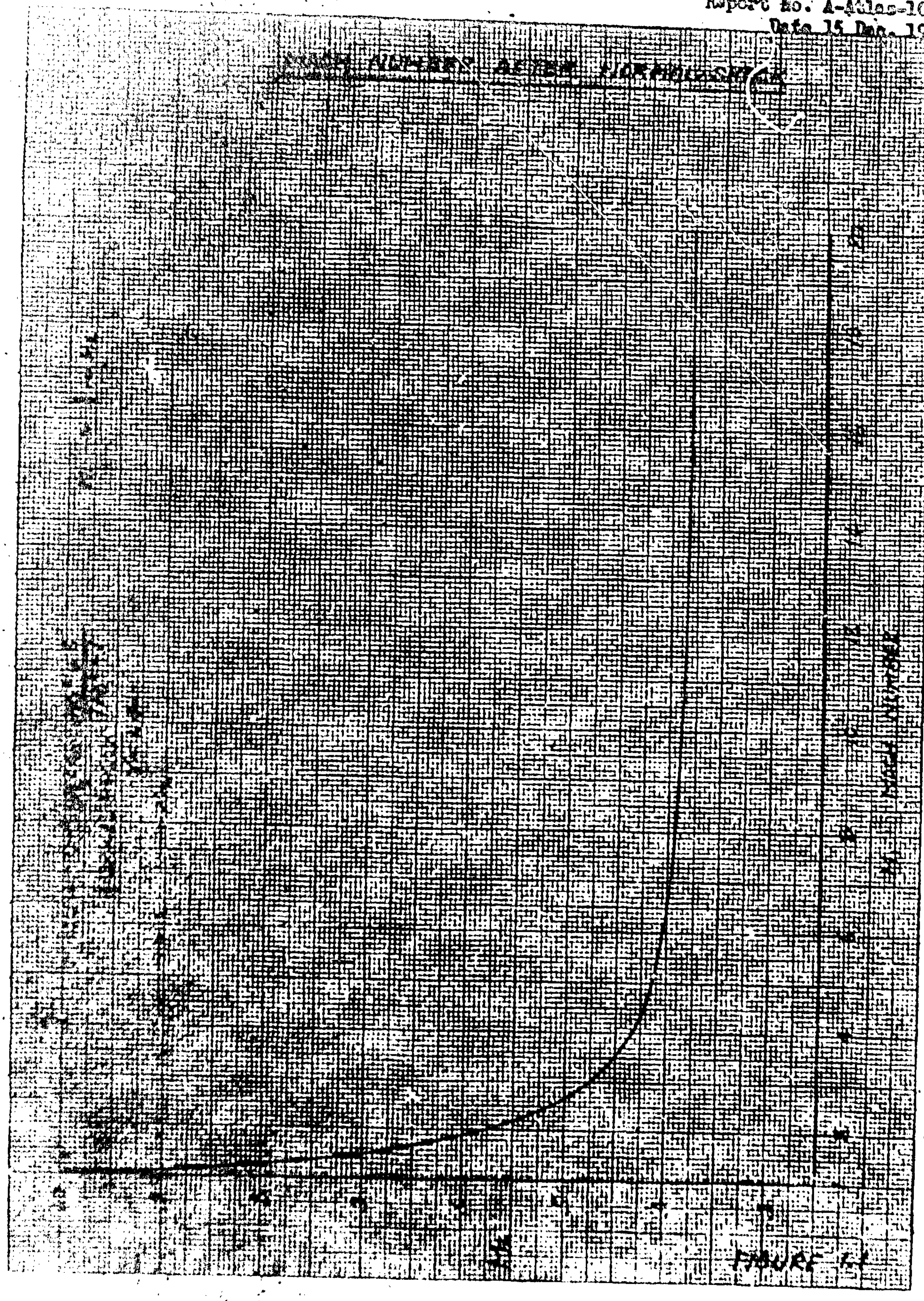

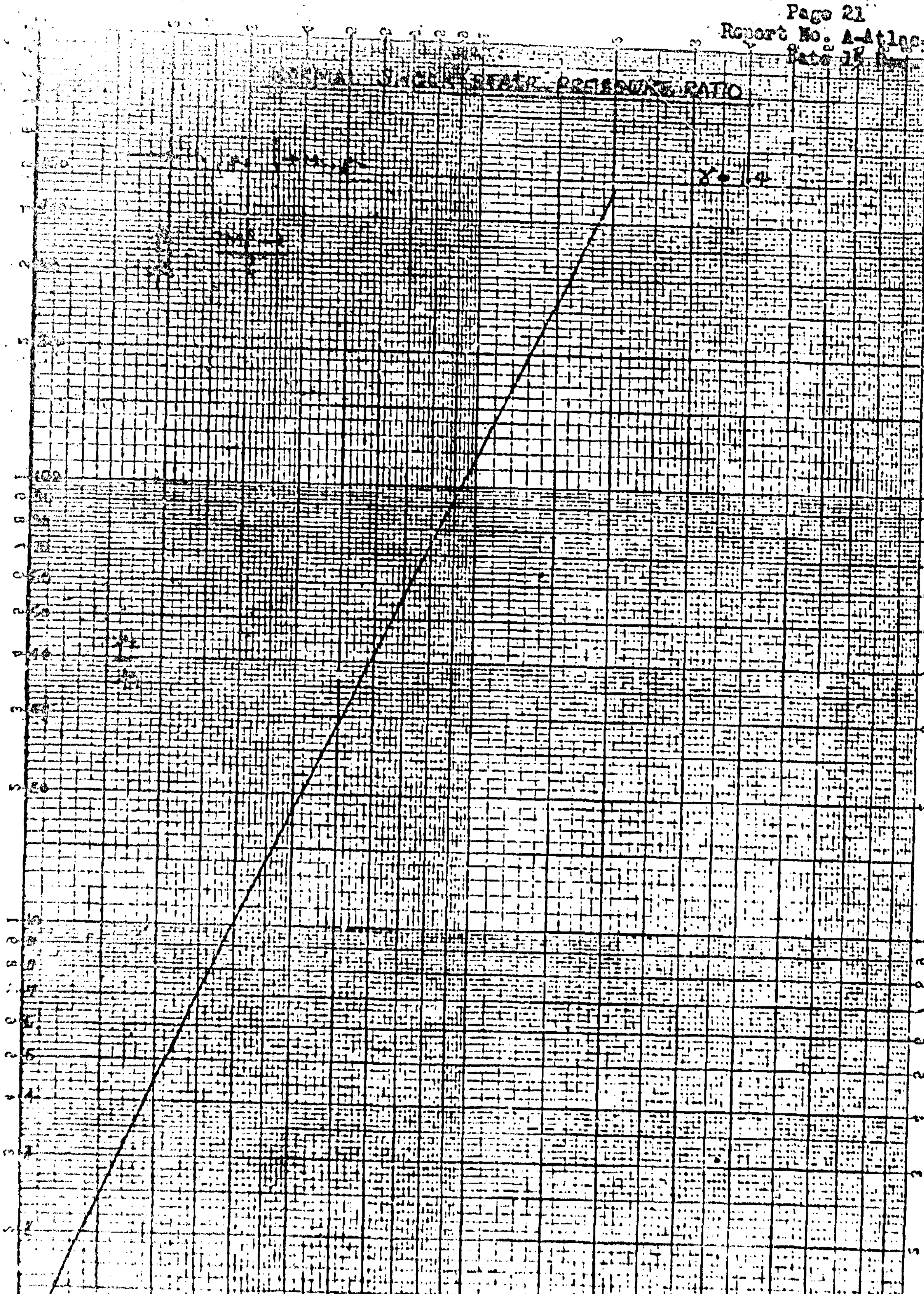

FIGURE 12

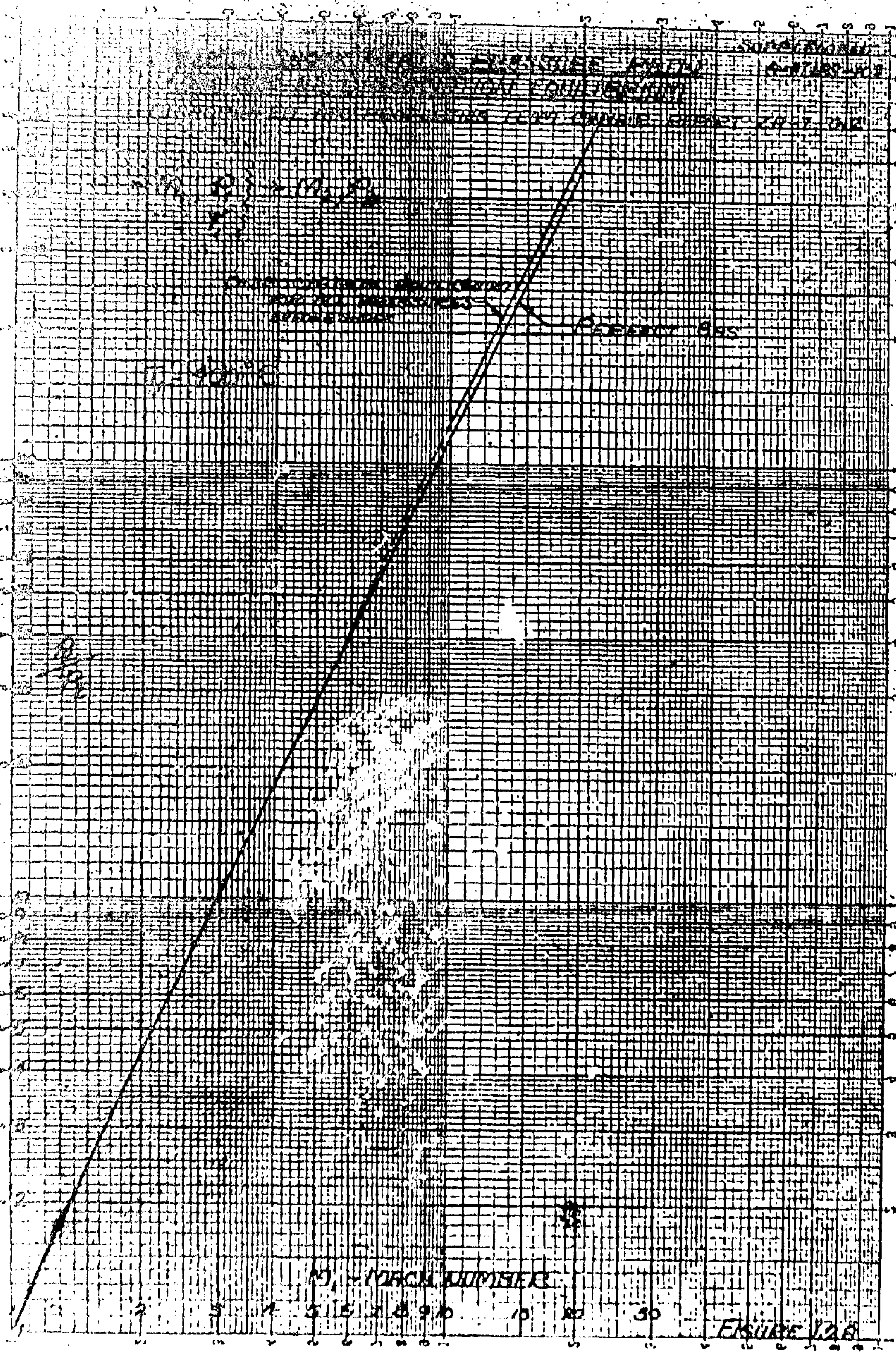

FIGURE 12A

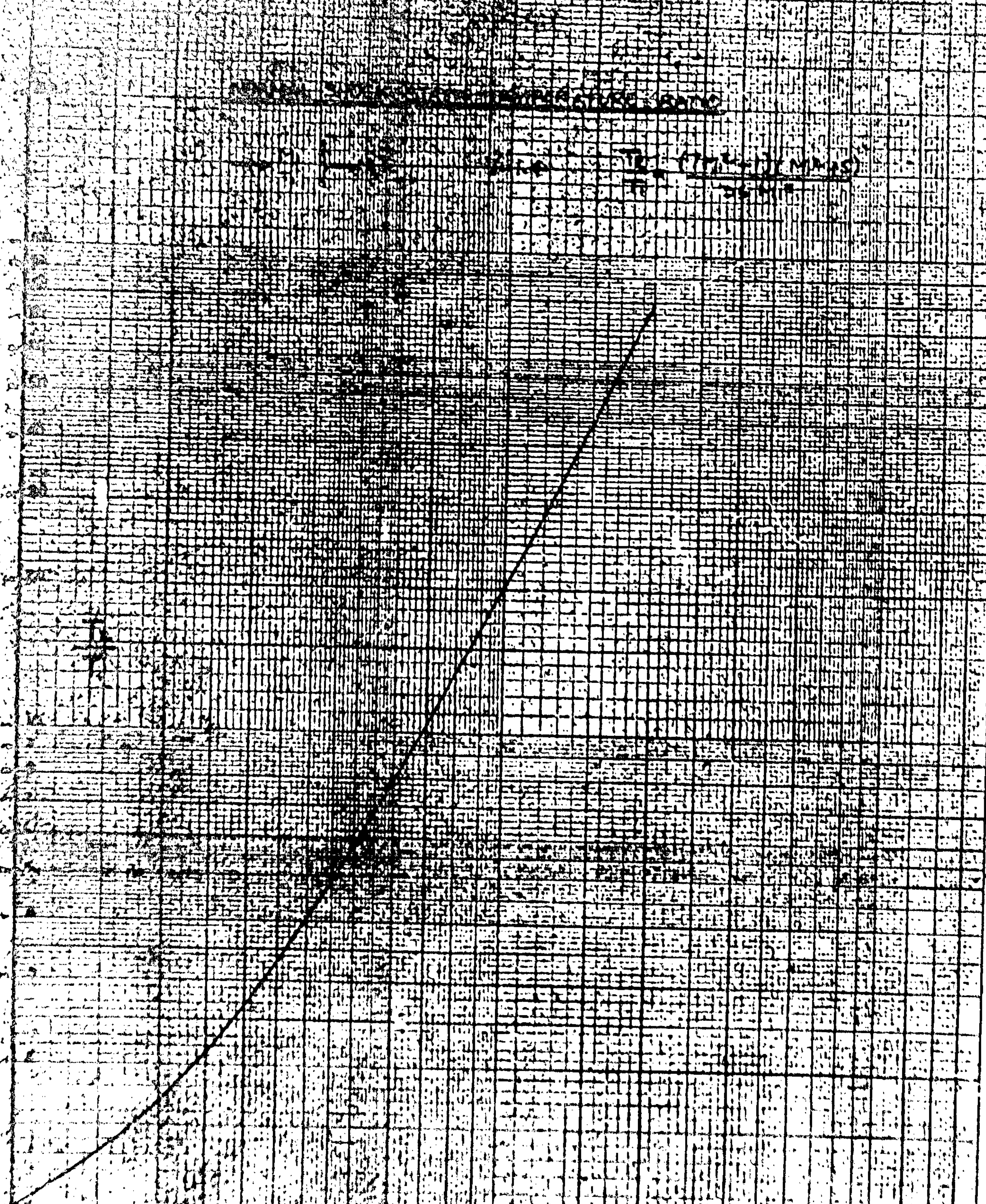

FIGURE 1-3

SUPPLEMENT
A-ATLAS-103

NORMAL SHOCK DENSITY RATIO FOR AIR AT DISSOCIATION EQUILIBRIUM

DISSOCIATED AIR PROPERTIES FROM CONVAIR REPORT ZA-7-012

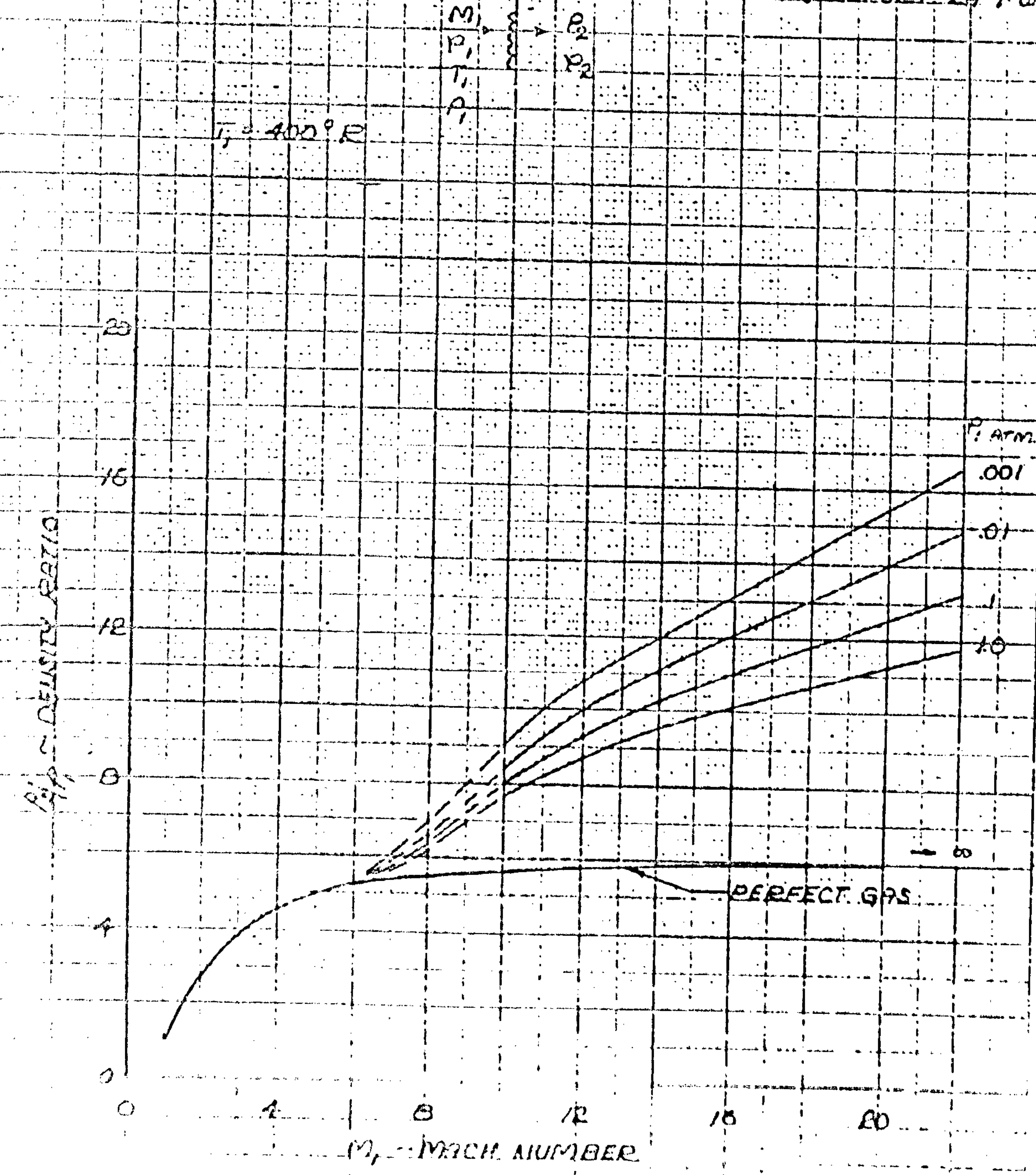

FIGURE 14A

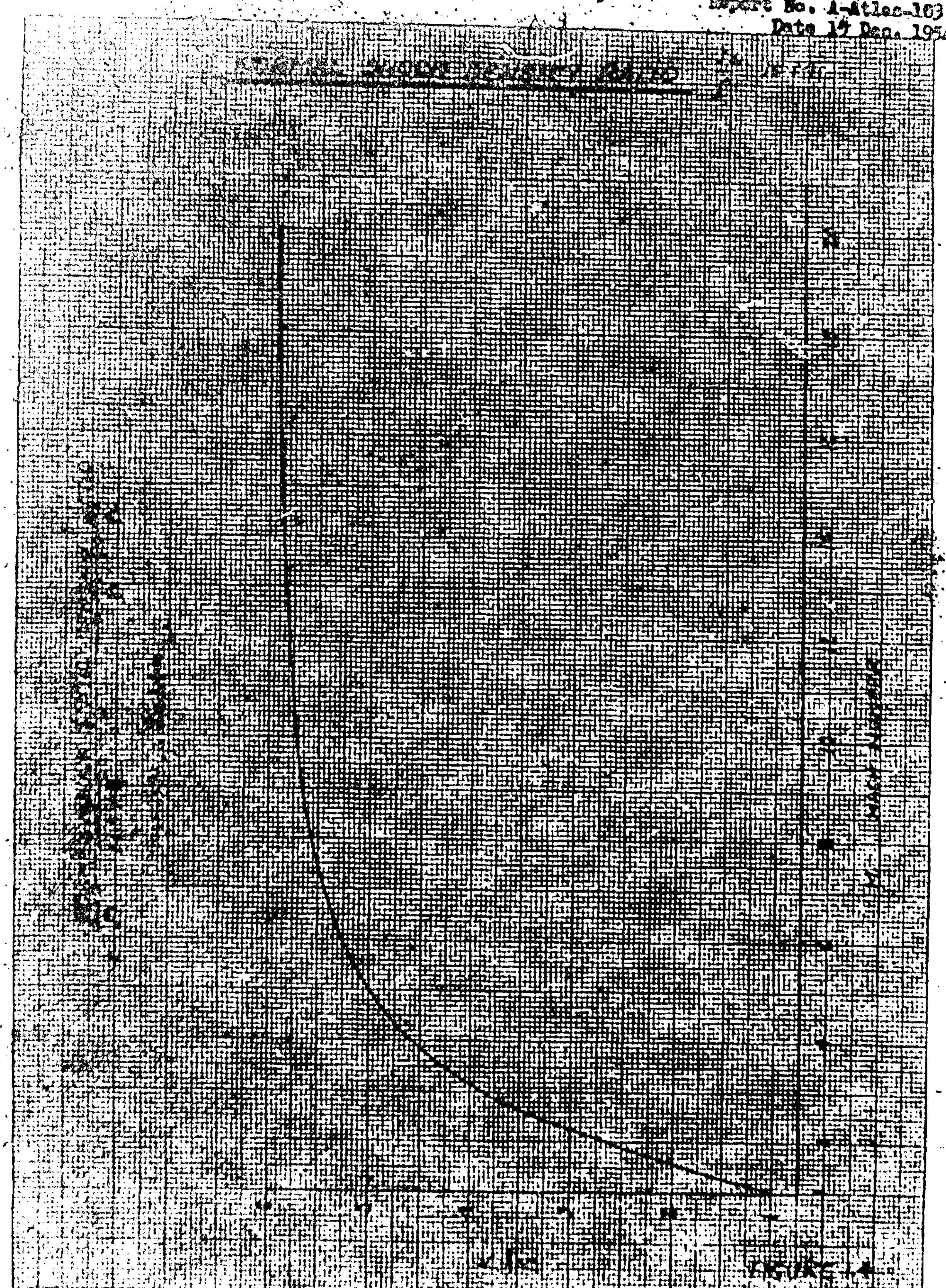

FIGURE 14

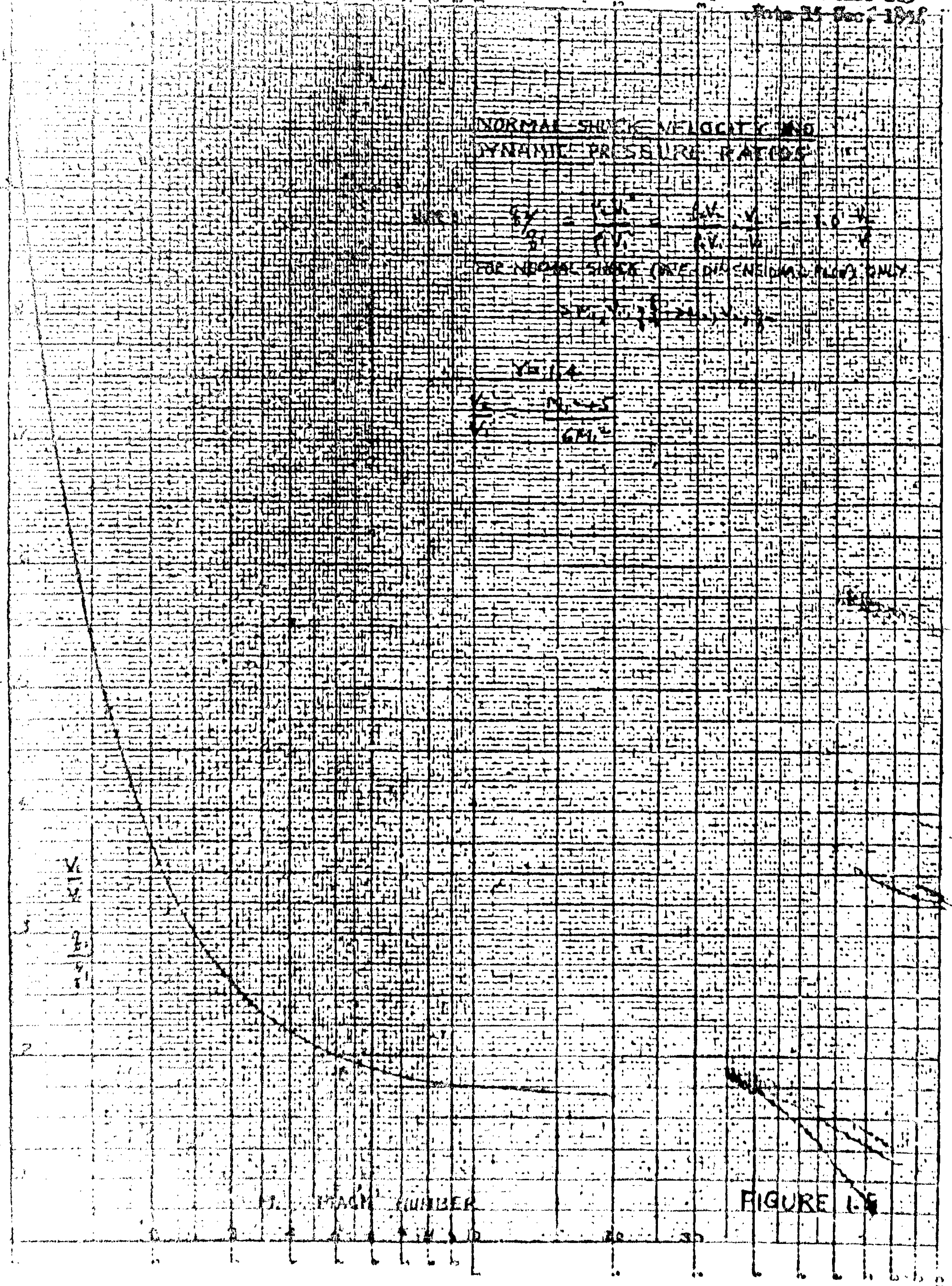
NORMAL SHOCK VELOCITY AND
DYNAMIC PRESSURE RATIOS
FOR NORMAL SHOCK (ONE-DIMENSIONAL FLOW) ONLY
γ = 1.4
$\frac{V_2}{V_1} = \frac{M_1^2+5}{6M_1^2}$
$\frac{V_2}{V_1}$
M₁ MACH NUMBER

FIGURE 1.6

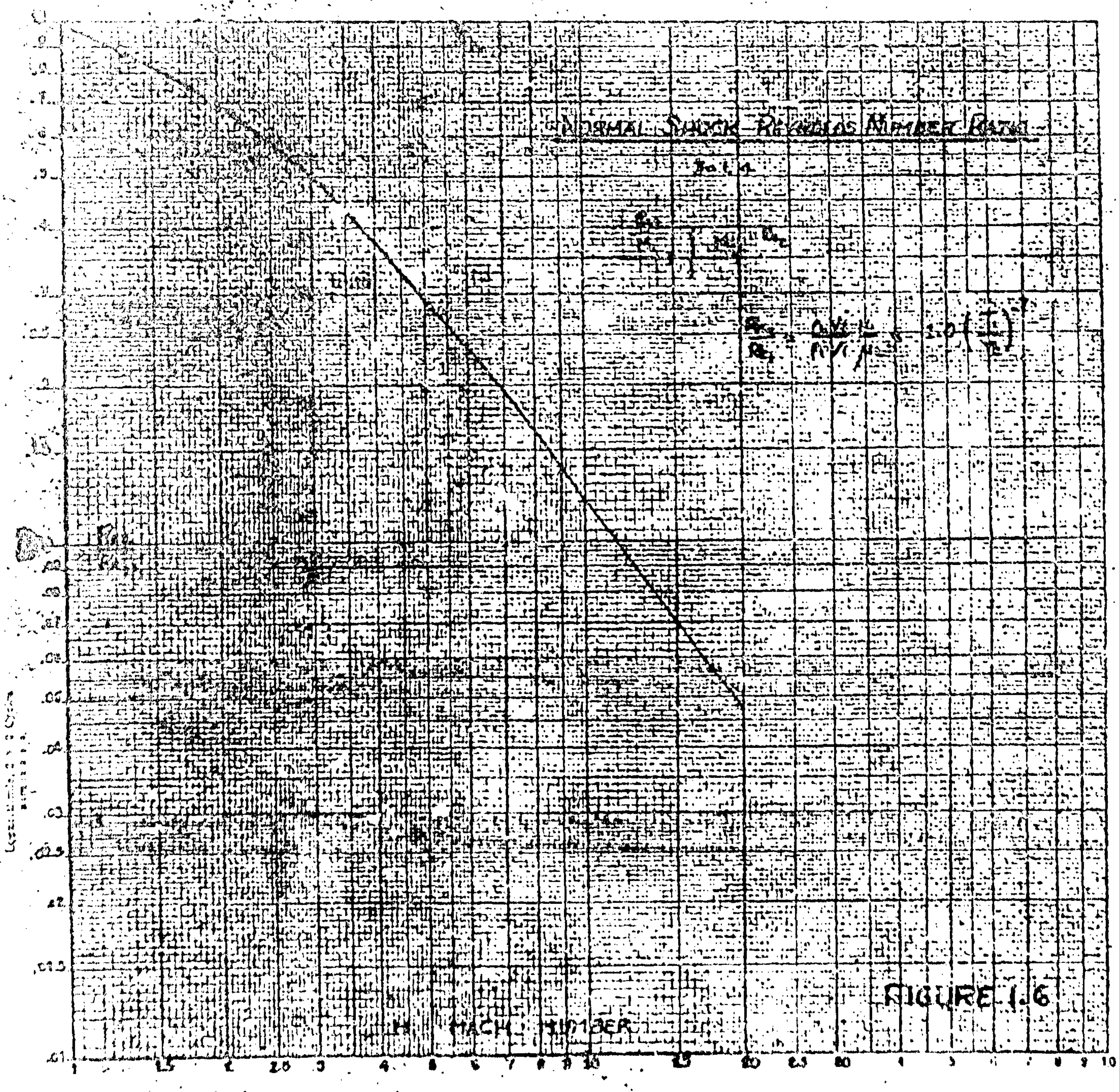
NORMAL SHOCK REYNOLDS NUMBER RATIO
M MACH NUMBER
FIGURE 1.6

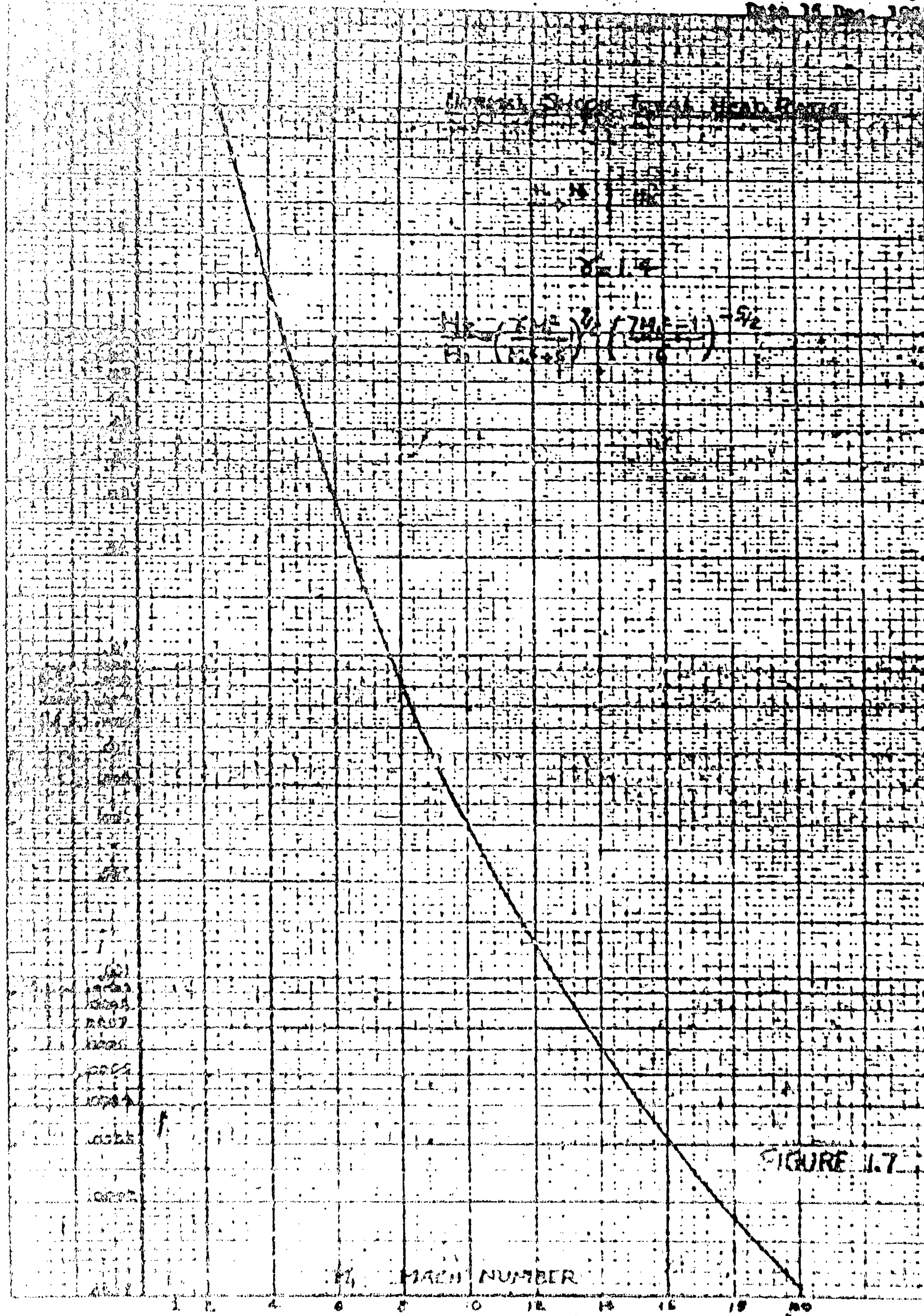
Normal Shock Total Head Ratio
γ = 1.4
MACH NUMBER
1
2
4
6
8
10
12
14
16
18
20

FIGURE 1.7

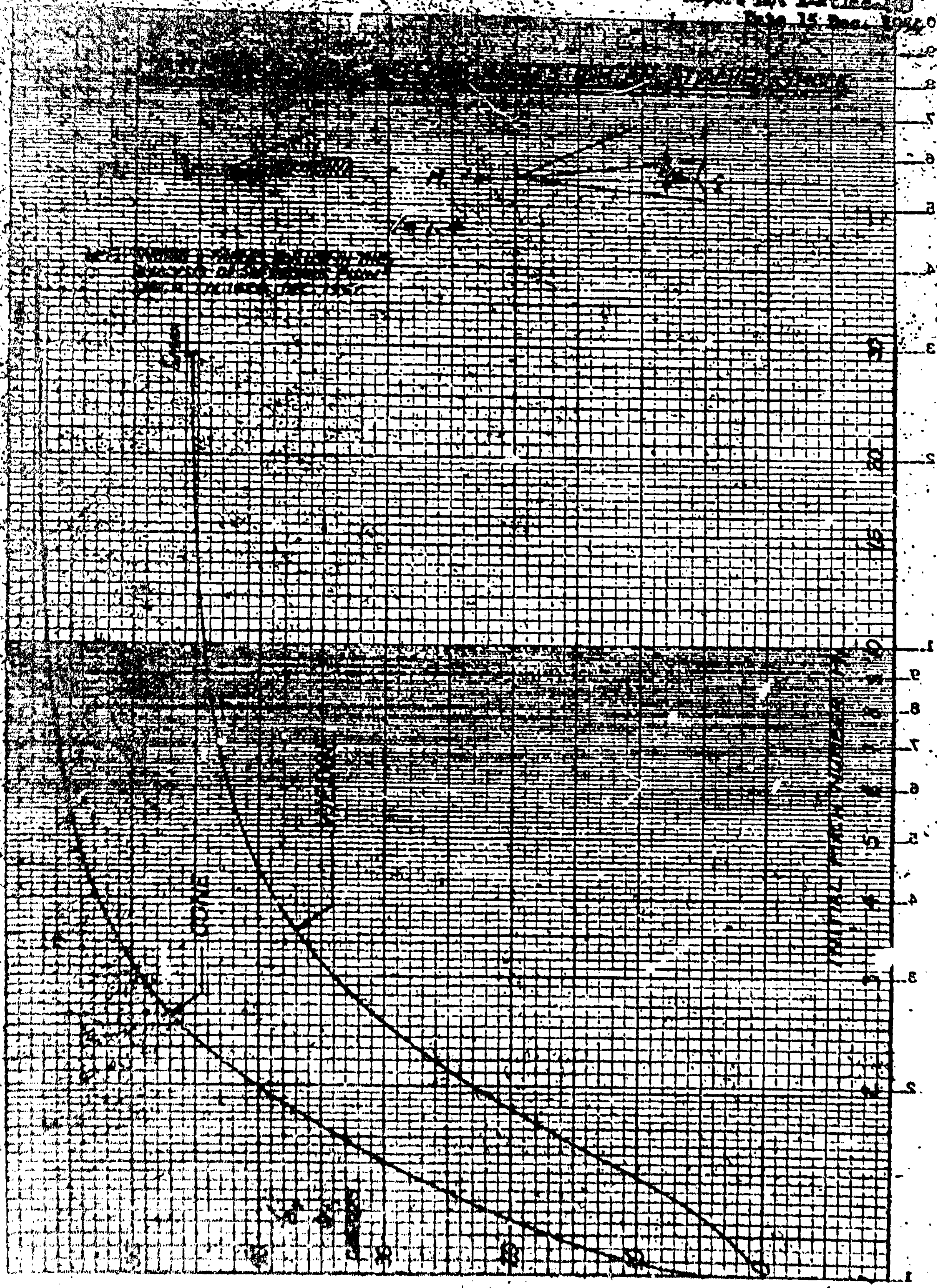

FIGURE 2.0

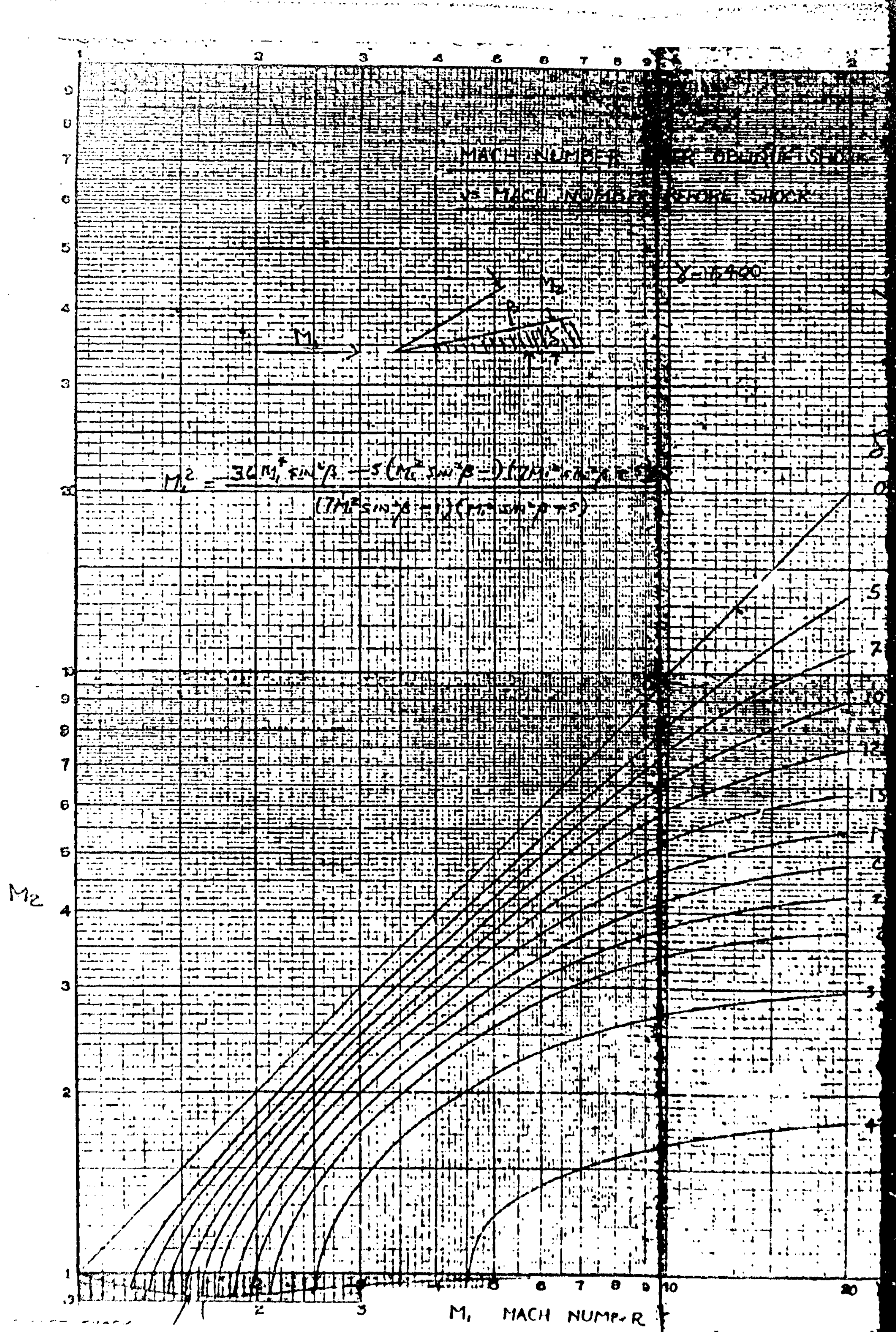
MACH NUMBER AFTER OBLIQUE SHOCK
VS MACH NUMBER BEFORE SHOCK
M₁
M₂
M₁ MACH NUMBER
M2

M_2 vs M_1

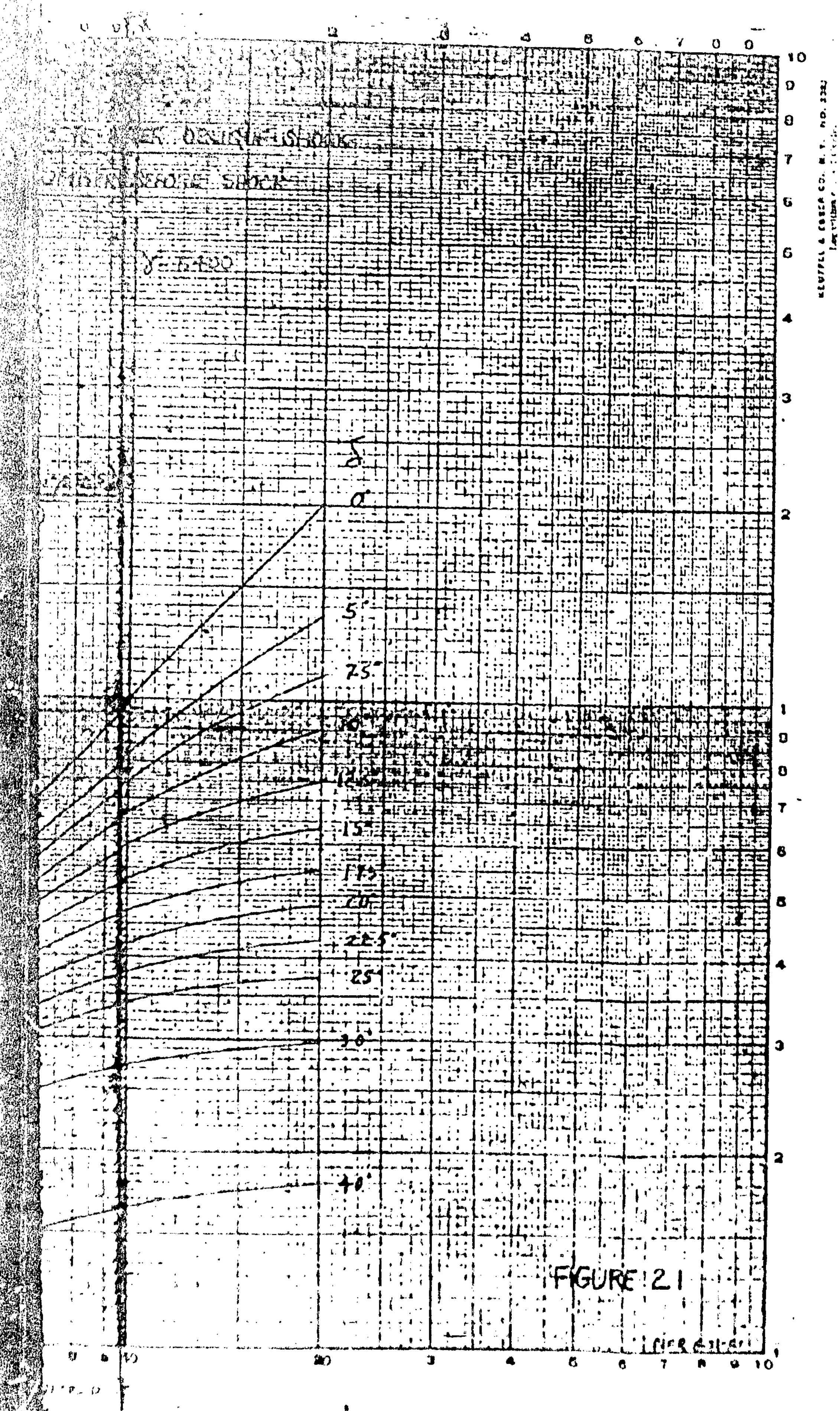

B

FIGURE 2.1

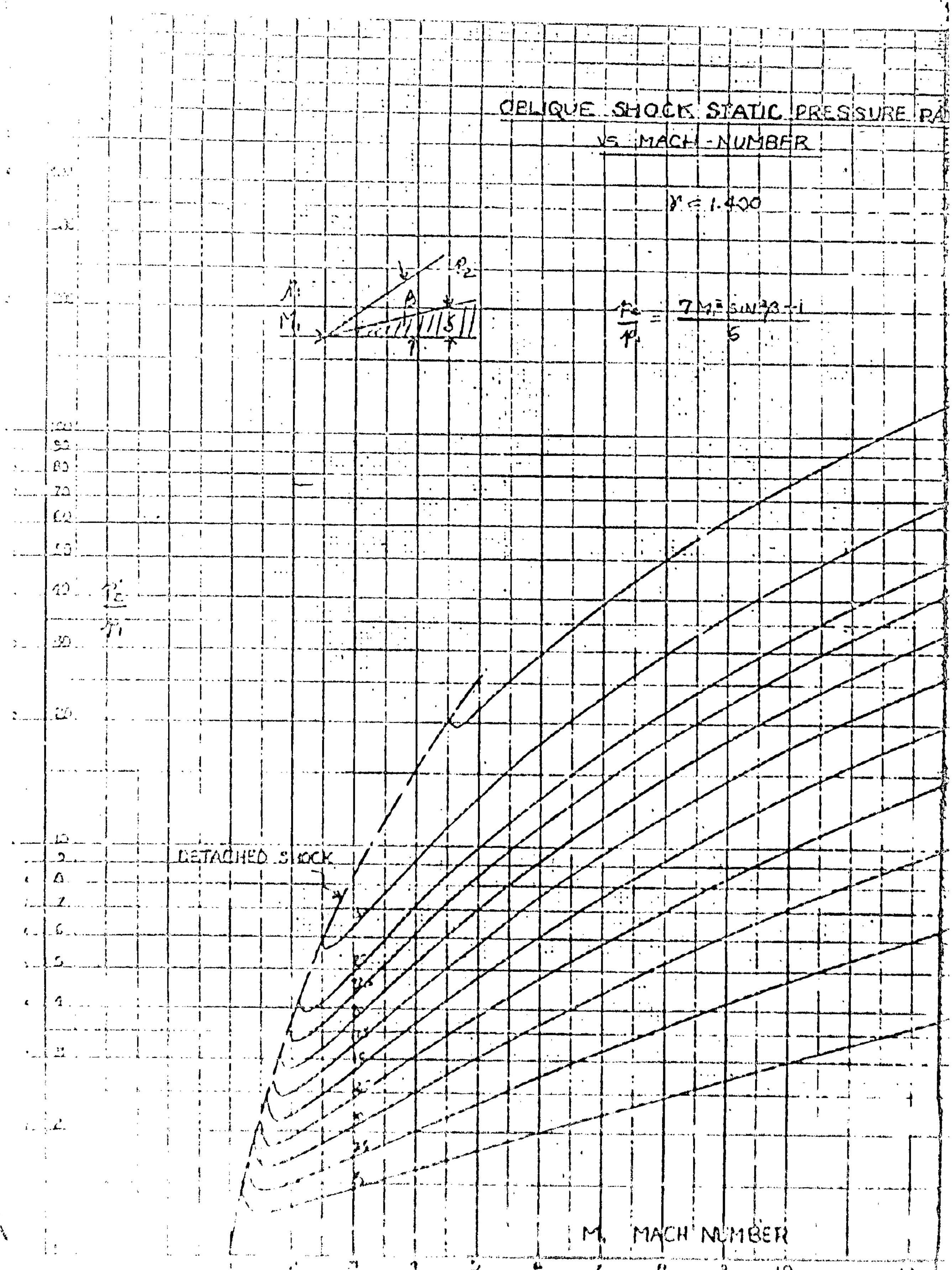

OBLIQUE SHOCK STATIC PRESSURE RA
VS MACH-NUMBER
$\gamma = 1.400$
$\frac{p_2}{p_1} = \frac{7 M_1^2 \sin^2\beta - 1}{6}$
p_1
M_1
p_2
β
δ
$\frac{p_2}{p_1}$
DETACHED SHOCK
M, MACH NUMBER
10
12

p_2/p_1 vs M_1

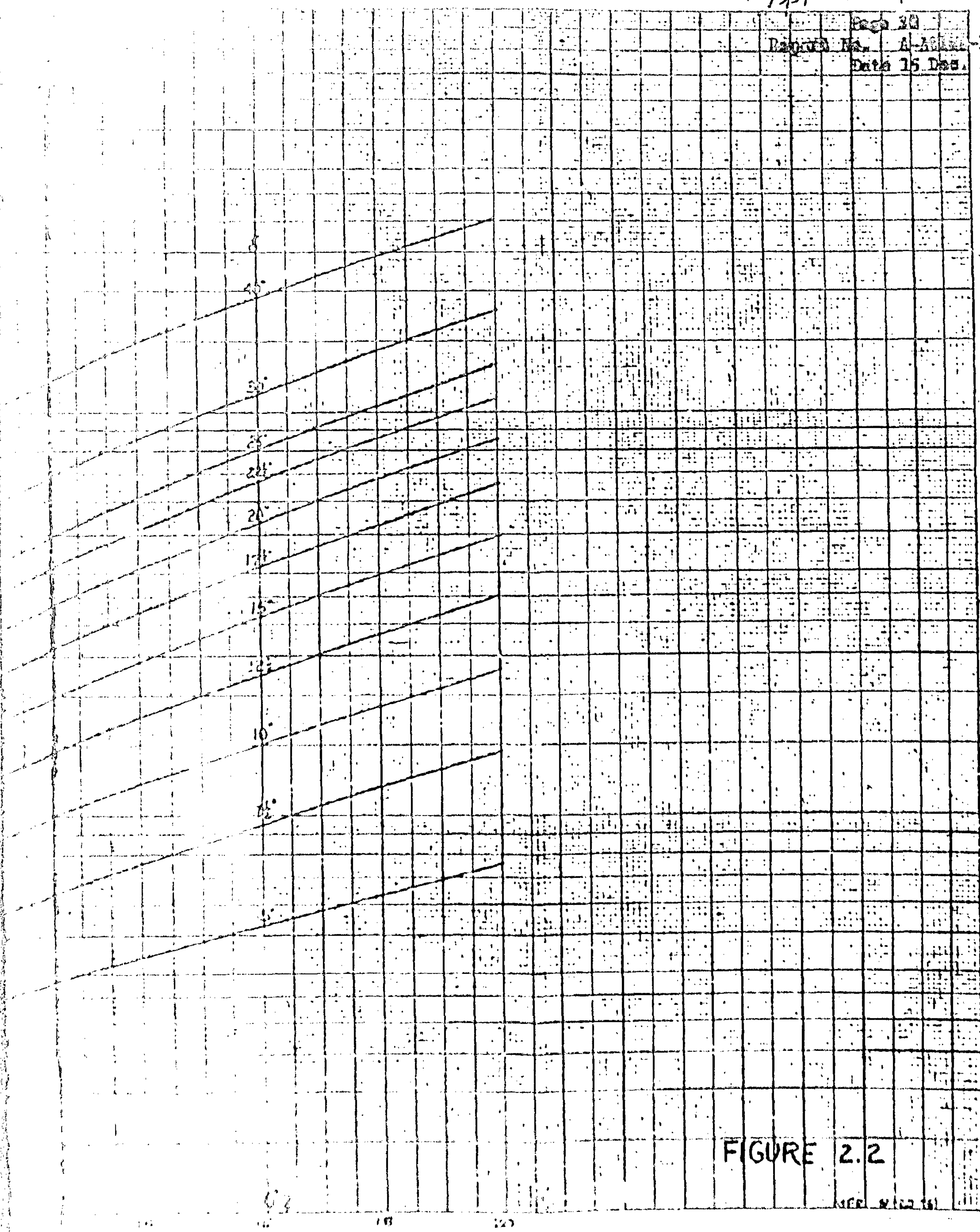

FIGURE 2.2

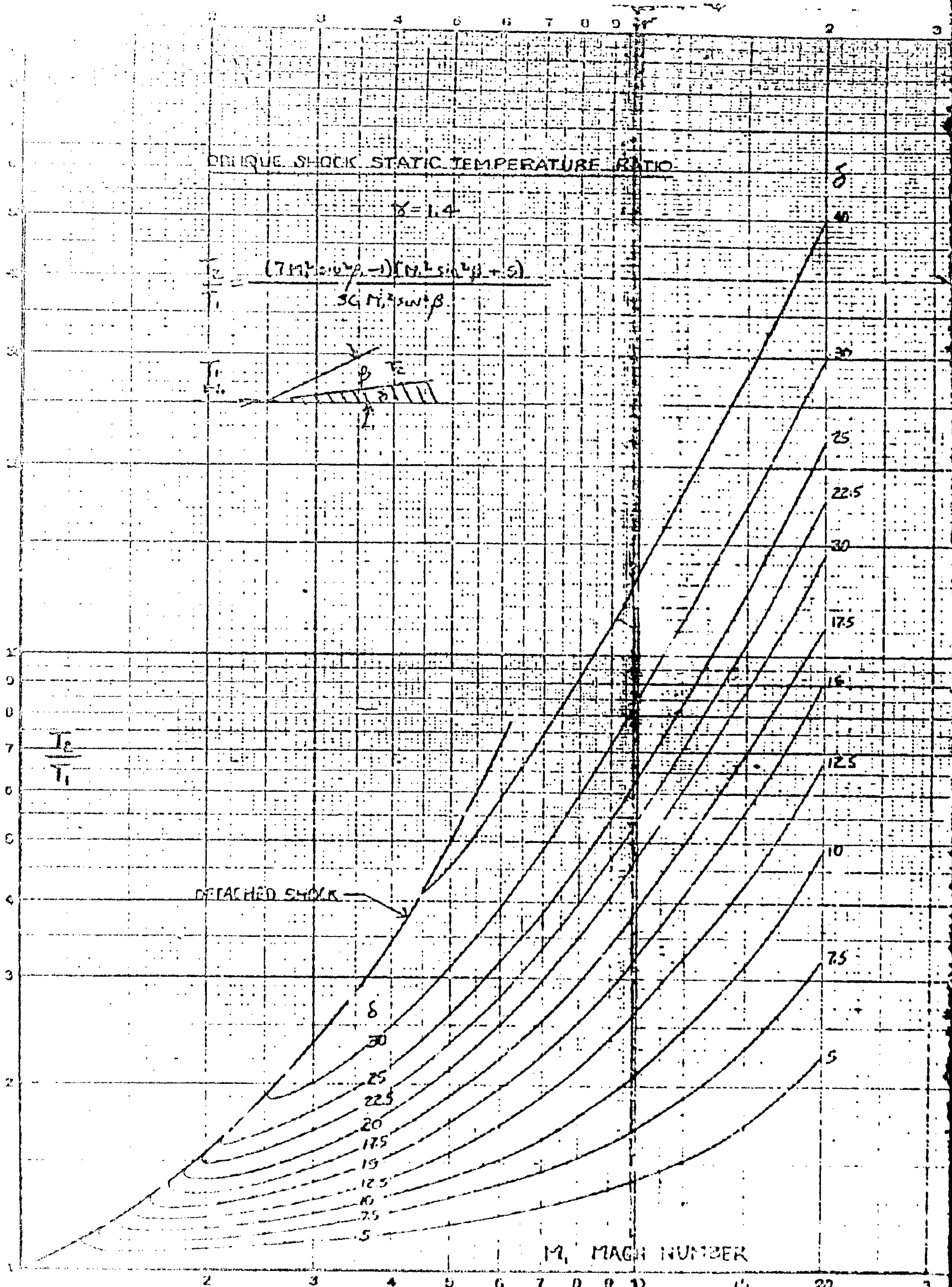

OBLIQUE SHOCK STATIC TEMPERATURE RATIO
$\gamma = 1.4$
$\frac{T_2}{T_1} = \frac{(7M_1^2\sin^2\beta - 1)(M_1^2\sin^2\beta + 5)}{36 M_1^2 \sin^2\beta}$
β
δ
T_1
T_2
$\frac{T_2}{T_1}$
DETACHED SHOCK
δ
40
30
25
22.5
20
17.5
15
12.5
10
7.5
5
M_1 MACH NUMBER

$\frac{T_2}{T_1}$ vs M_1

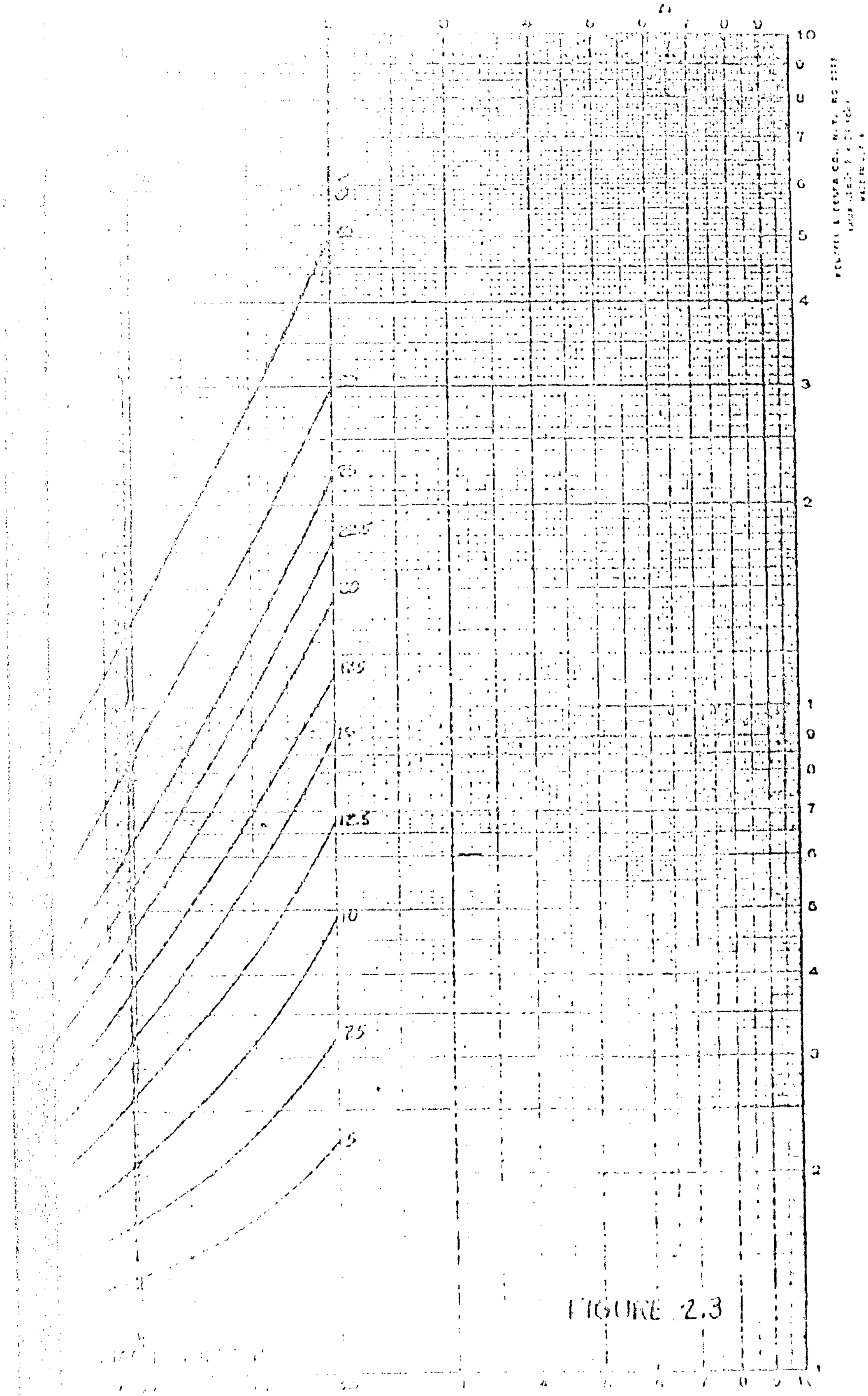

FIGURE 2.3

FIGURE 2.3

B

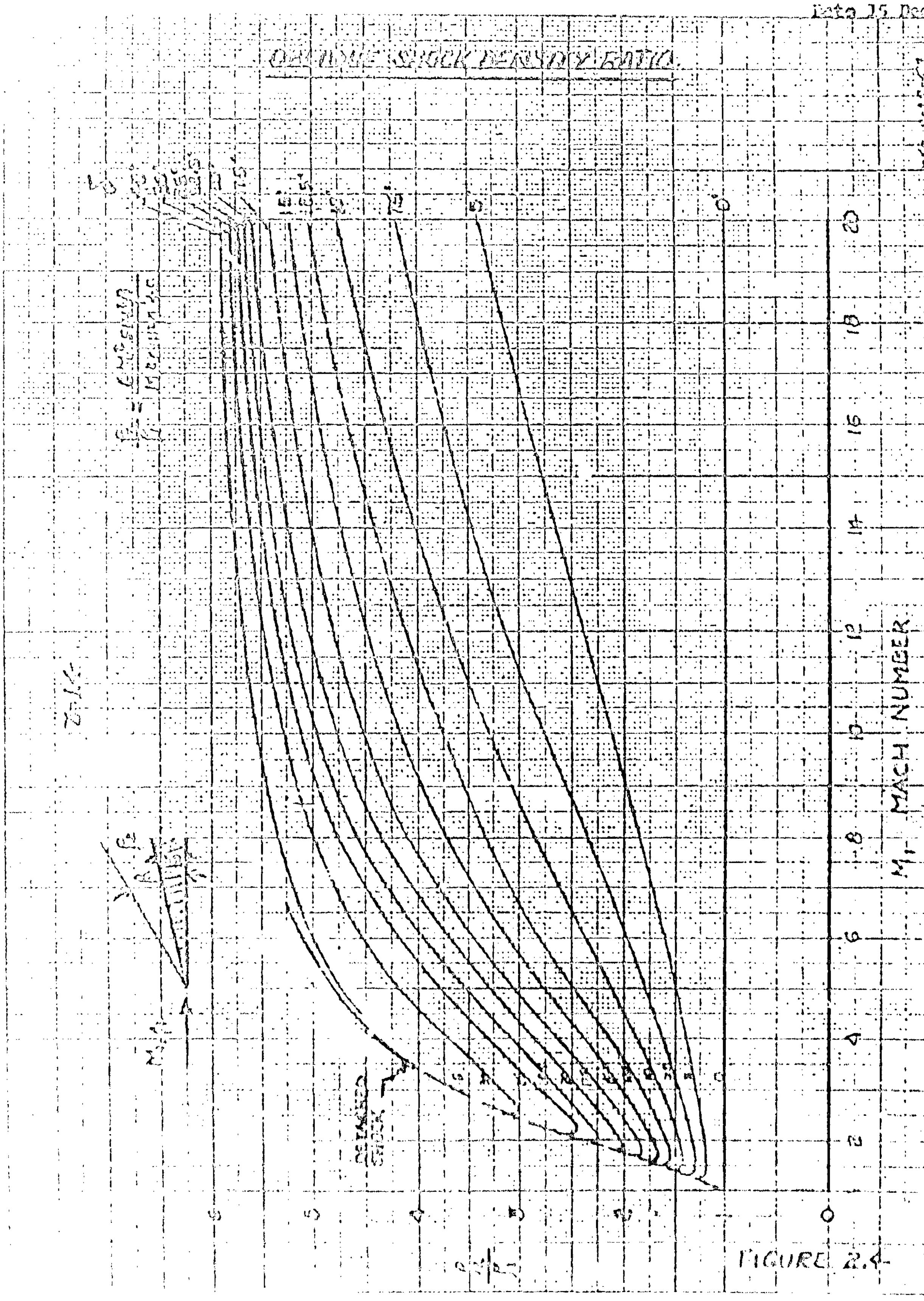

FIGURE 2.4

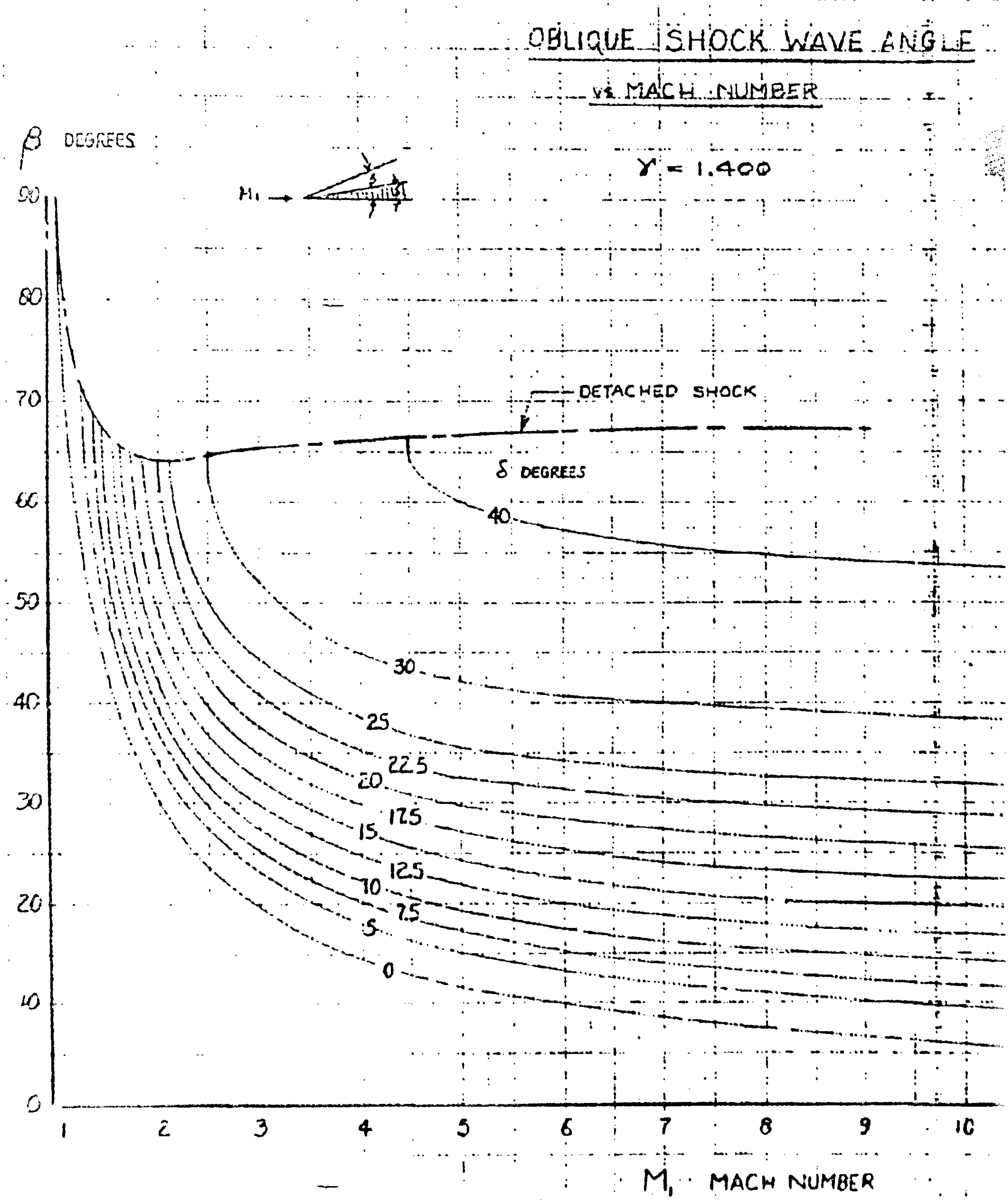

OBLIQUE SHOCK WAVE ANGLE
vs MACH NUMBER
γ = 1.400
β DEGREES
M₁
DETACHED SHOCK
δ DEGREES
40
30
25
22.5
20
17.5
15
12.5
10
7.5
5
0
M₁ MACH NUMBER

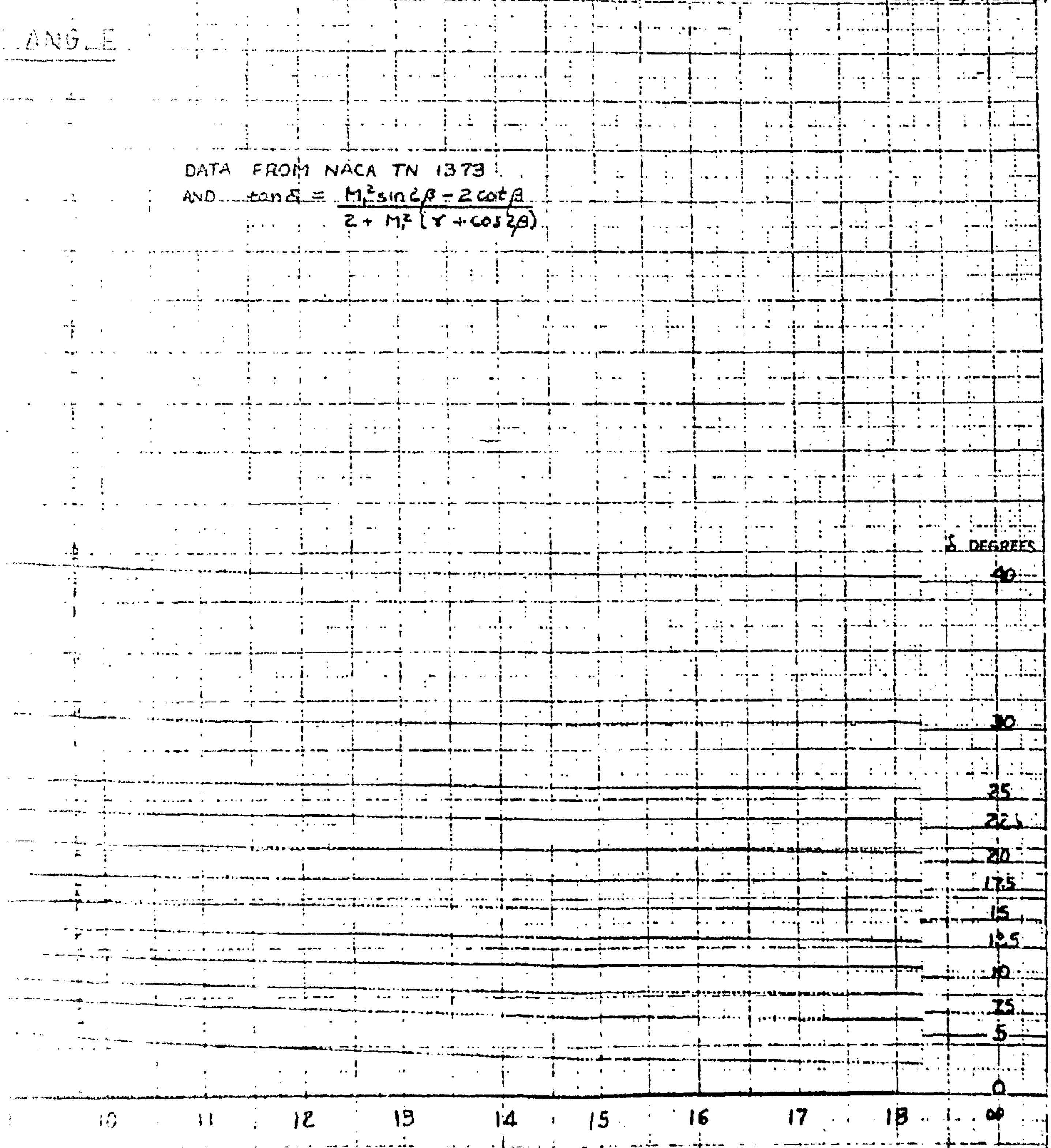

ANGLE
DATA FROM NACA TN 1373
AND $\tan\delta = \dfrac{M_1^2 \sin 2\beta - 2\cot\beta}{2 + M_1^2(\gamma + \cos 2\beta)}$
δ DEGREES
40
30
25
22.5
20
17.5
15
12.5
10
7.5
5
0
10
11
12
13
14
15
16
17
18
∞

FIGURE 2.5

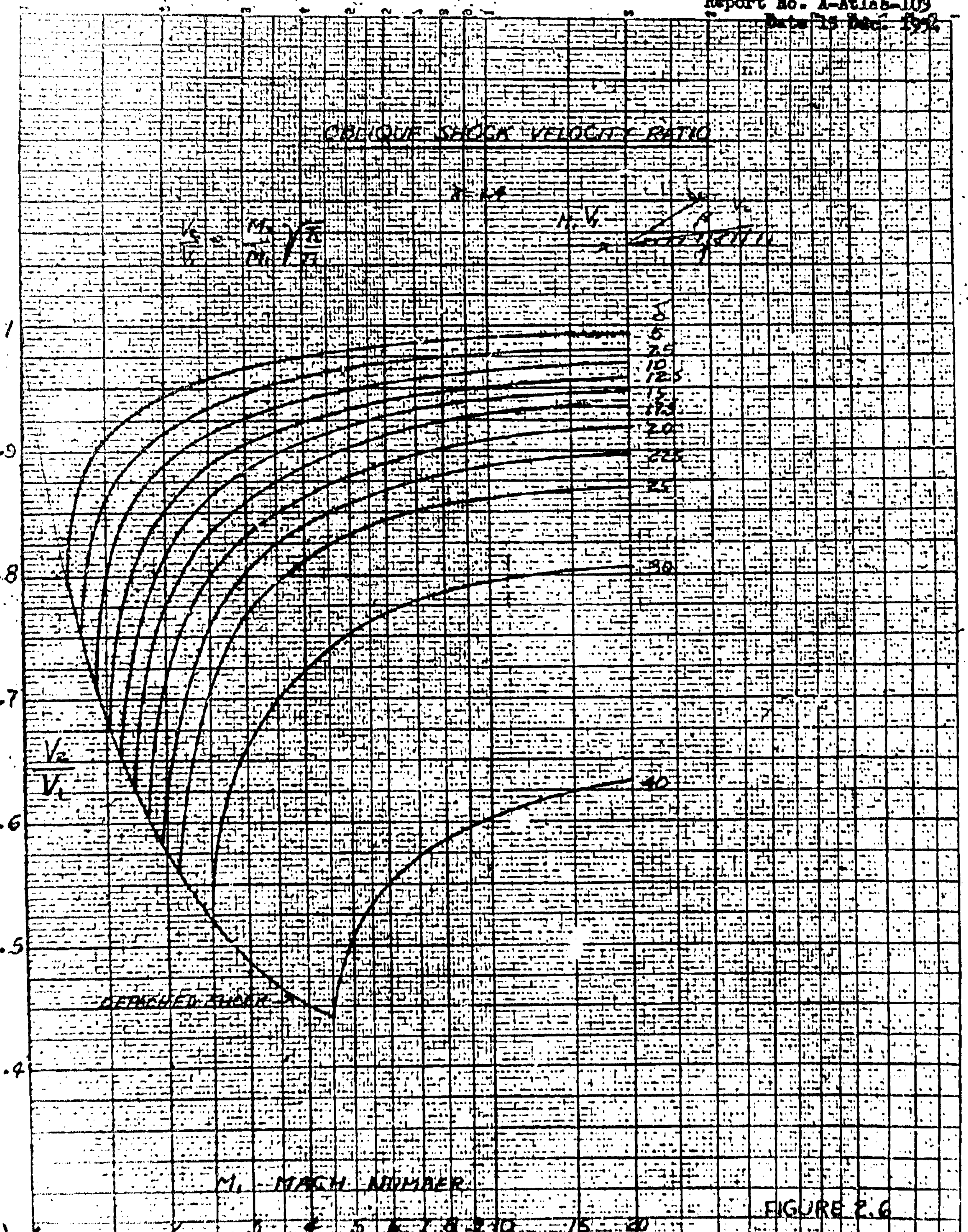
OBLIQUE SHOCK VELOCITY RATIO
δ
5
7.5
10
12.5
15
17.5
20
22.5
25
30
40
DETACHED SHOCK
$\frac{V_2}{V_1}$
1
.9
.8
.7
.6
.5
.4
M₁ MACH NUMBER
1
2
3
4
5
6
7
8
9
10
15
20

FIGURE 2.6

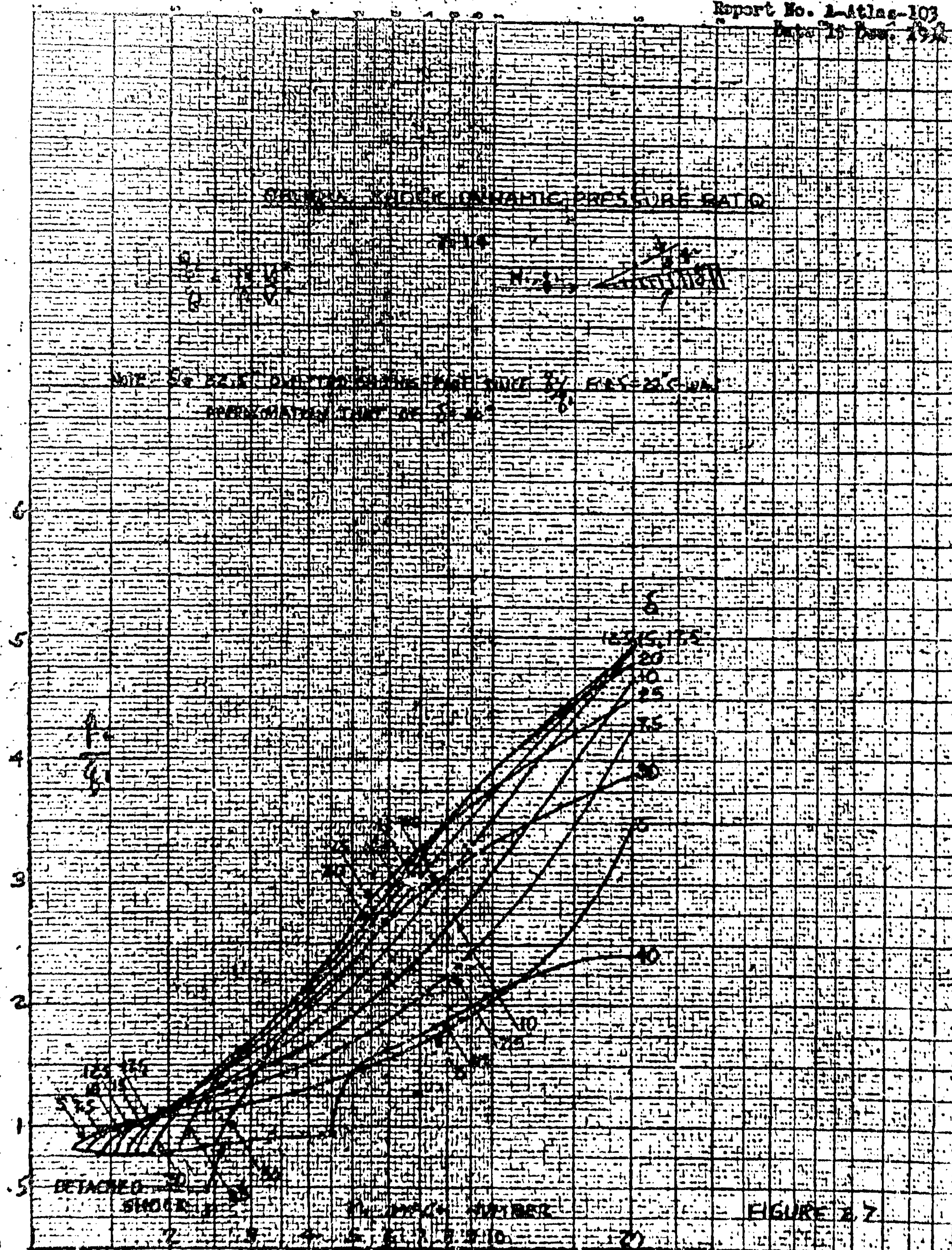
OBLIQUE SHOCK DYNAMIC PRESSURE RATIO
δ
12.5 15 17.5
20
10
25
7.5
30
35
40
10
DETACHED SHOCK
MACH NUMBER
2
3
4
5
6
7
8
9
10
20
1
2
3
4
5
6

FIGURE 2.7

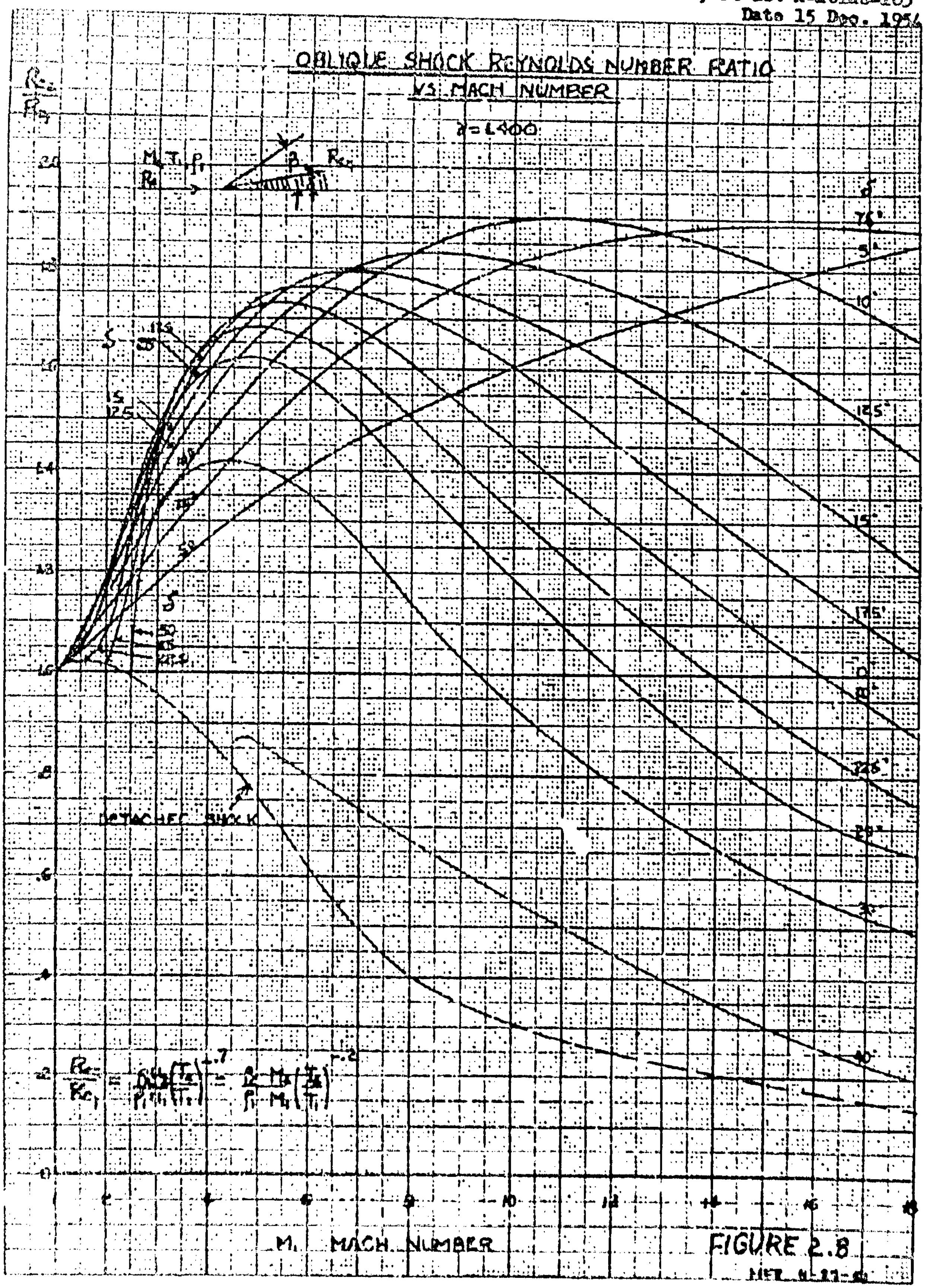
OBLIQUE SHOCK REYNOLDS NUMBER RATIO
VS MACH NUMBER
$\gamma = 1.400$
$\frac{R_{e_2}}{R_{e_1}}$
DETACHED SHOCK
$\frac{R_{e_2}}{R_{e_1}} = \frac{\rho_2 u_2}{\rho_1 u_1}\left(\frac{T_2}{T_1}\right)^{-.7} = \frac{\rho_2}{\rho_1}\frac{M_2}{M_1}\left(\frac{T_2}{T_1}\right)^{.2}$
M_1 MACH NUMBER
FIGURE 2.8

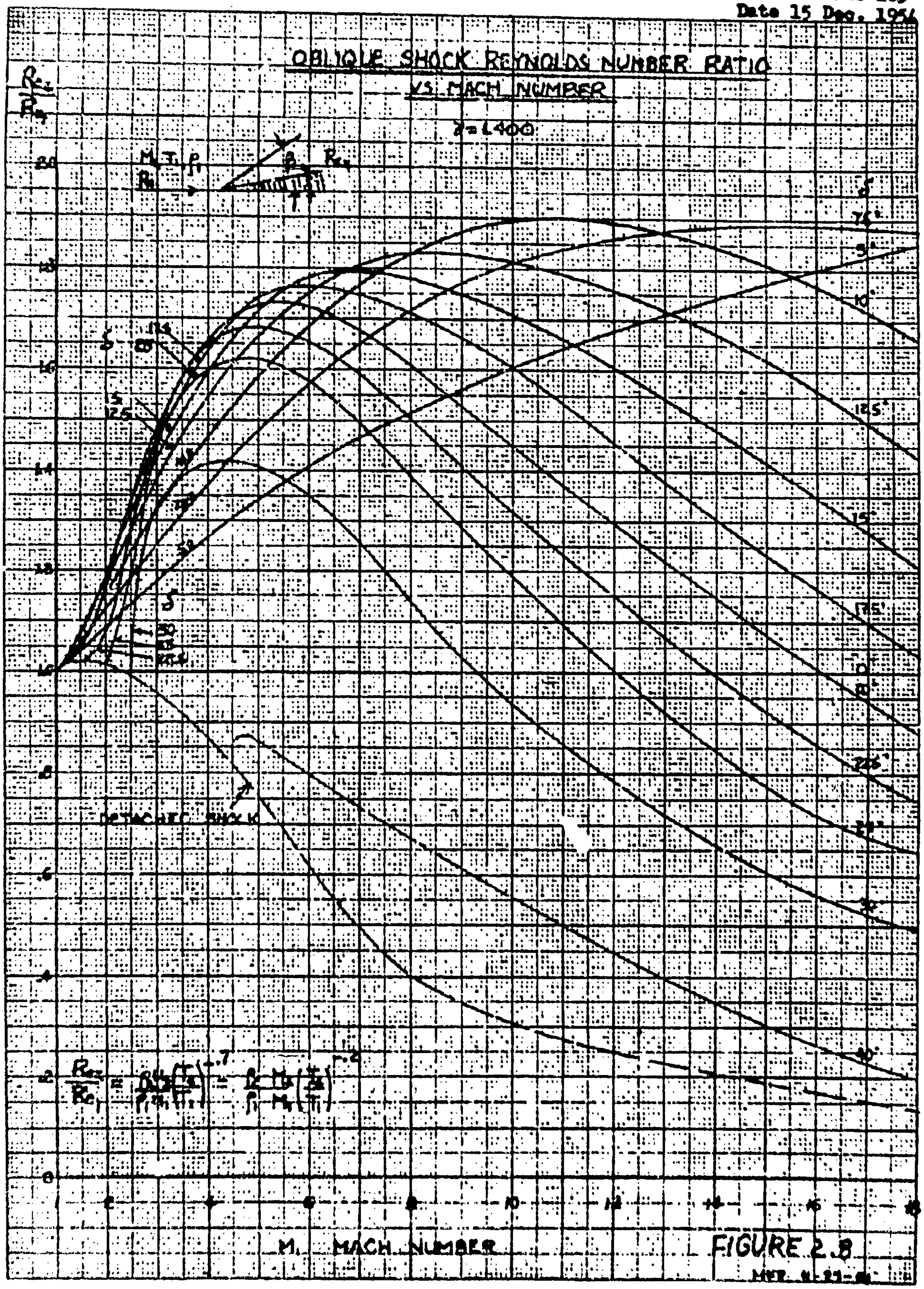
OBLIQUE SHOCK REYNOLDS NUMBER RATIO
VS MACH NUMBER
γ = 1.400
DETACHED SHOCK
M, MACH NUMBER

FIGURE 2.8

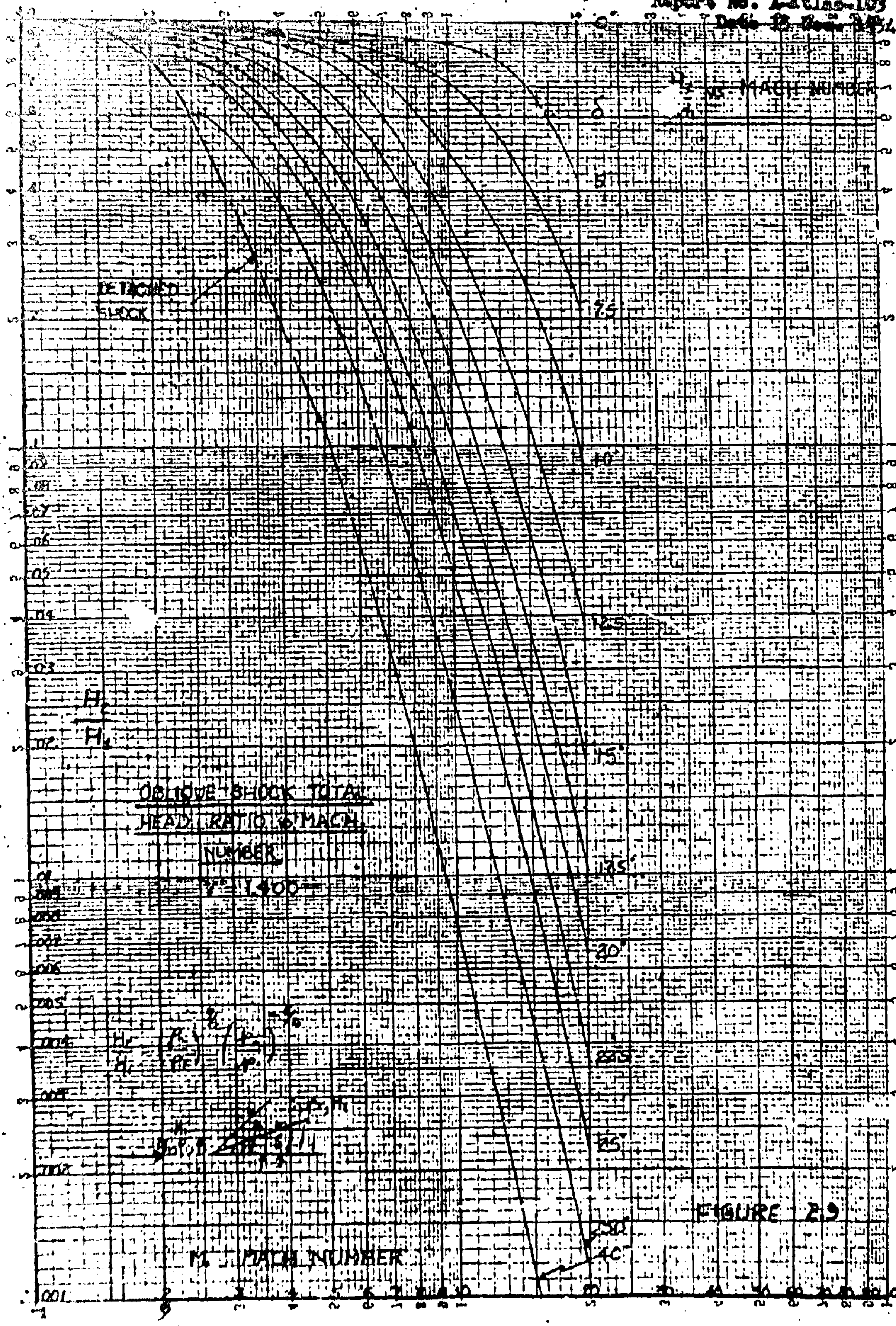
$\frac{H_2}{H_1}$ VS MACH NUMBER
DETACHED SHOCK
$\frac{H_2}{H_1}$
OBLIQUE SHOCK TOTAL HEAD RATIO vs MACH NUMBER
γ = 1.400
M - MACH NUMBER

FIGURE 29

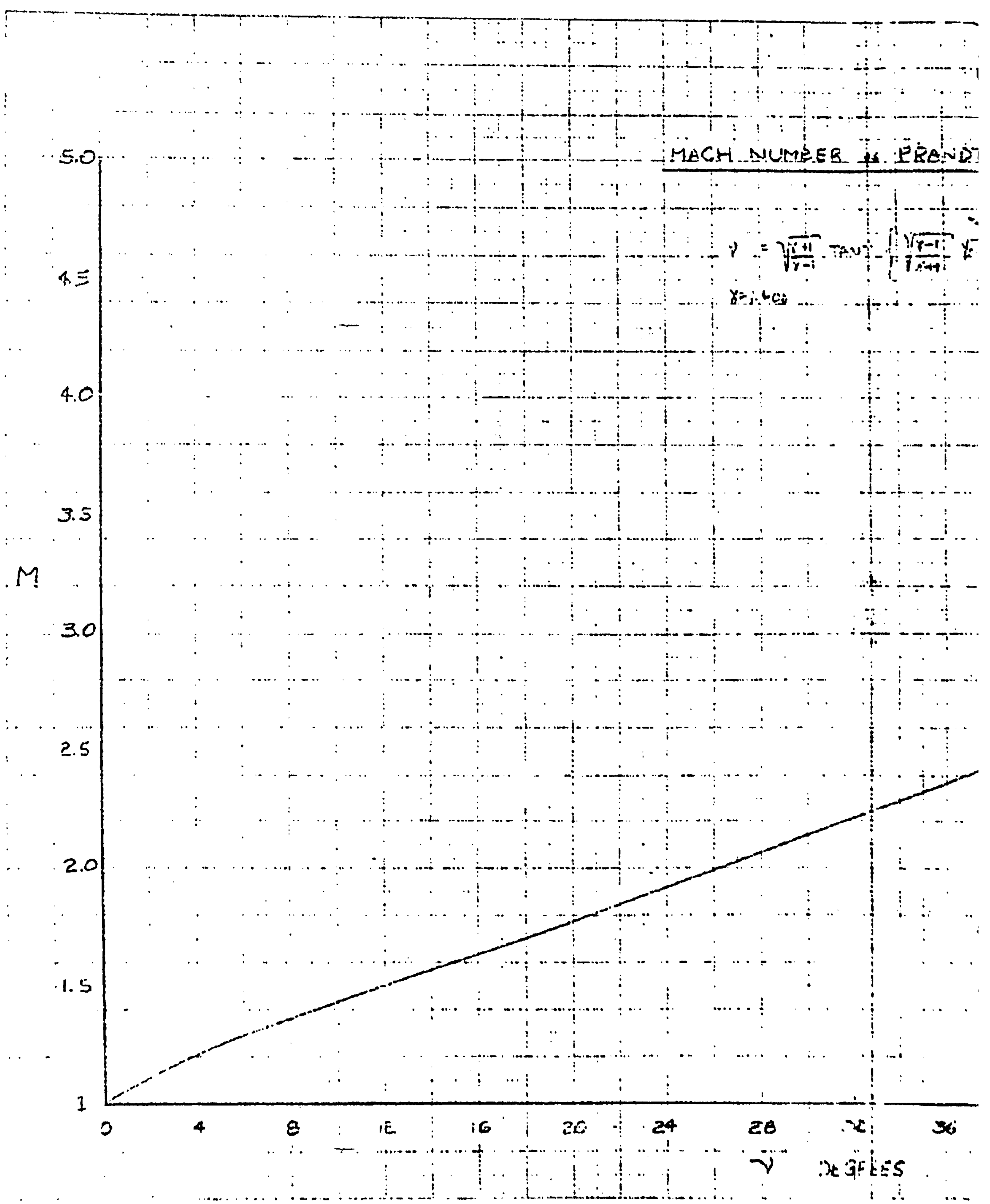
MACH NUMBER vs PRAND
M
5.0
4.5
4.0
3.5
3.0
2.5
2.0
1.5
1
0
4
8
16
20
24
28
36
ν DEGREES
γ = 1.40
A

M vs ν

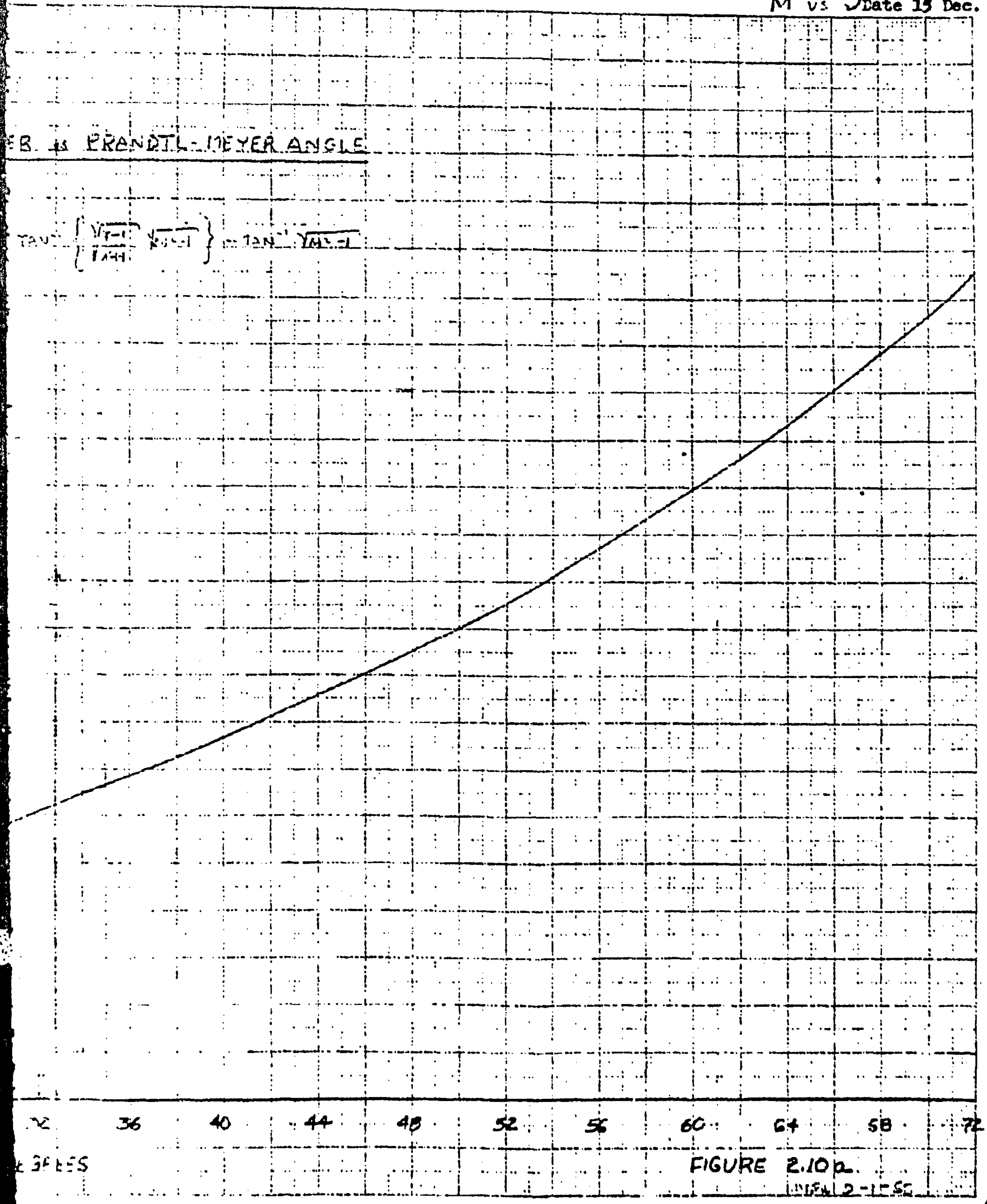

FIGURE 2.10 b.

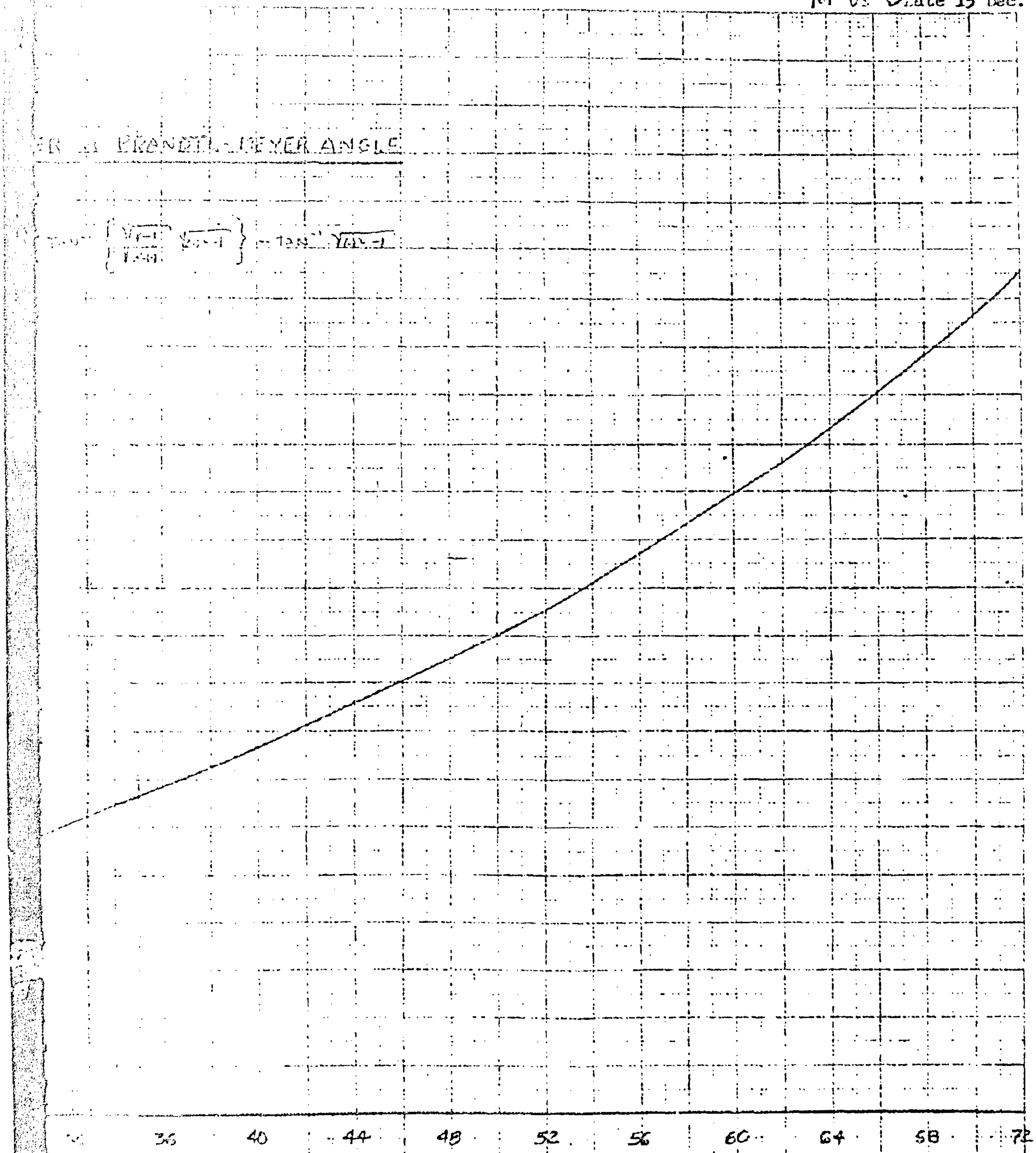

FIGURE 2.10p.

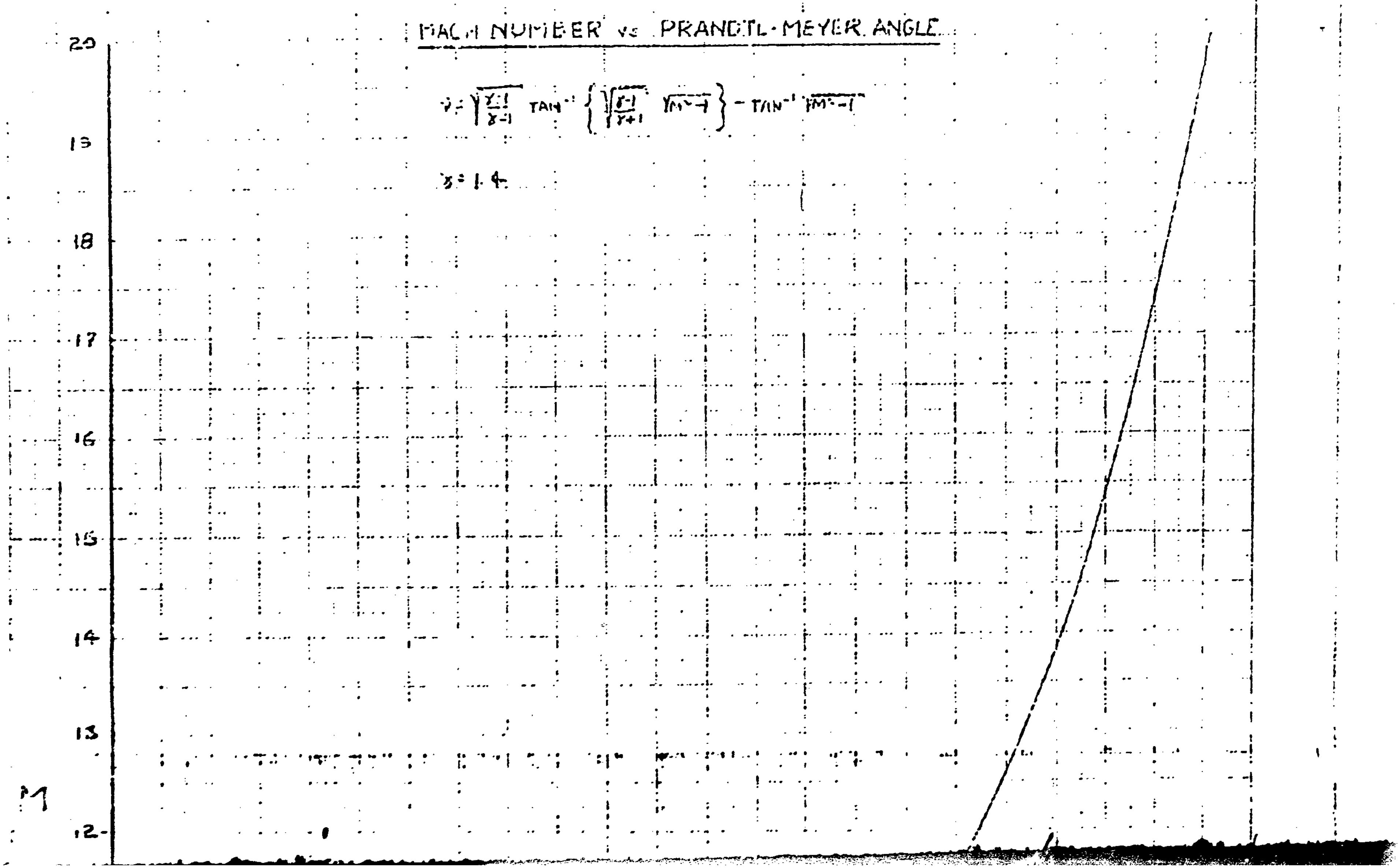
MACH NUMBER vs PRANDTL-MEYER ANGLE
$\nu = \sqrt{\frac{\gamma+1}{\gamma-1}} \tan^{-1}\left\{\sqrt{\frac{\gamma-1}{\gamma+1}}\sqrt{M^2-1}\right\} - \tan^{-1}\sqrt{M^2-1}$
$\gamma = 1.4$
20
19
18
17
16
15
14
13
12
M

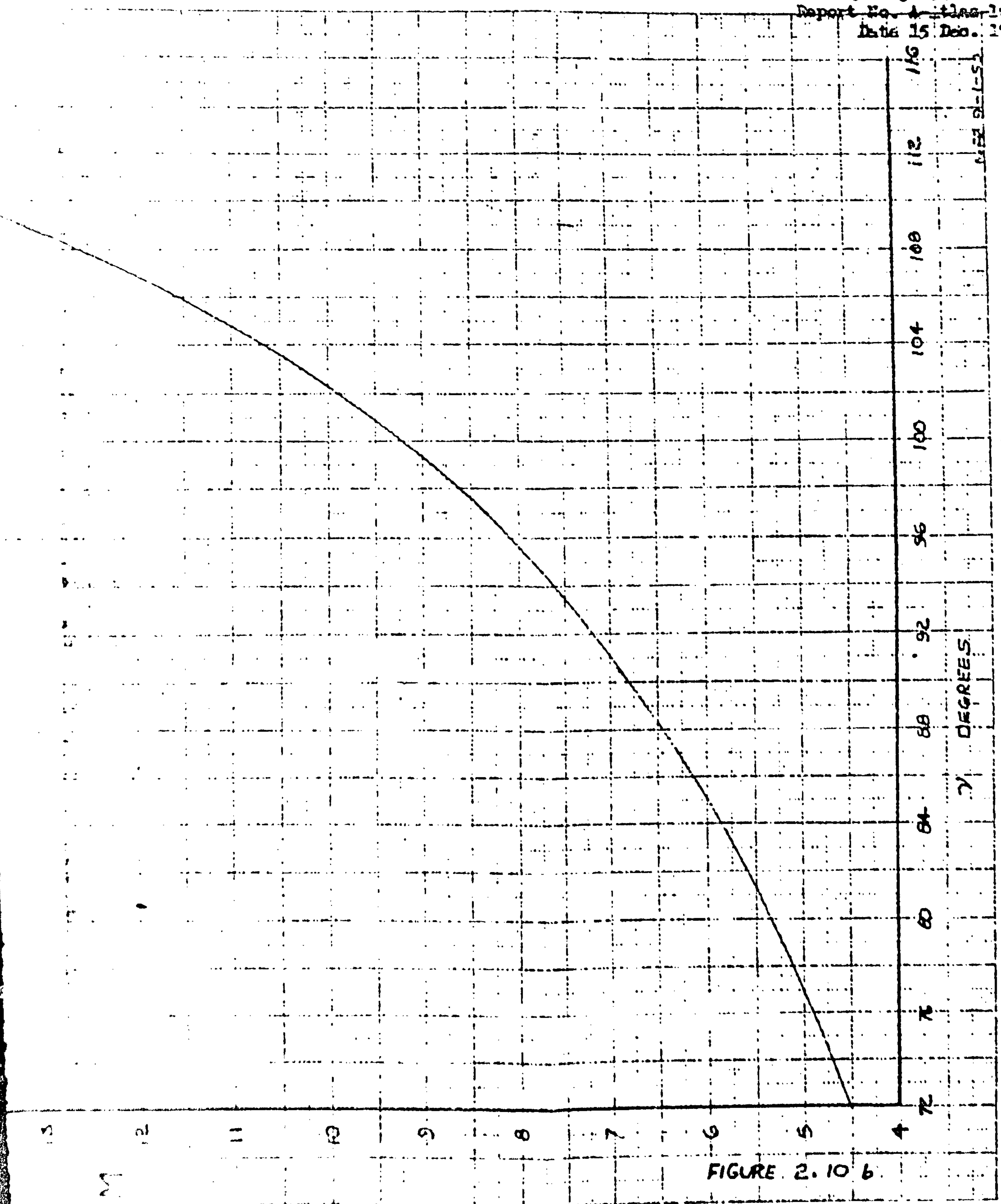

FIGURE 2.10 b

B

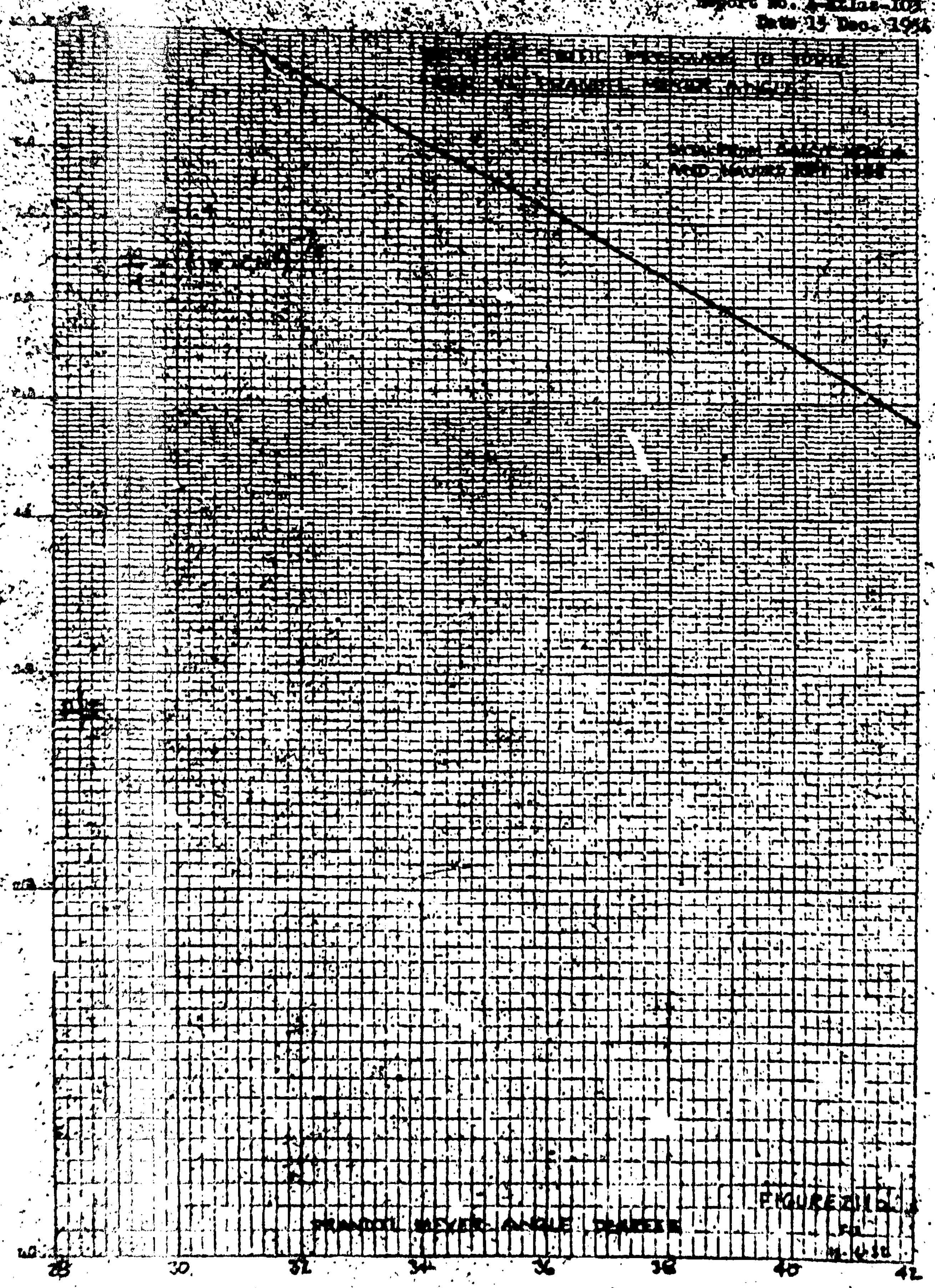
28
30
32
34
36
38
40
42

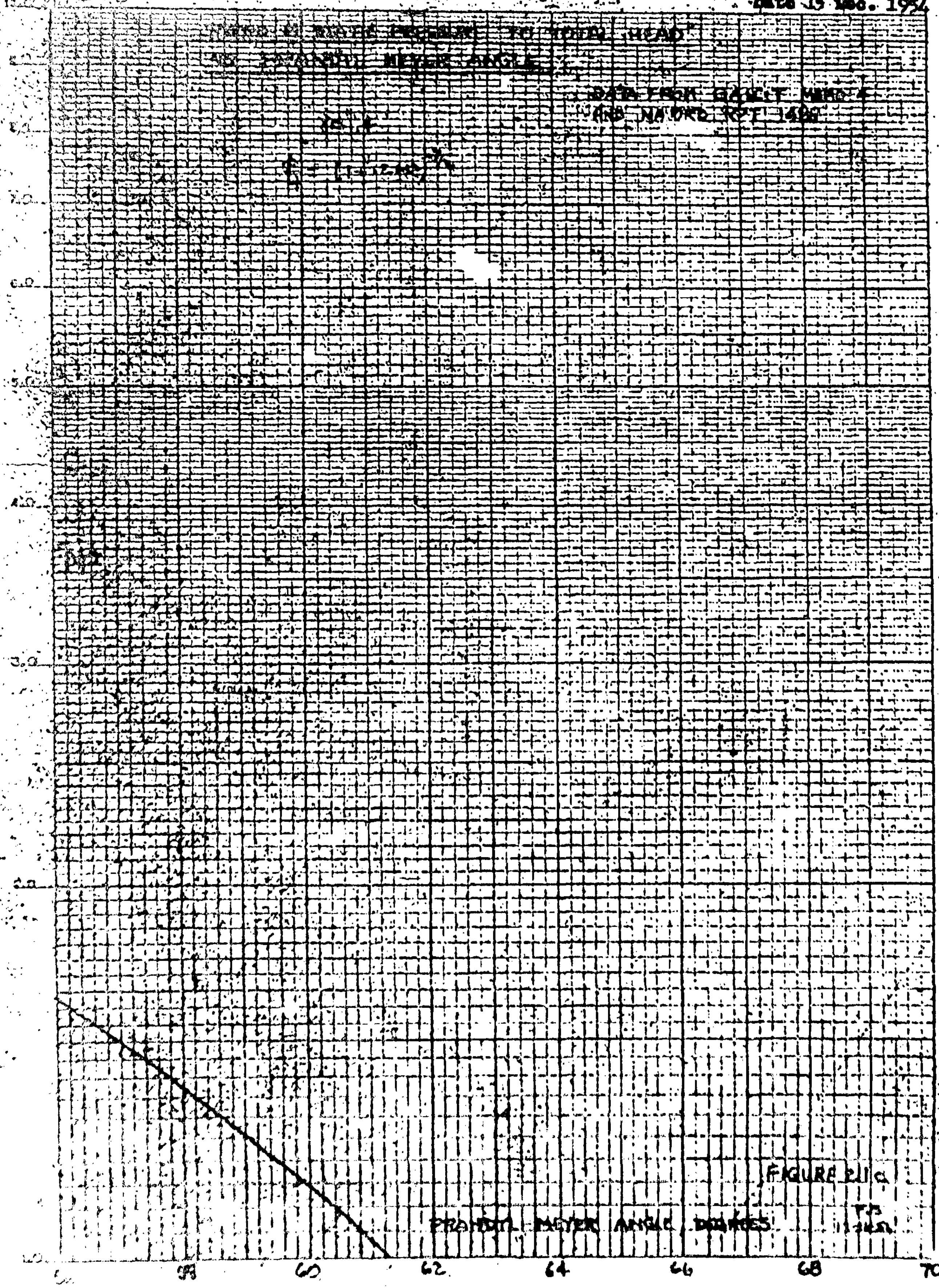
HEAD
METER ANGLE
PRANDTL METER ANGLE DEGREES
6.0
5.0
4.0
3.0
2.0
60
62
64
66
68
70

FIGURE 21a

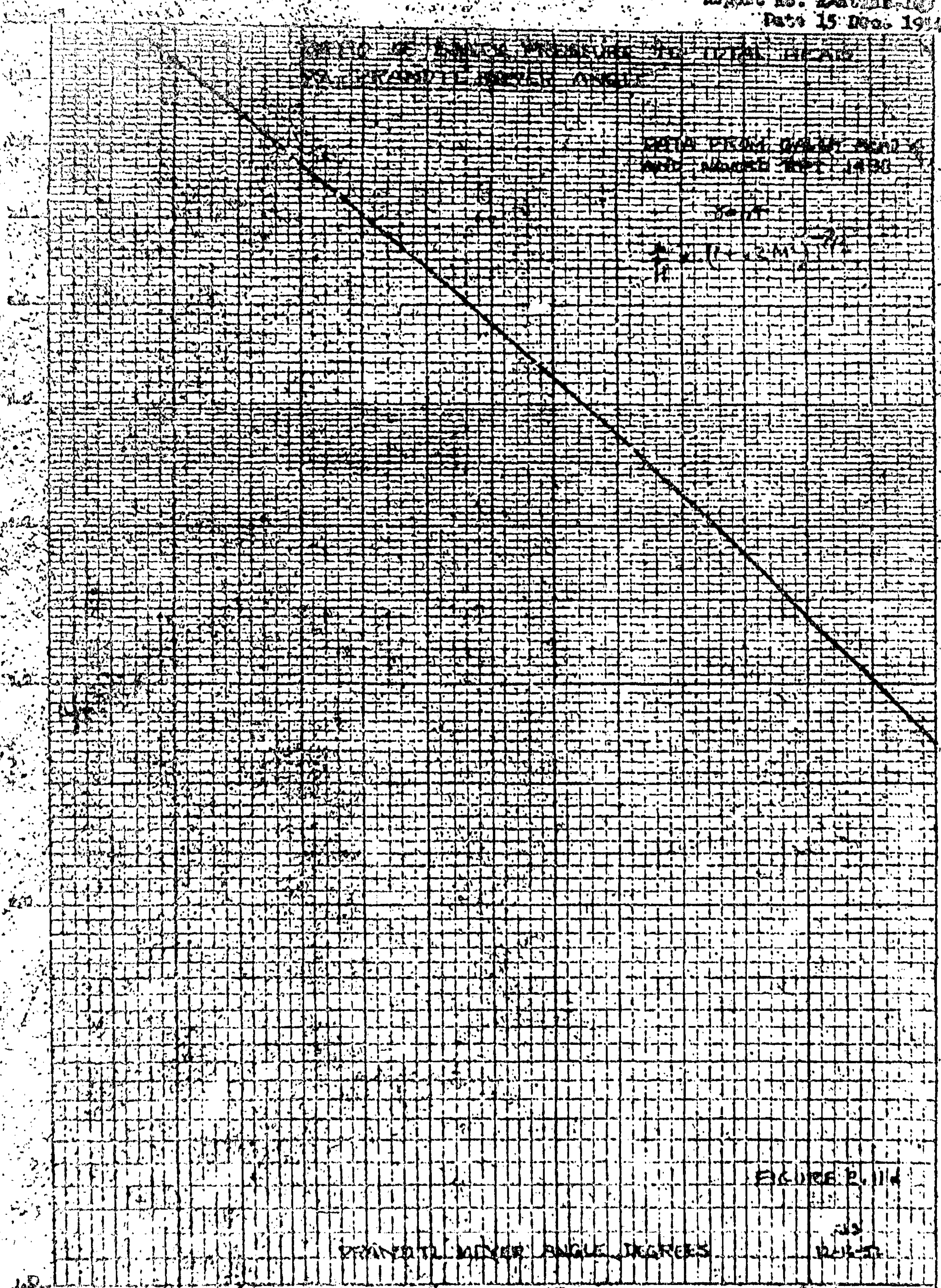
RATIO OF [illegible] PRESSURE TO TOTAL HEAD
VS. PRANDTL MEYER ANGLE
DATA FROM [illegible]
AND [illegible] 1490
FIGURE 2.114
PRANDTL MEYER ANGLE DEGREES
60
62
64
66
68
70
72
74

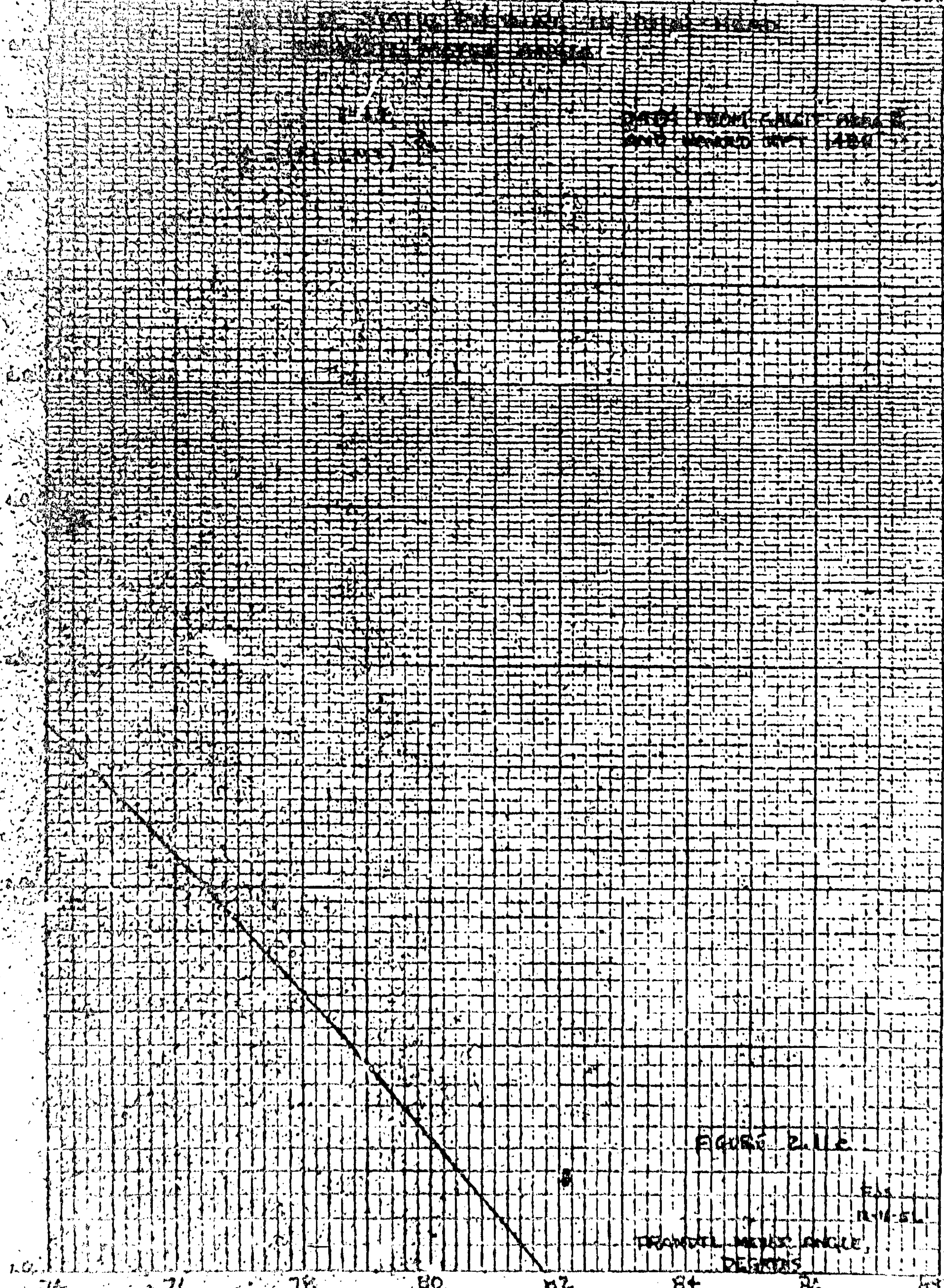
1.0
2.0
4.0
74
76
78
80
82
84
86
88
FIGURE 2.11c
PRANDTL MEYER ANGLE,
DEGREES

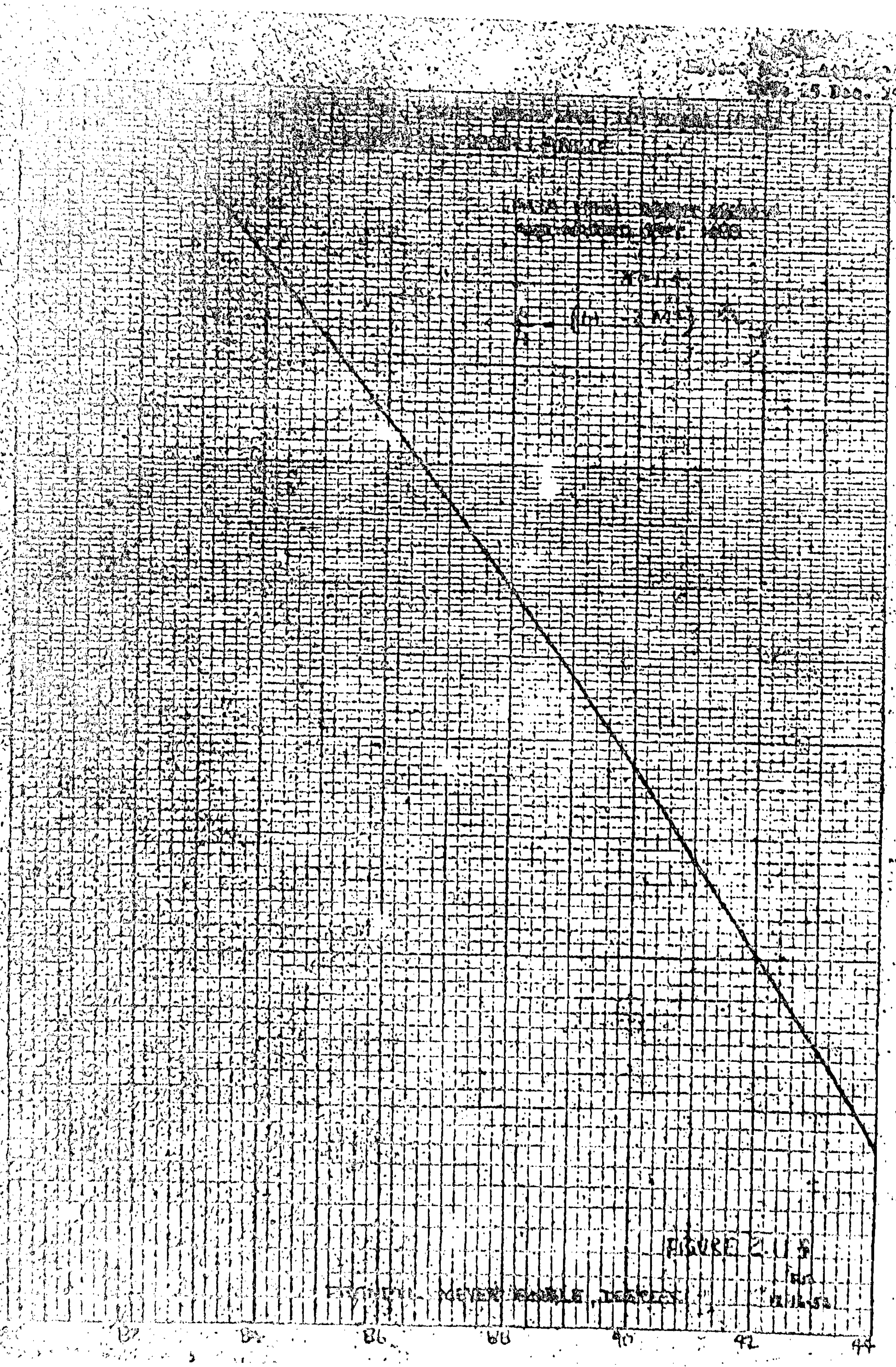

FIGURE 2.11.5

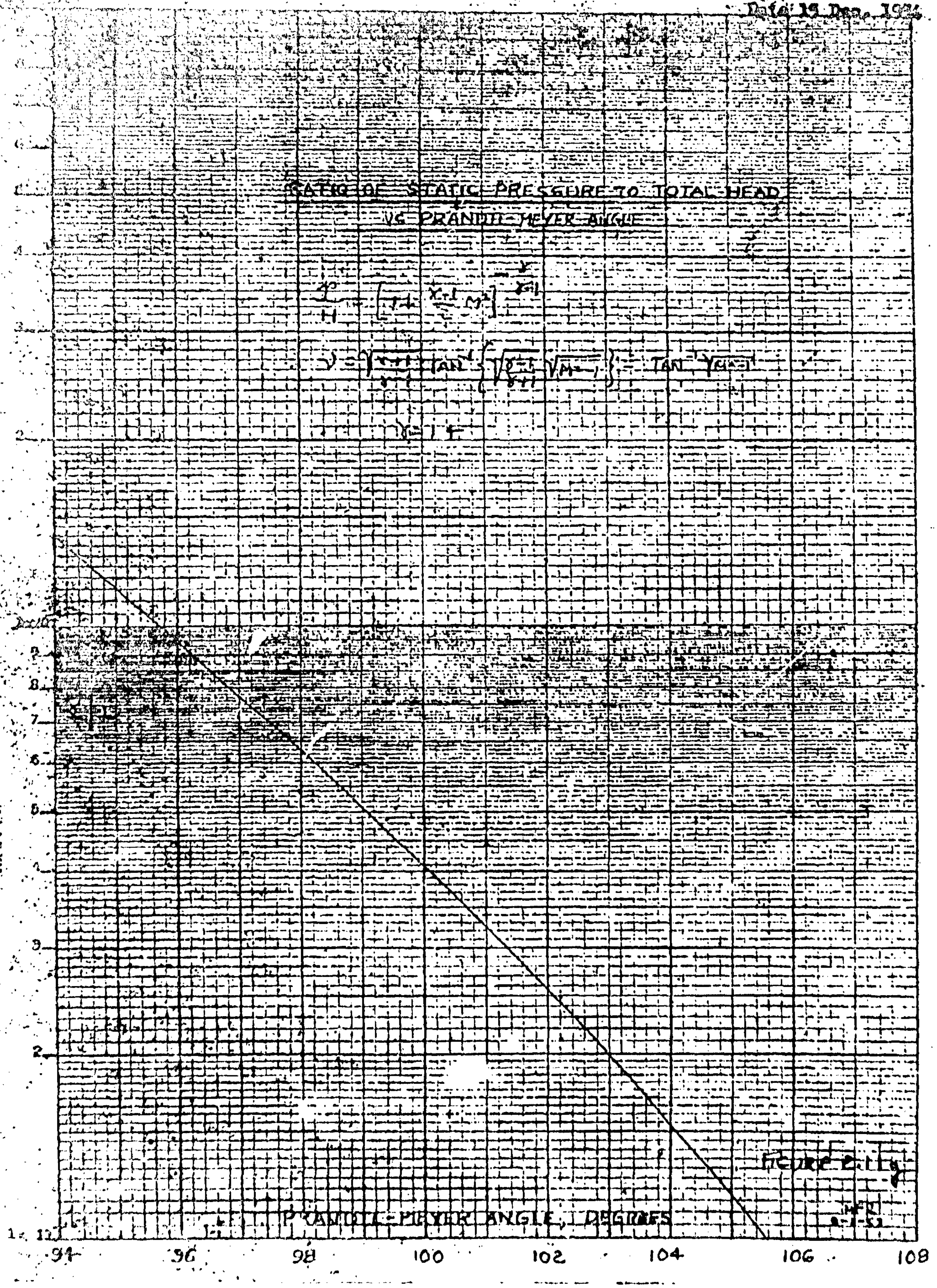
RATIO OF STATIC PRESSURE TO TOTAL HEAD
VS PRANDTL-MEYER ANGLE
$\frac{p}{H} = \left[1 + \frac{\gamma-1}{2} M^2\right]^{-\frac{\gamma}{\gamma-1}}$
$\nu = \sqrt{\frac{\gamma+1}{\gamma-1}} \tan^{-1}\left\{\sqrt{\frac{\gamma-1}{\gamma+1}}\sqrt{M^2-1}\right\} - \tan^{-1}\sqrt{M^2-1}$
$\gamma = 1.4$
PRANDTL-MEYER ANGLE, DEGREES
94
96
98
100
102
104
106
108

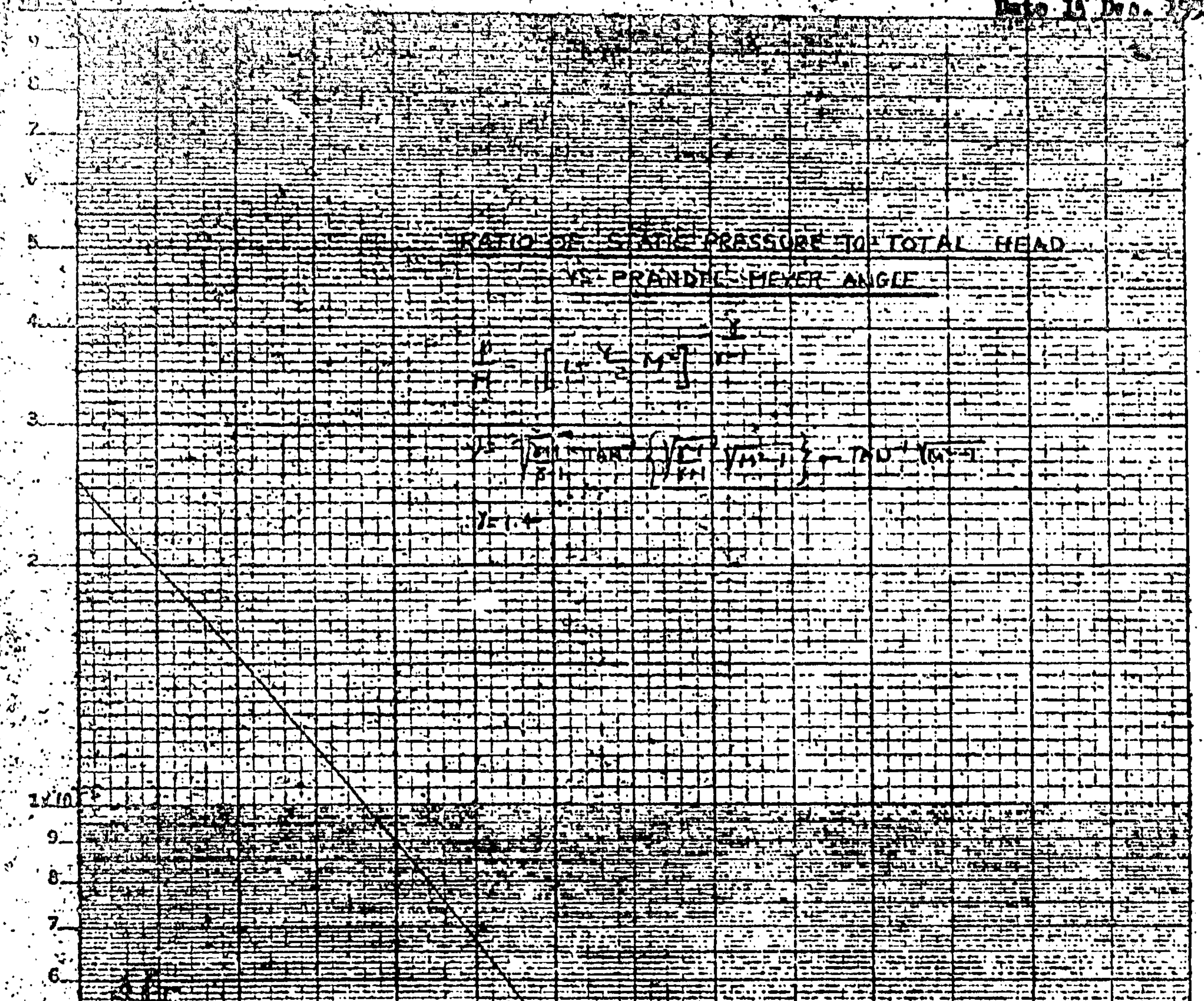
RATIO OF STATIC PRESSURE TO TOTAL HEAD
VS PRANDTL-MEYER ANGLE
PRANDTL-MEYER ANGLE, DEGREES
102
104
106
108
110
112
114
116
1 x 10
9
8
7
6
5
4
3
2
FIGURE

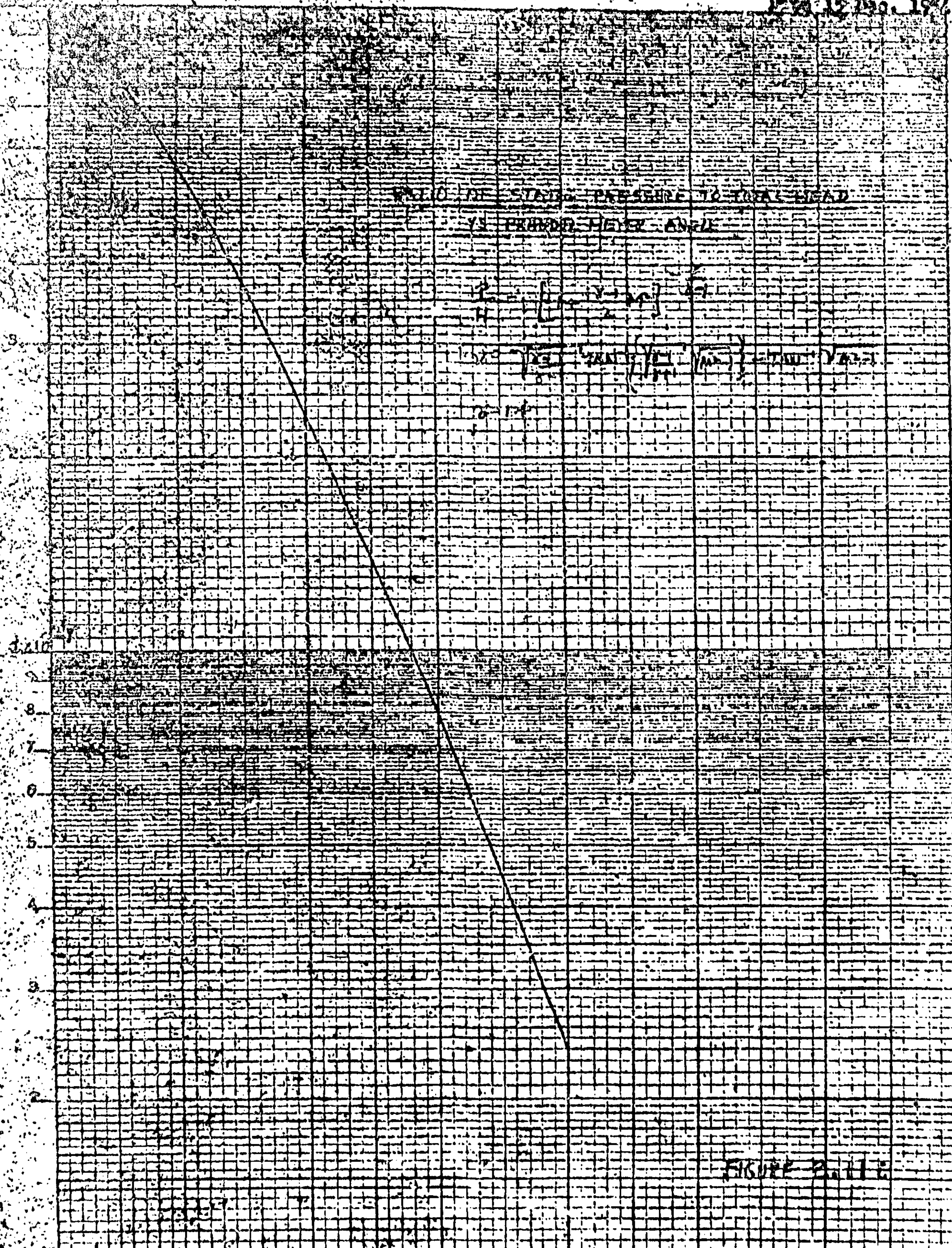
RATIO OF STATIC PRESSURE TO TOTAL HEAD
VS PRANDTL MEYER ANGLE
γ = 1.4
FIGURE
PRANDTL-MEYER ANGLE, DEGREES
112
114
116
118
120
122

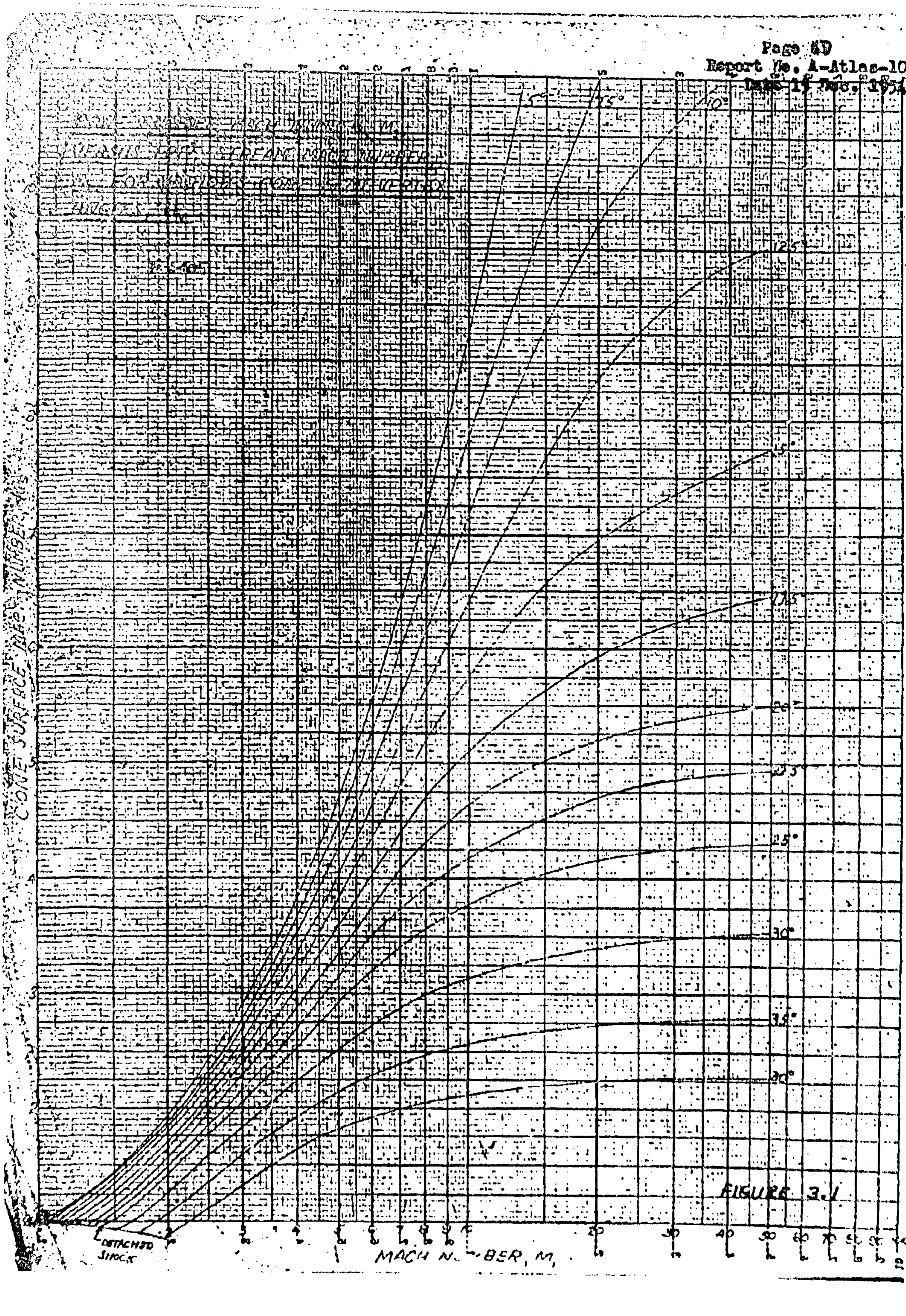
CONE SURFACE MACH NUMBER, M_s
MACH N BER, M_1
DETACHED SHOCK
5°
7.5°
10°
12.5°
15°
17.5°
20°
22.5°
25°
30°
35°
40°

FIGURE 3.1

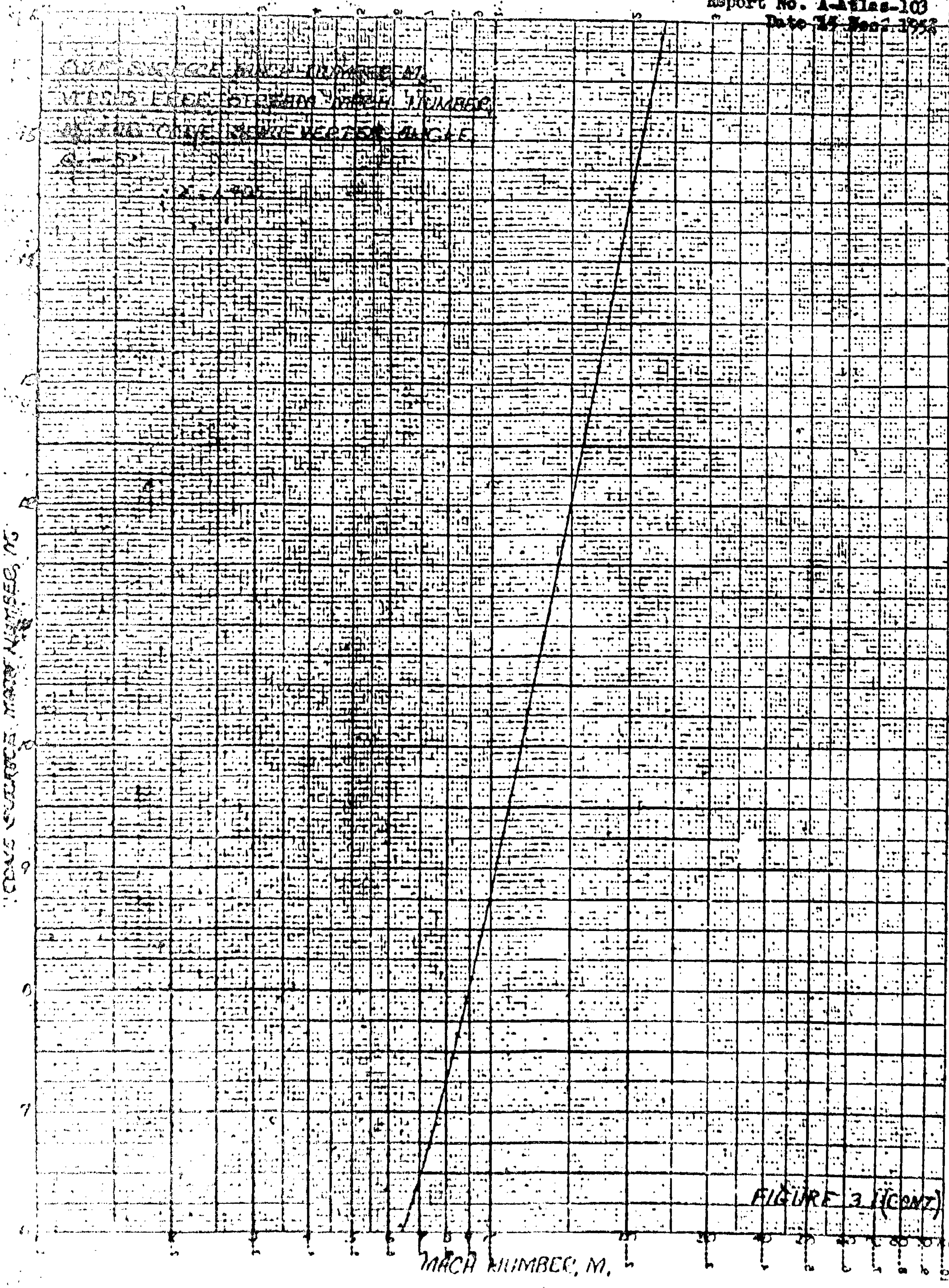

FIGURE 3 (CONT)

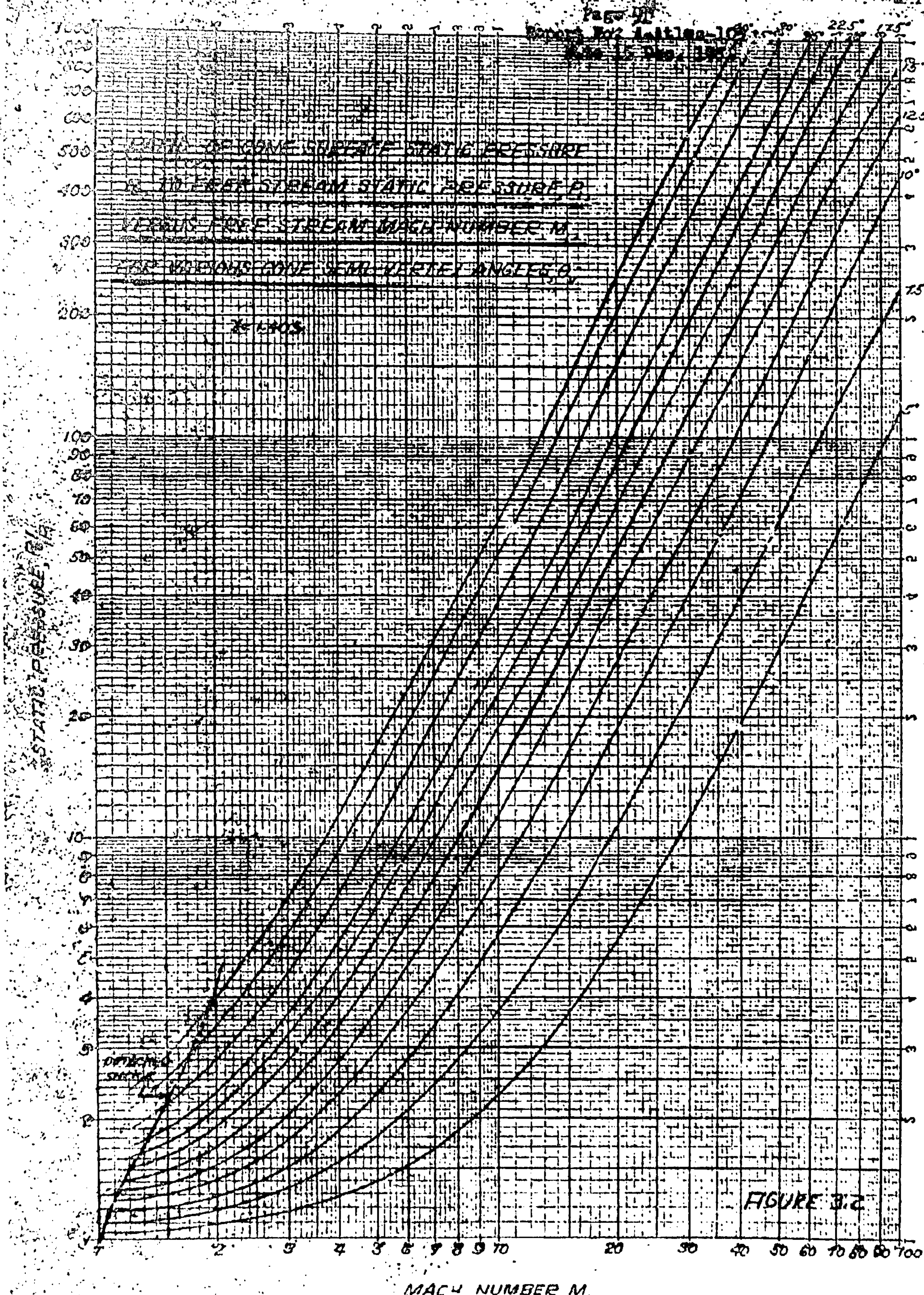
RATIO OF CONE SURFACE STATIC PRESSURE
TO FREE STREAM STATIC PRESSURE
VERSUS FREE STREAM MACH NUMBER M_1
FOR VARIOUS CONE SEMI-VERTEX ANGLES
$\gamma = 1.405$
22.5°
17.5°
12.5°
10°
7.5°
5°
DETACHED SHOCK
STATIC PRESSURE
MACH NUMBER, M_1

FIGURE 3.2

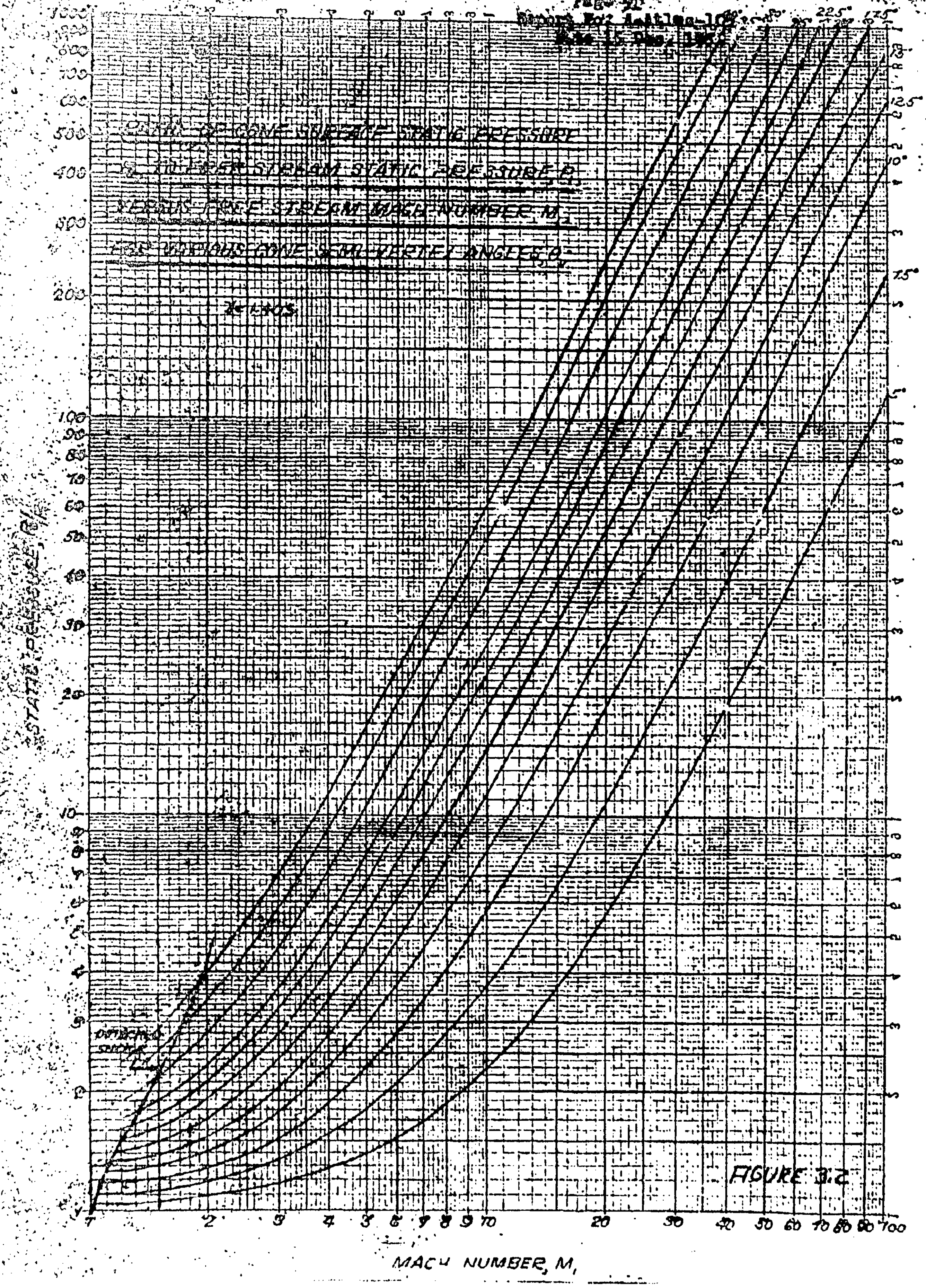
RATIO OF CONE SURFACE STATIC PRESSURE
TO FREE STREAM STATIC PRESSURE
VERSUS FREE STREAM MACH NUMBER M_1
FOR VARIOUS CONE SEMI-VERTEX ANGLES
γ = 1.405
22.5°
17.5°
12.5°
10°
7.5°
5°
DETACHED SHOCK
STATIC PRESSURE RATIO
MACH NUMBER, M_1

FIGURE 3.2

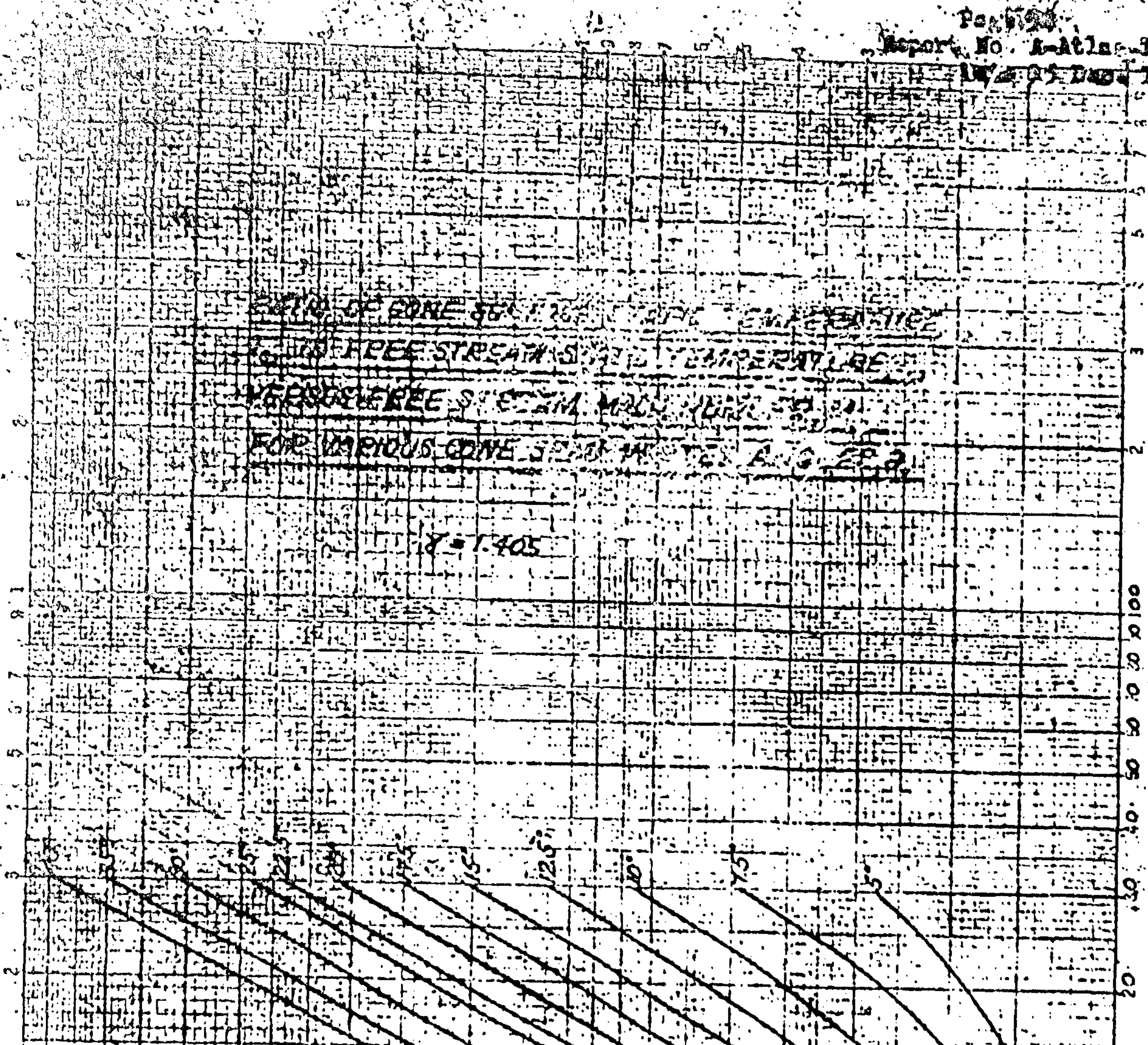

FIGURE 33

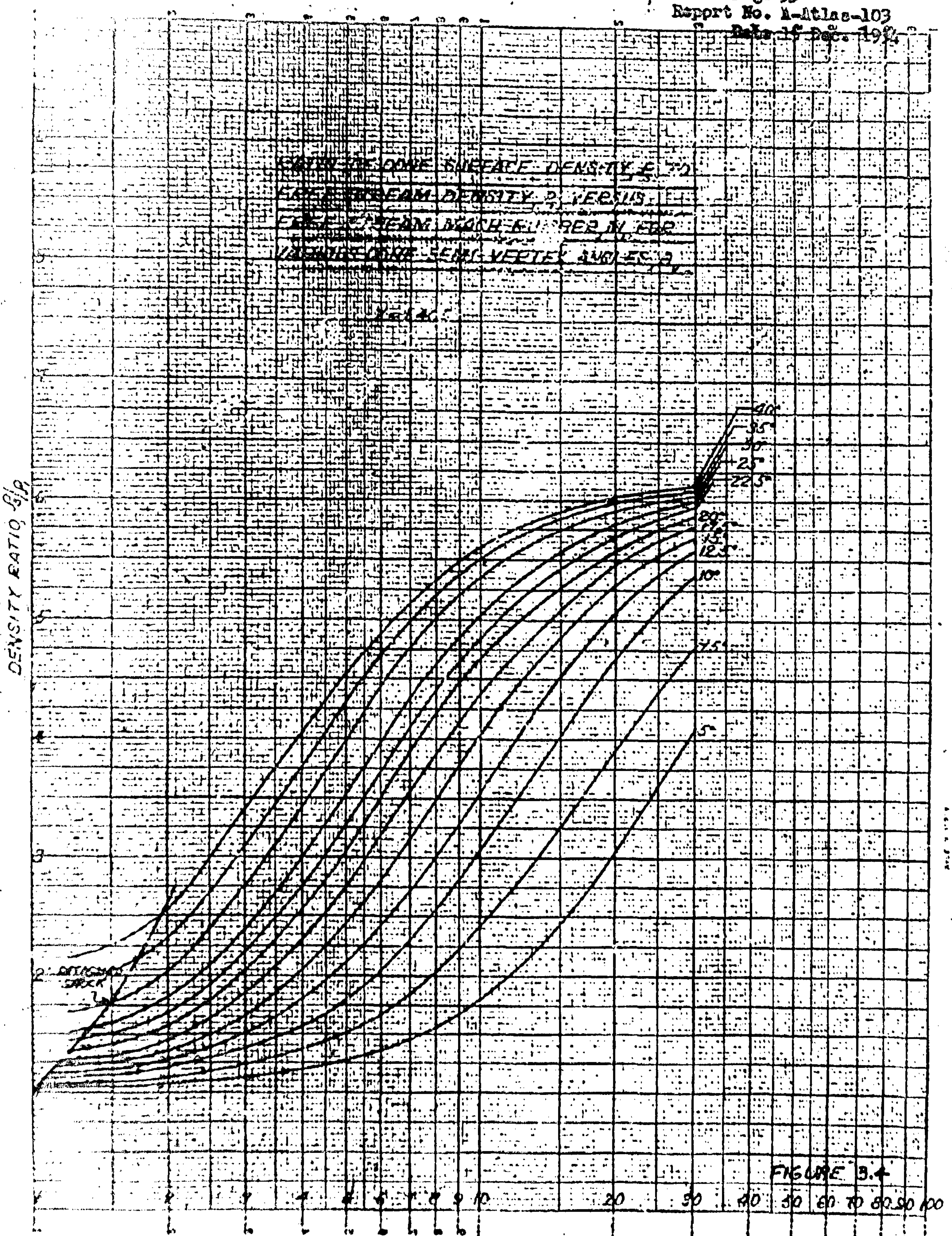
RATIO OF CONE SURFACE DENSITY TO
FREE STREAM DENSITY VERSUS
FREE STREAM MACH NUMBER M FOR
VARIOUS CONE SEMI-VERTEX ANGLES
γ=1.40
40°
35°
30°
25°
22.5°
20°
17.5°
15°
12.5°
10°
7.5°
5°
DETACHED SHOCK
DENSITY RATIO ρs/ρ
1
2
3
4
5
6
7
8
9
10
20
30
40
50
60
70
80
90
100
MACH NUMBER, M
FIGURE B.4

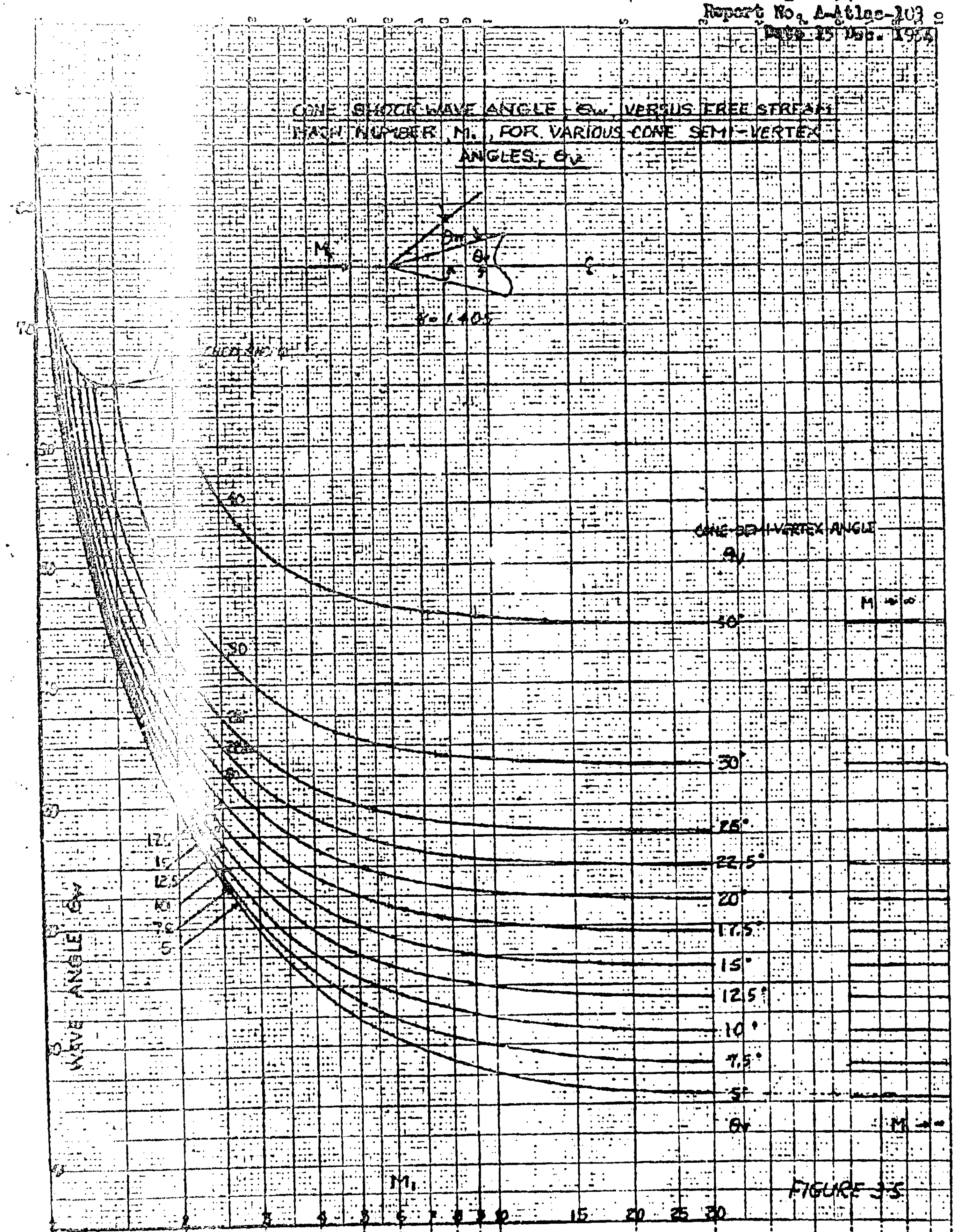
CONE SHOCK WAVE ANGLE, θw VERSUS FREE STREAM MACH NUMBER, M1, FOR VARIOUS CONE SEMI-VERTEX ANGLES, θv
M1
θw
θv
℄
γ = 1.405
CONE SEMI-VERTEX ANGLE
θv
M → ∞
40°
30°
25°
22.5°
20°
17.5°
15°
12.5°
10°
7.5°
5°
WAVE ANGLE θw
M1
1.5
2
3
4
5
6
7
8
9
10
15
20
25
30
70

FIGURE 35

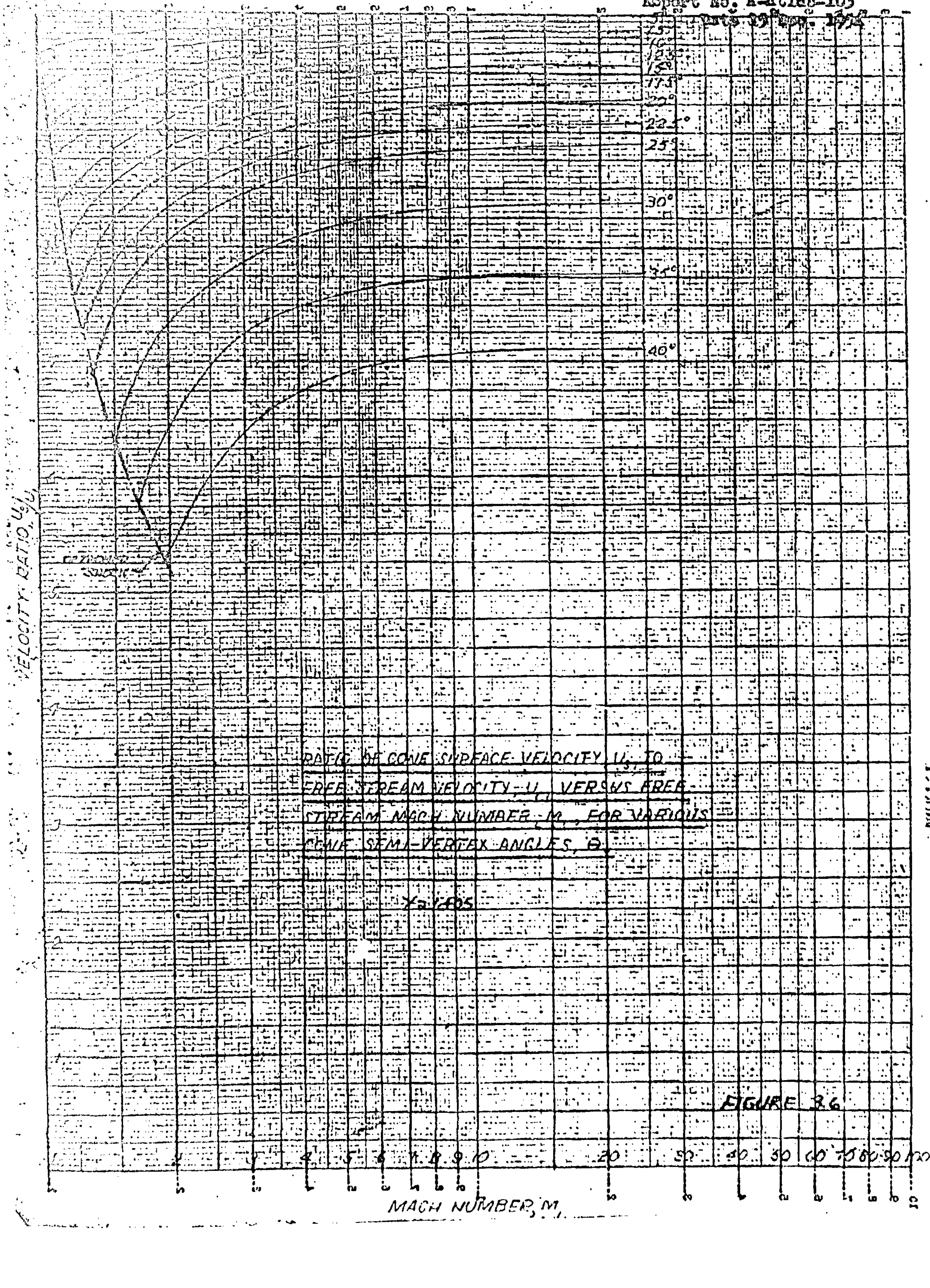
VELOCITY RATIO, U_s/U_1
MACH NUMBER, M_1
15°
20°
22.5°
25°
30°
35°
40°
RATIO OF CONE SURFACE VELOCITY U_s TO FREE STREAM VELOCITY U_1 VERSUS FREE STREAM MACH NUMBER M_1 FOR VARIOUS CONE SEMI-VERTEX ANGLES, θ.
$\gamma = 1.405$
FIGURE 3.6

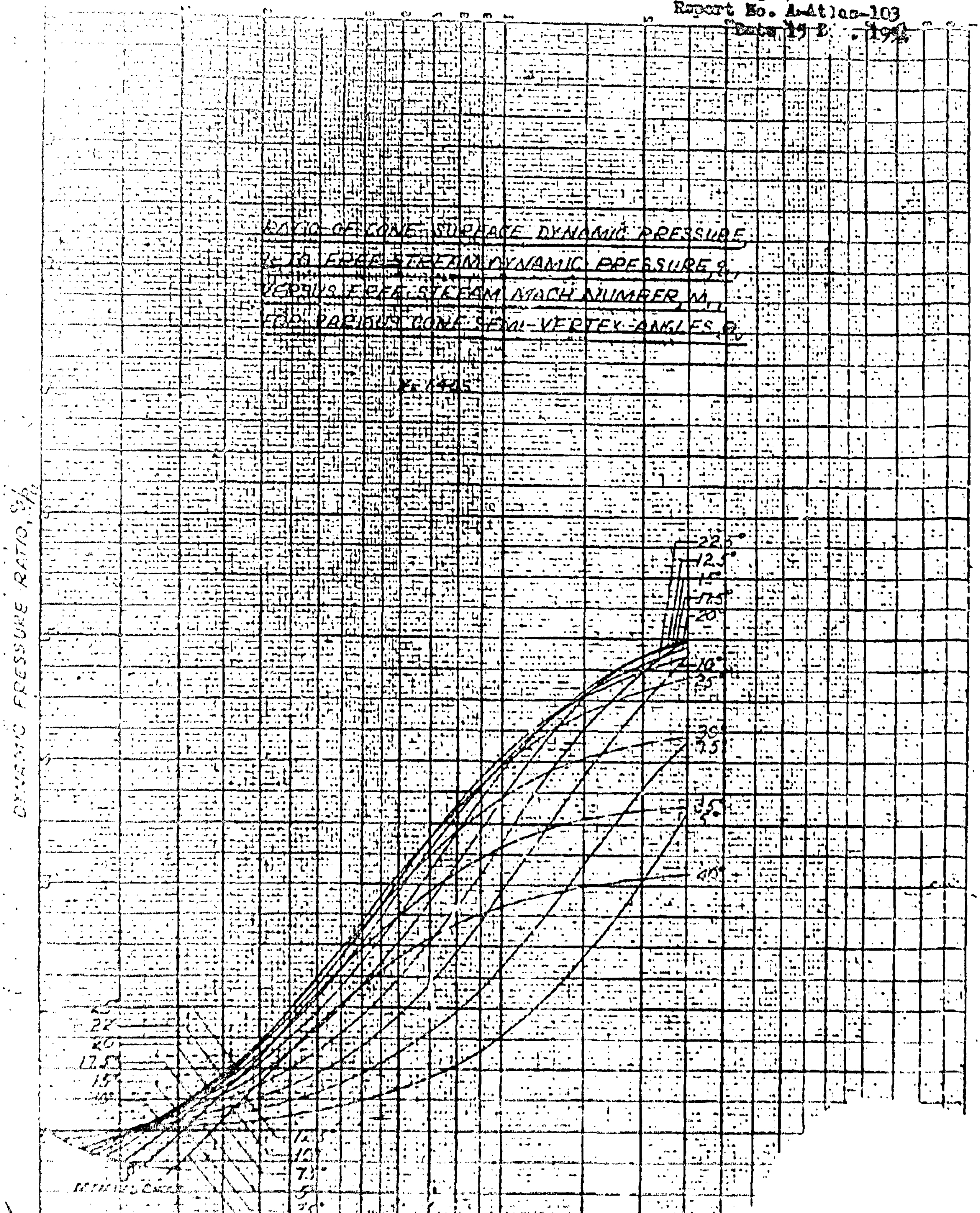
RATIO OF CONE SURFACE DYNAMIC PRESSURE
TO FREE STREAM DYNAMIC PRESSURE
VERSUS FREE STREAM MACH NUMBER
FOR VARIOUS CONE SEMI-VERTEX ANGLES
22.5°
12.5°
15°
17.5°
20°
10°
25°
30°
7.5°
35°
40°
DYNAMIC PRESSURE RATIO
MACH NUMBER

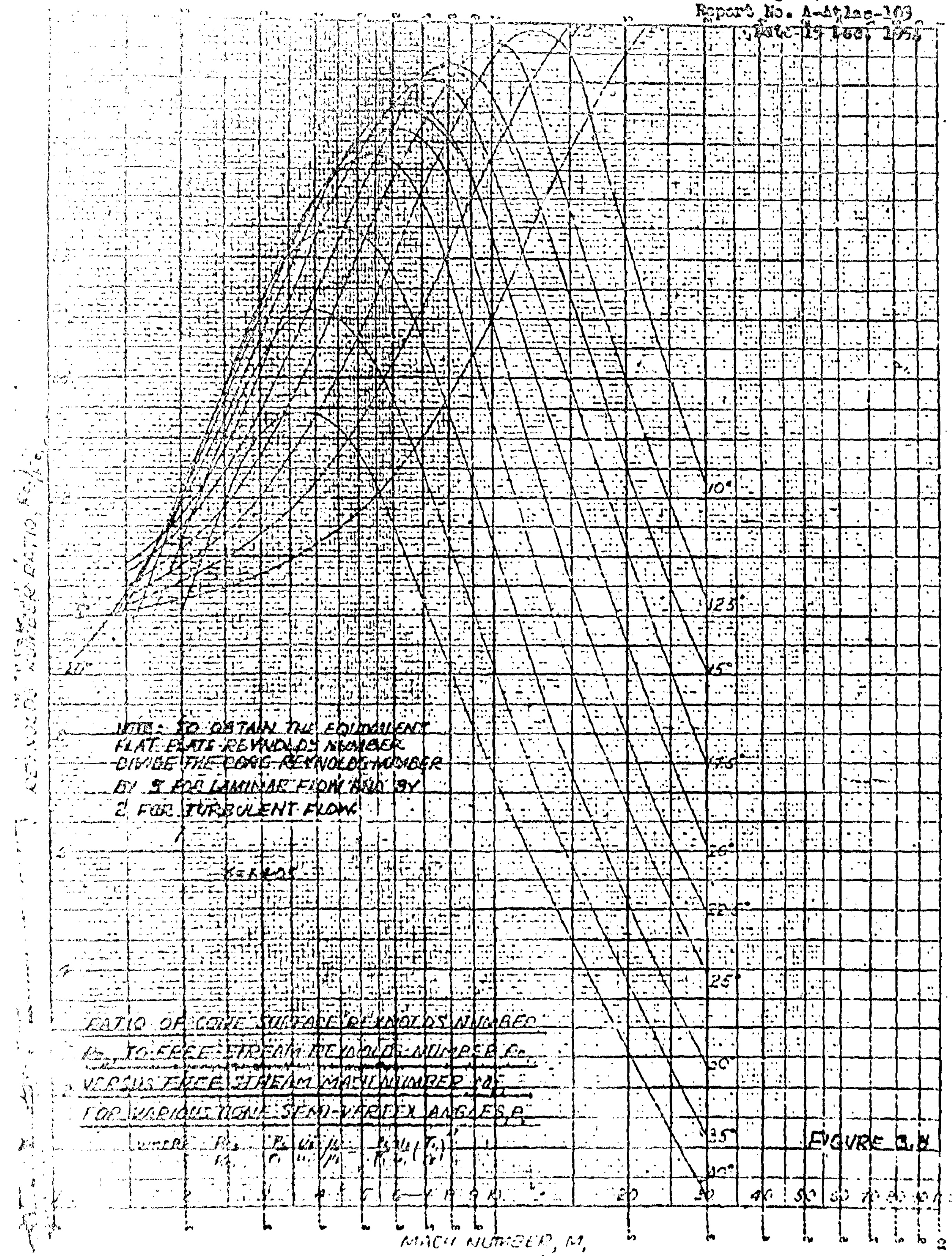
10°
12.5°
15°
17.5°
20°
22.5°
25°
30°
35°
NOTE: TO OBTAIN THE EQUIVALENT FLAT PLATE REYNOLDS NUMBER DIVIDE THE CONE REYNOLDS NUMBER BY 3 FOR LAMINAR FLOW AND BY 2 FOR TURBULENT FLOW.
RATIO OF CONE SURFACE REYNOLDS NUMBER
TO FREE STREAM REYNOLDS NUMBER
VERSUS FREE STREAM MACH NUMBER
FOR VARIOUS CONE SEMI-VERTEX ANGLES
2
3
4
5
6
7
8
9
10
20
30
40
50
MACH NUMBER, M,

FIGURE 3.8

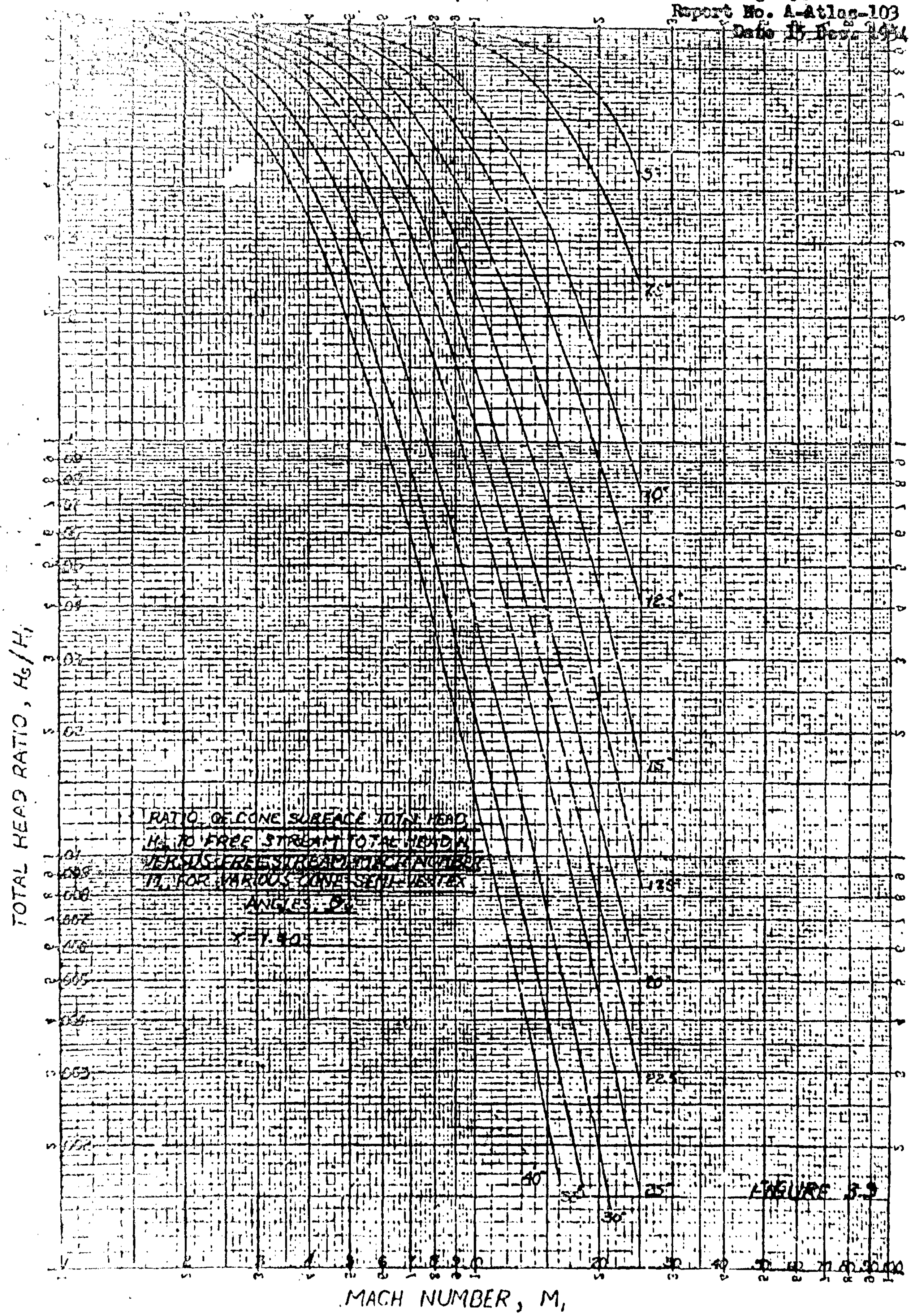
RATIO OF CONE SURFACE TOTAL HEAD
H_s TO FREE STREAM TOTAL HEAD H_1
VERSUS FREE STREAM MACH NUMBER
M_1 FOR VARIOUS CONE SEMI-VERTEX
ANGLES, θ_s
$\gamma = 1.40$
5°
7.5°
10°
12.5°
15°
17.5°
20°
22.5°
25°
30°
35°
40°
TOTAL HEAD RATIO, H_s/H_1
MACH NUMBER, M_1

FIGURE 3.3

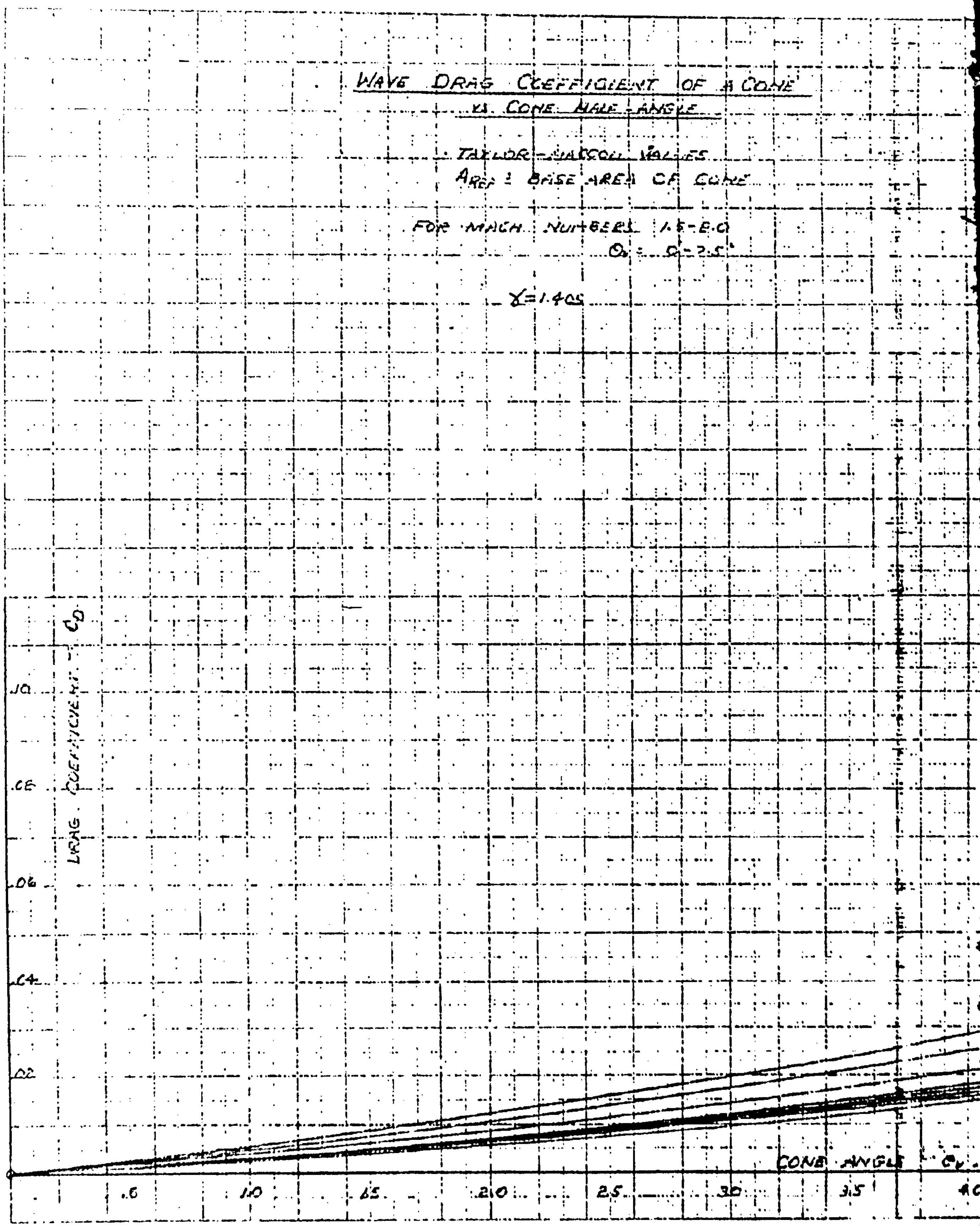

WAVE DRAG COEFFICIENT OF A CONE
vs. CONE HALF-ANGLE
TAYLOR-MACCOLL VALUES
AREF = BASE AREA OF CONE
FOR MACH NUMBERS 1.5-8.0
γ=1.405
DRAG COEFFICIENT - C_D
.10
.08
.06
.04
.02
.5
1.0
1.5
2.0
2.5
3.0
3.5
4.0
CONE ANGLE

C_D vs Θ_V

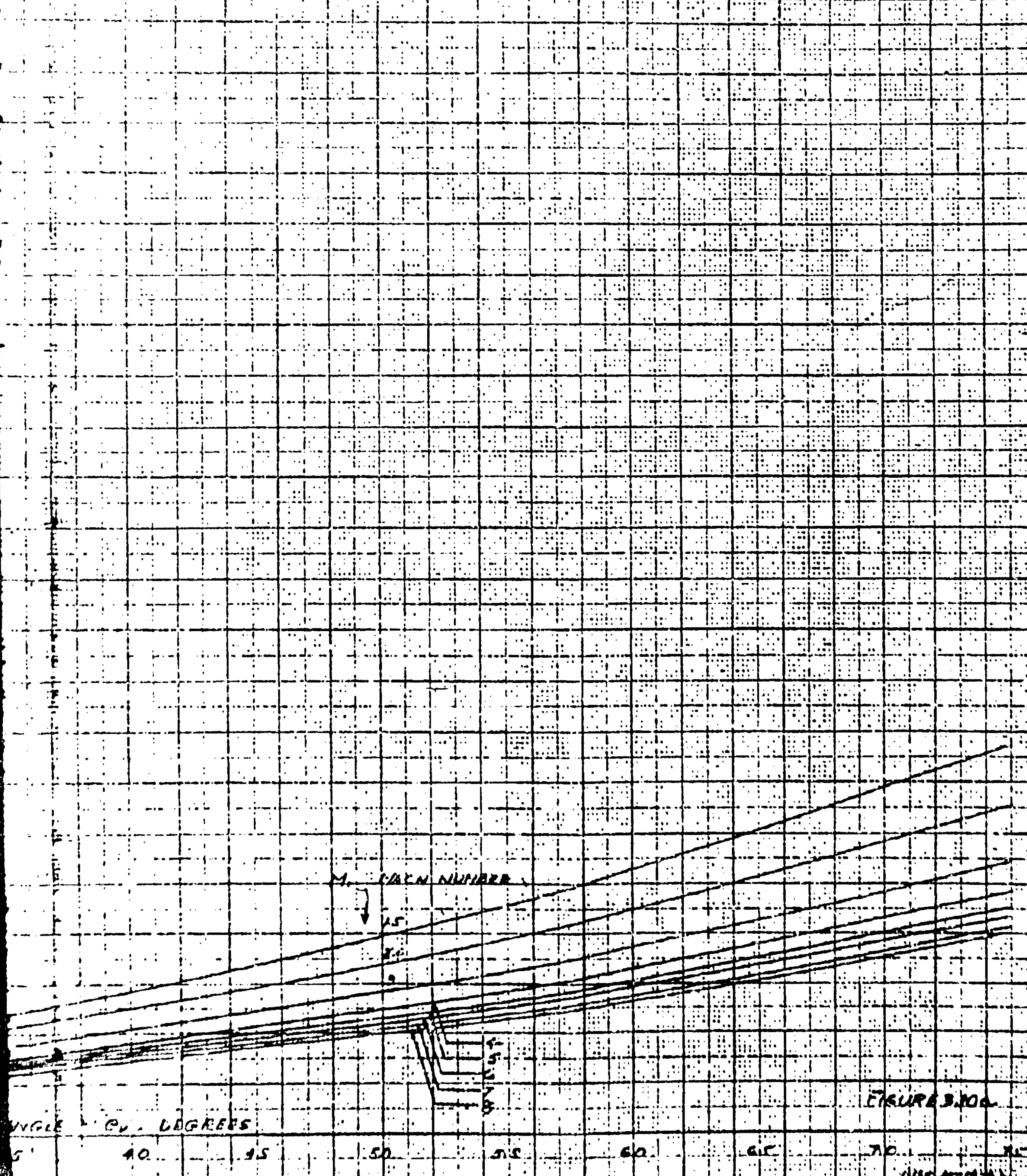

FIGURE 3.10a

C_D vs Θ_V

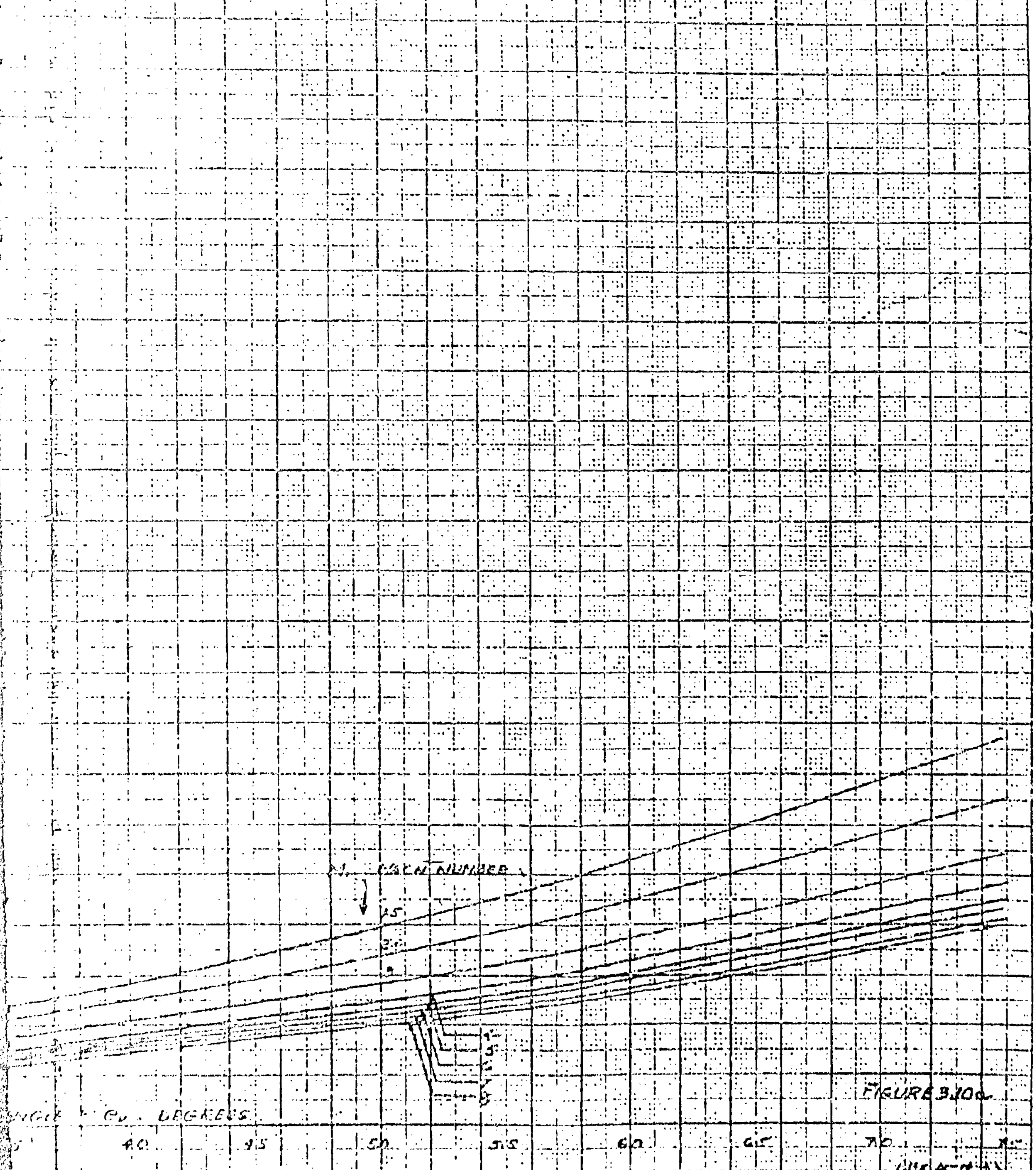

FIGURE 3.10a

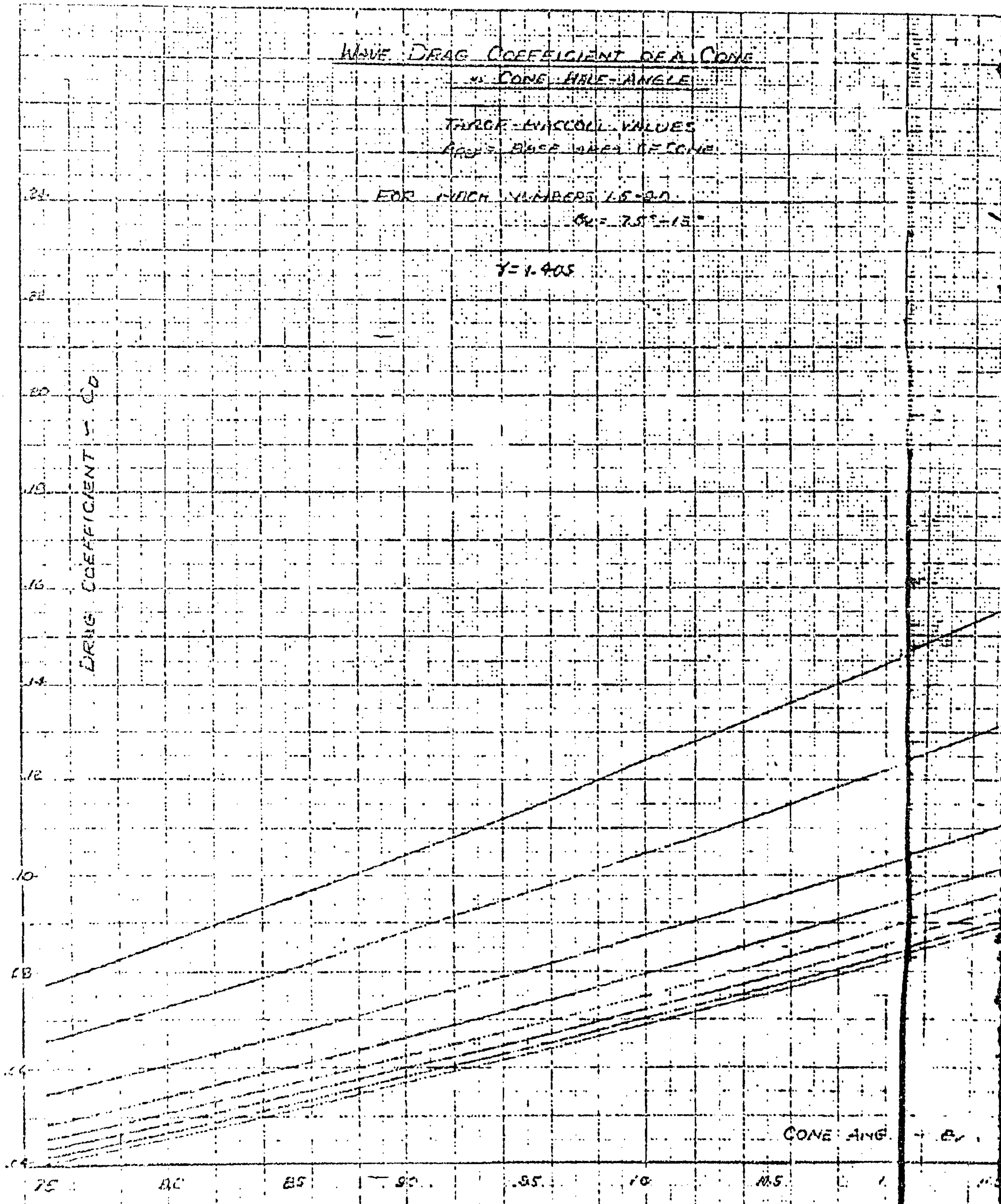
WAVE DRAG COEFFICIENT OF A CONE
vs CONE HALF-ANGLE
TAYLOR-MACCOLL VALUES
FOR MACH NUMBERS 1.5-2.0
γ = 1.405
DRAG COEFFICIENT - C_D
CONE ANG
.24
.22
.20
.18
.16
.14
.12
.10
.08
.06
.04
7.5
8.0
8.5
9.0
9.5
10
10.5

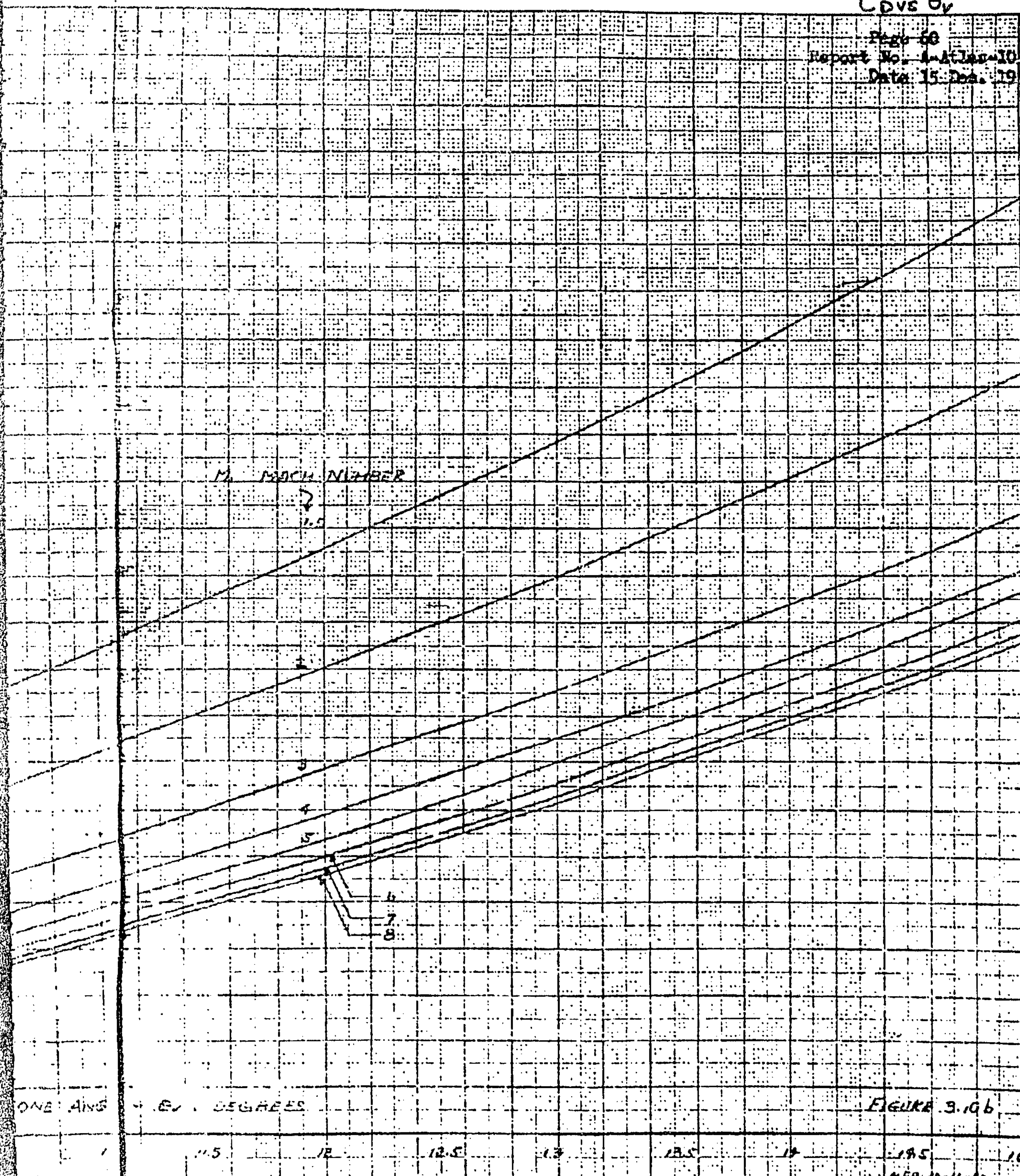

FIGURE 3.10b

B

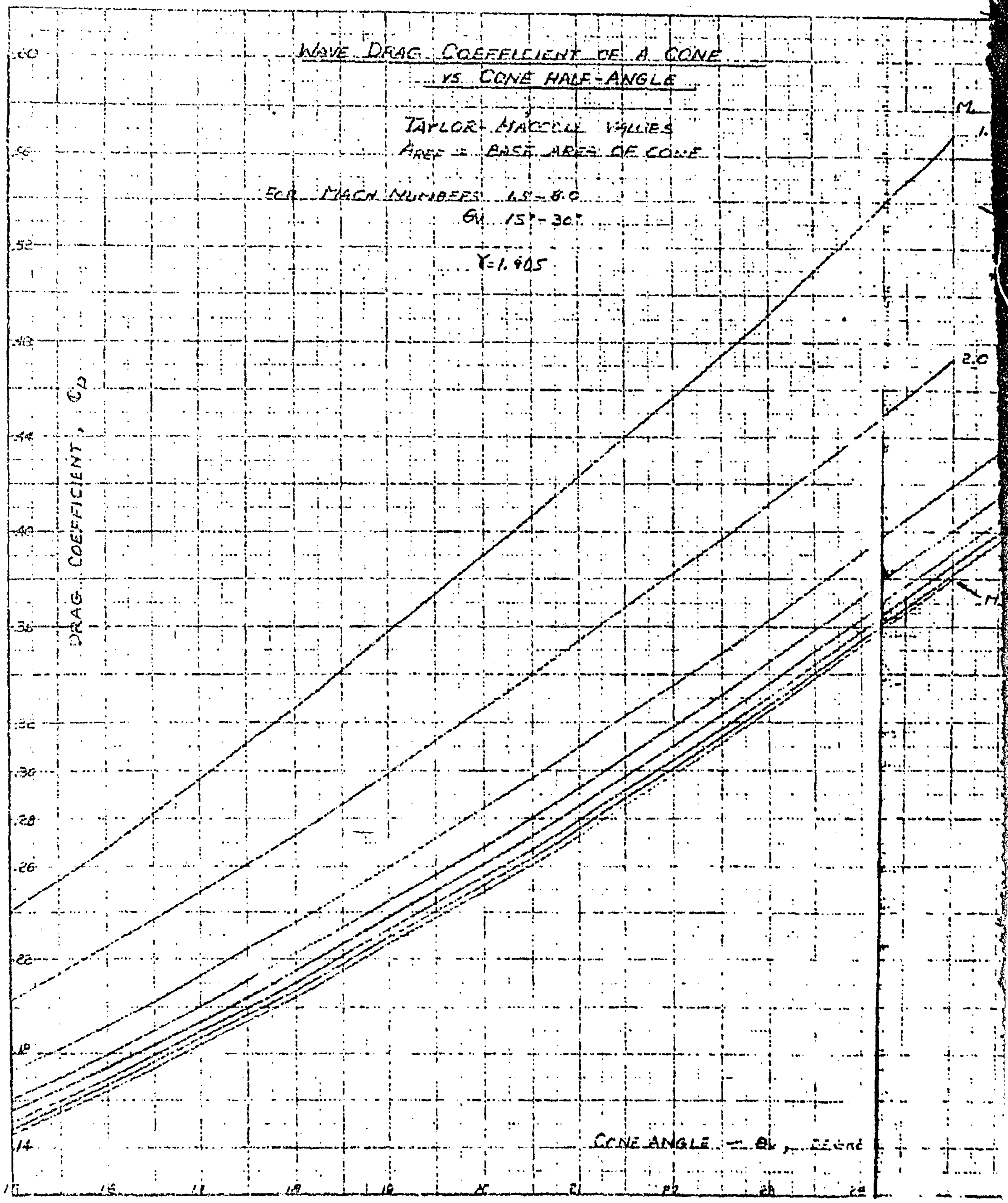
WAVE DRAG COEFFICIENT OF A CONE
VS CONE HALF-ANGLE
TAYLOR-MACCOLL VALUES
AREF = BASE AREA OF CONE
FOR MACH NUMBERS 1.5 - 8.0
θV 15° - 30°
γ=1.405
DRAG COEFFICIENT, C_D
CONE ANGLE — θV, DEGREE
.60
.56
.52
.48
.44
.40
.38
.36
.30
.28
.26
.22
.18
.14
15
M
2.0

C_D vs θ_v

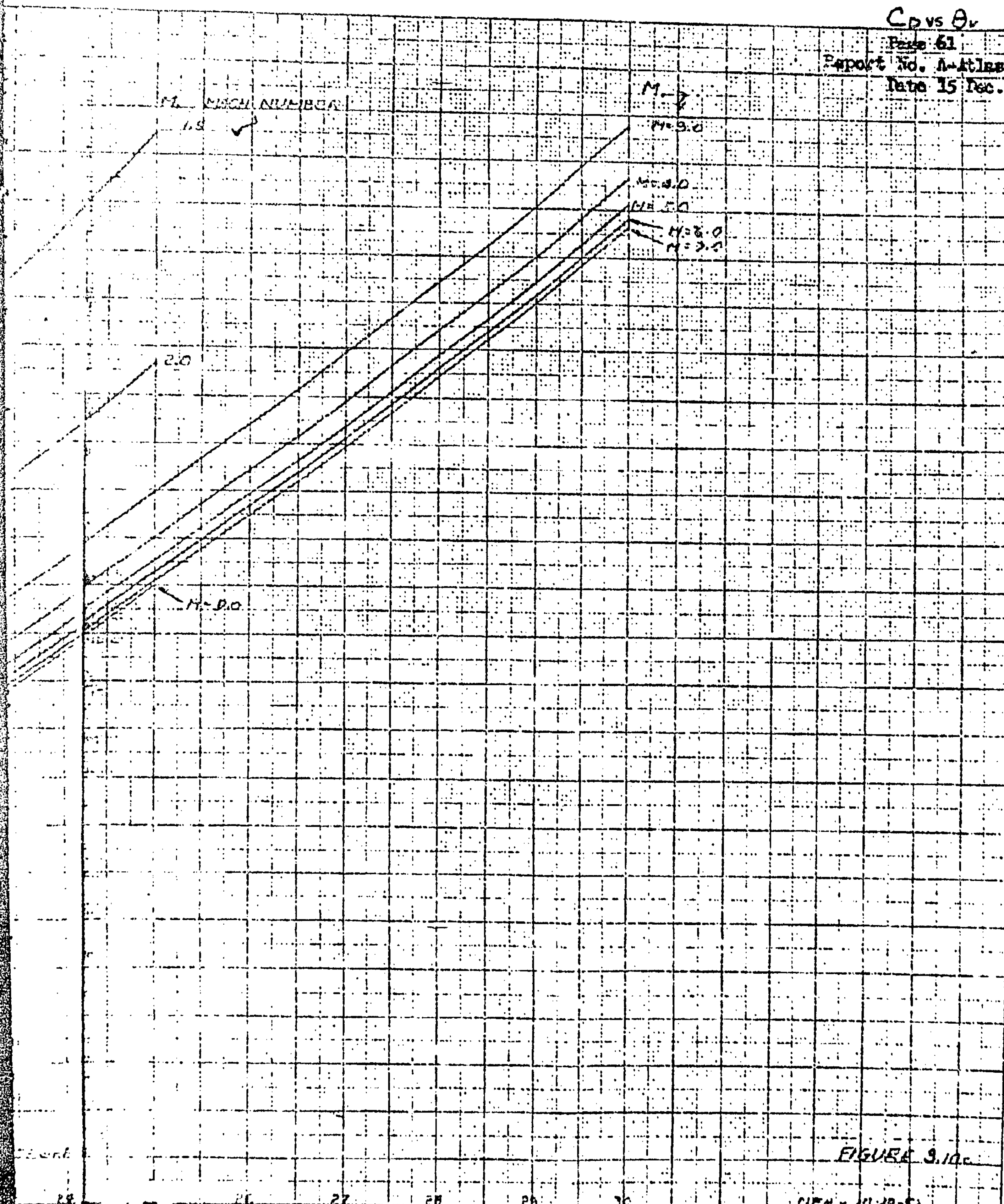

FIGURE 9.10c

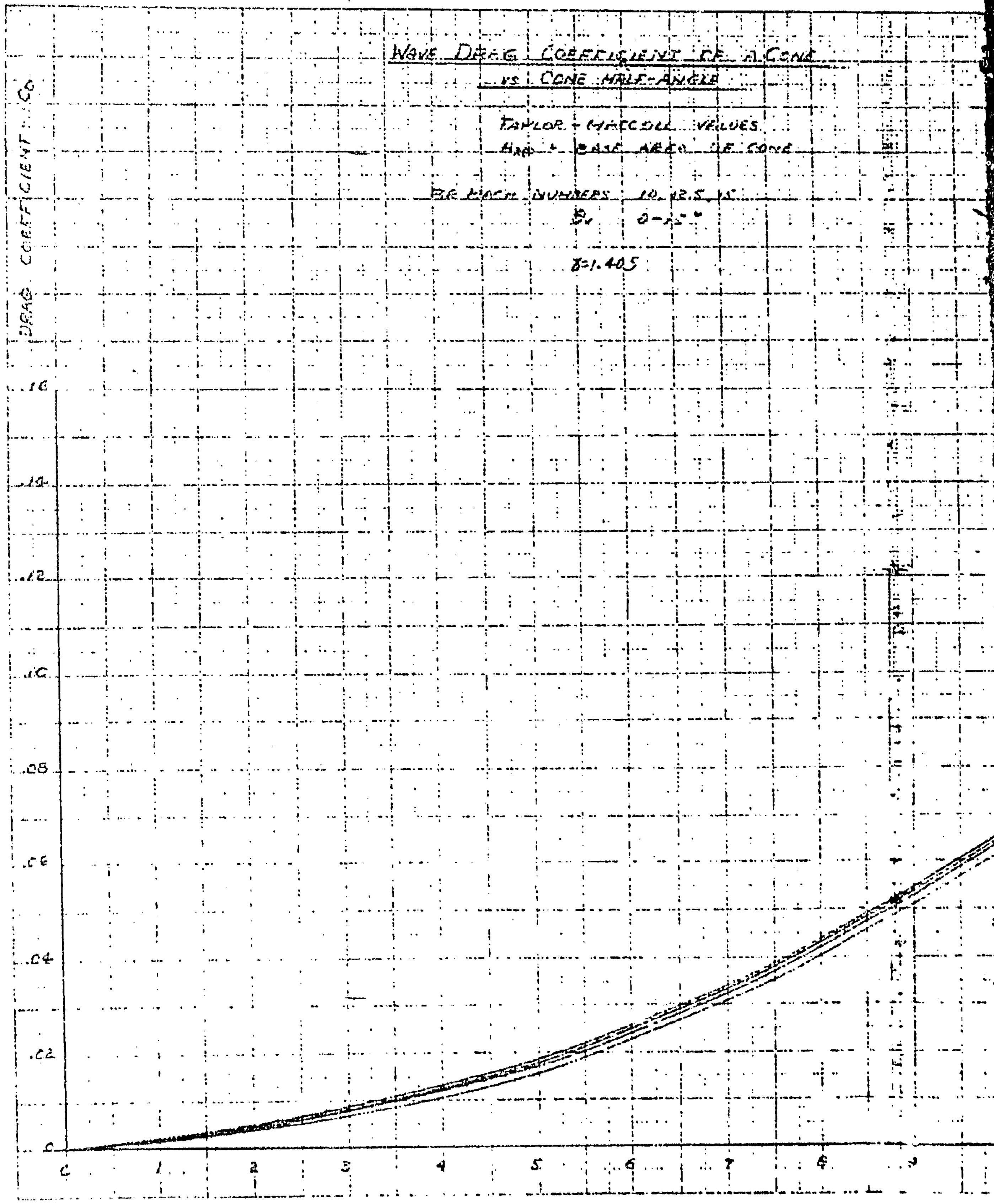
WAVE DRAG COEFFICIENT OF A CONE
VS CONE HALF-ANGLE
TAYLOR - MACCOLL VALUES
BASE AREA OF CONE
MACH NUMBERS 10, 12.5, 15
γ=1.405
DRAG COEFFICIENT C_D
.16
.14
.12
.10
.08
.06
.04
.02
0
0
1
2
3
4
5
6
7
8
9

A

C_D vs θ_v

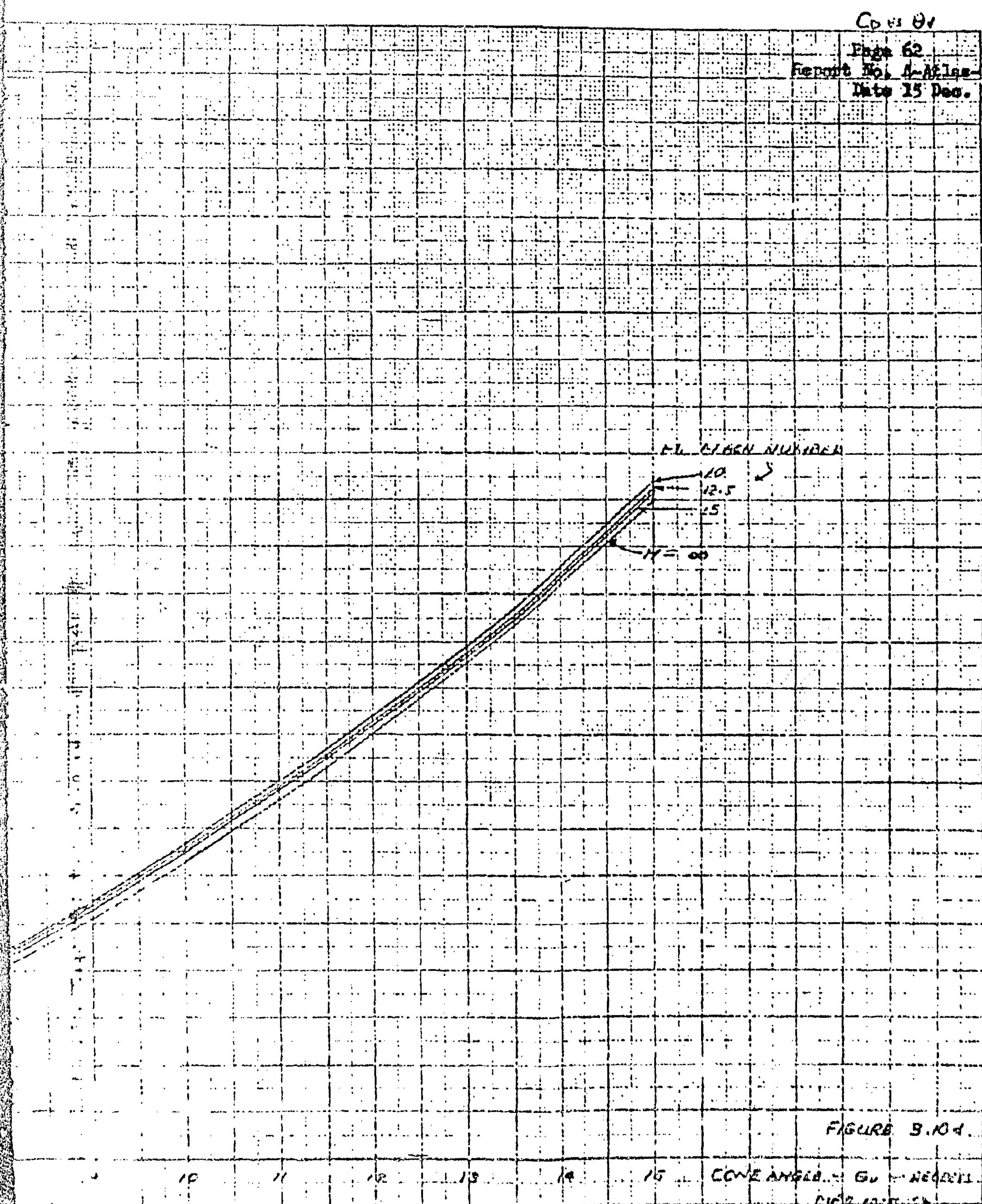

FIGURE 3.10.4.

B

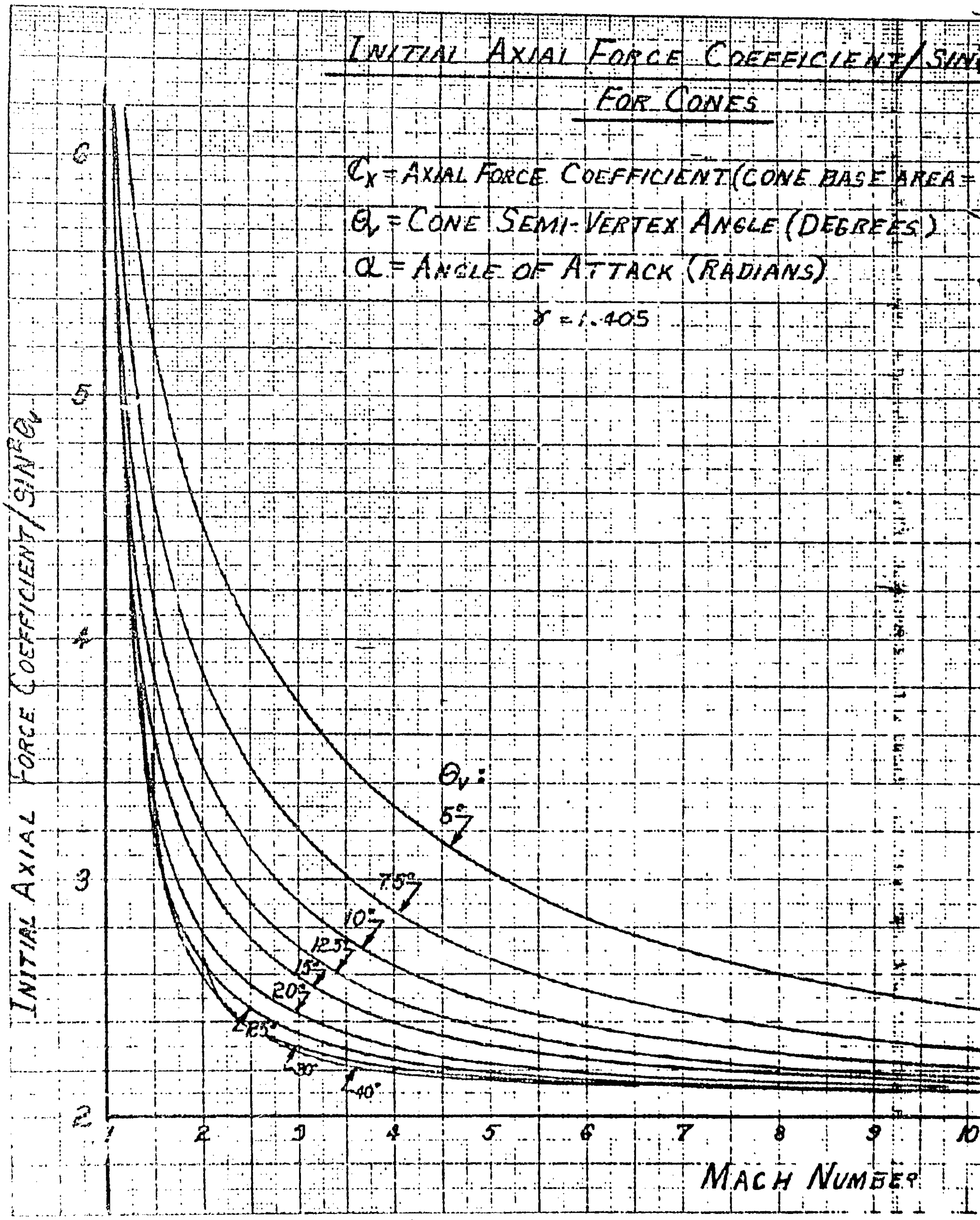

INITIAL AXIAL FORCE COEFFICIENT/SIN
FOR CONES
C_X = AXIAL FORCE COEFFICIENT (CONE BASE AREA =
θ_v = CONE SEMI-VERTEX ANGLE (DEGREES)
α = ANGLE OF ATTACK (RADIANS)
γ = 1.405
INITIAL AXIAL FORCE COEFFICIENT/SIN² θ_v
θ_v:
5°
7.5°
10°
12.5°
15°
20°
25°
30°
40°
6
5
4
3
2
1
2
3
4
5
6
7
8
9
10
MACH NUMBER

C_x vs M_1

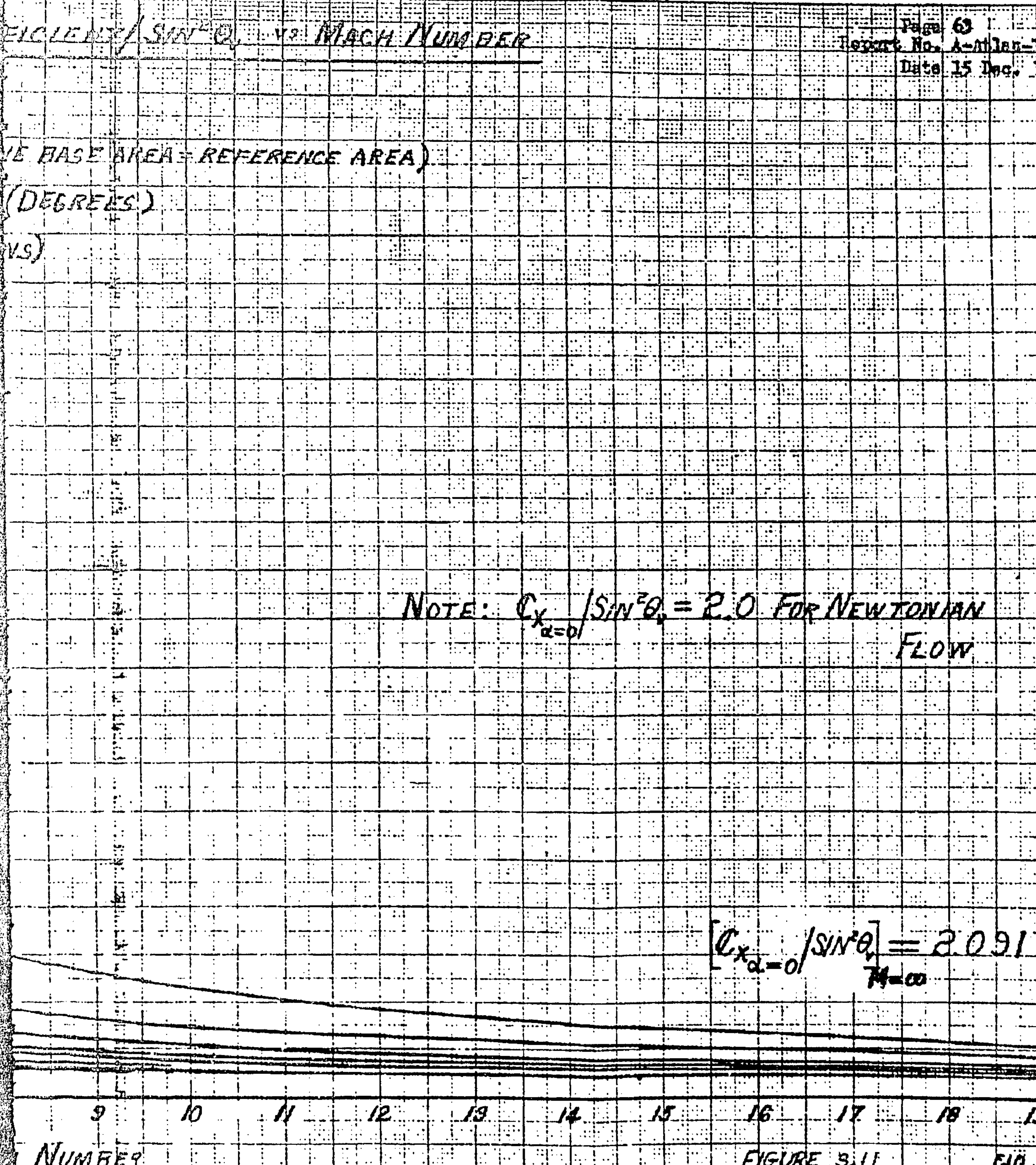

FIGURE 3.11

FJD
5-22-53

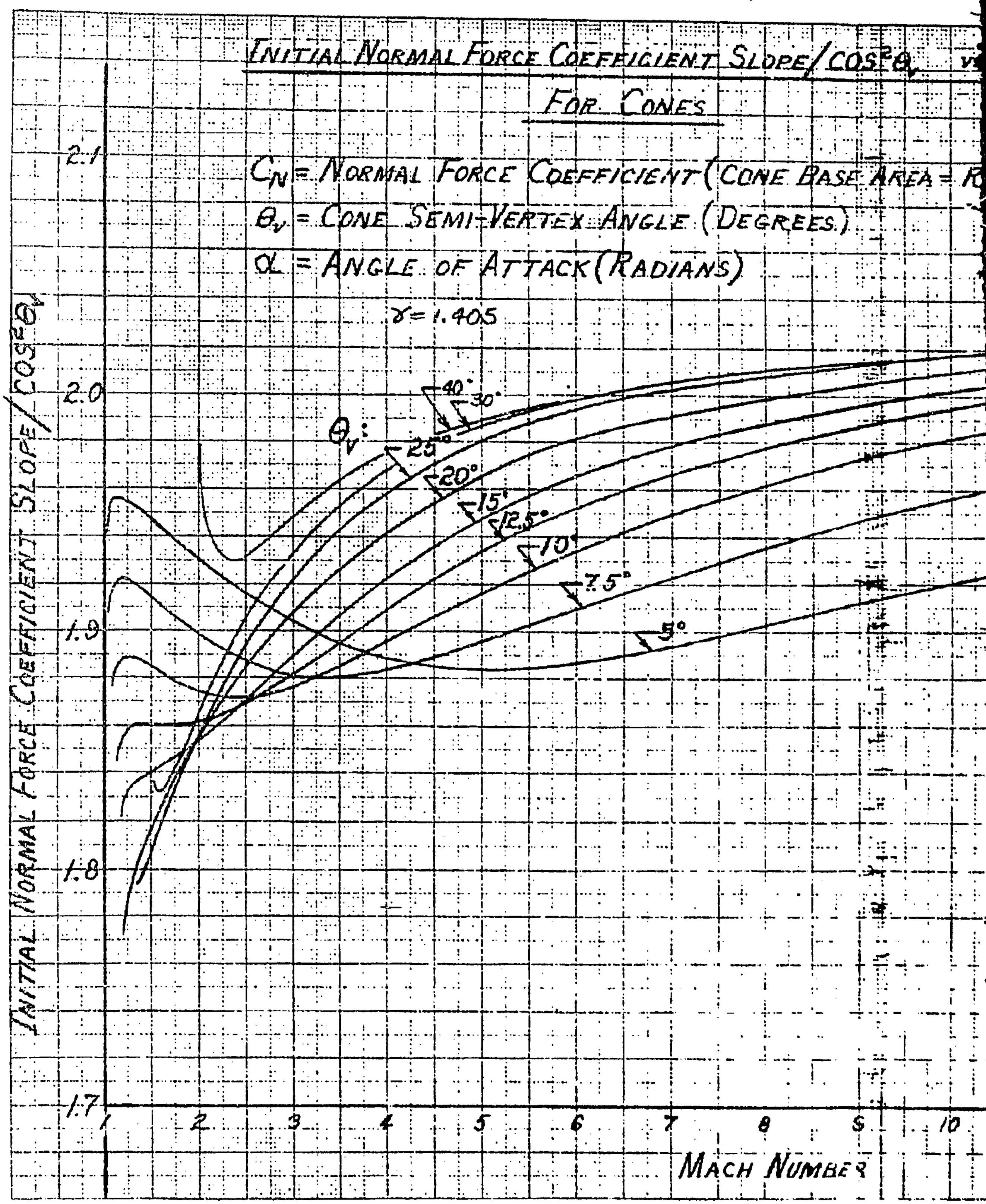
INITIAL NORMAL FORCE COEFFICIENT SLOPE/COS²θv vs
FOR CONES
CN = NORMAL FORCE COEFFICIENT (CONE BASE AREA = R
θv = CONE SEMI-VERTEX ANGLE (DEGREES)
α = ANGLE OF ATTACK (RADIANS)
γ = 1.405
θv:
40°
30°
25°
20°
15°
12.5°
10°
7.5°
5°
2.1
2.0
1.9
1.8
1.7
1
2
3
4
5
6
7
8
9
10
MACH NUMBER
INITIAL NORMAL FORCE COEFFICIENT SLOPE/COS²θv
A

$\left(\frac{dC_N}{d\alpha}\right)_{\alpha=0} / \cos^2\theta_v$ vs M_1

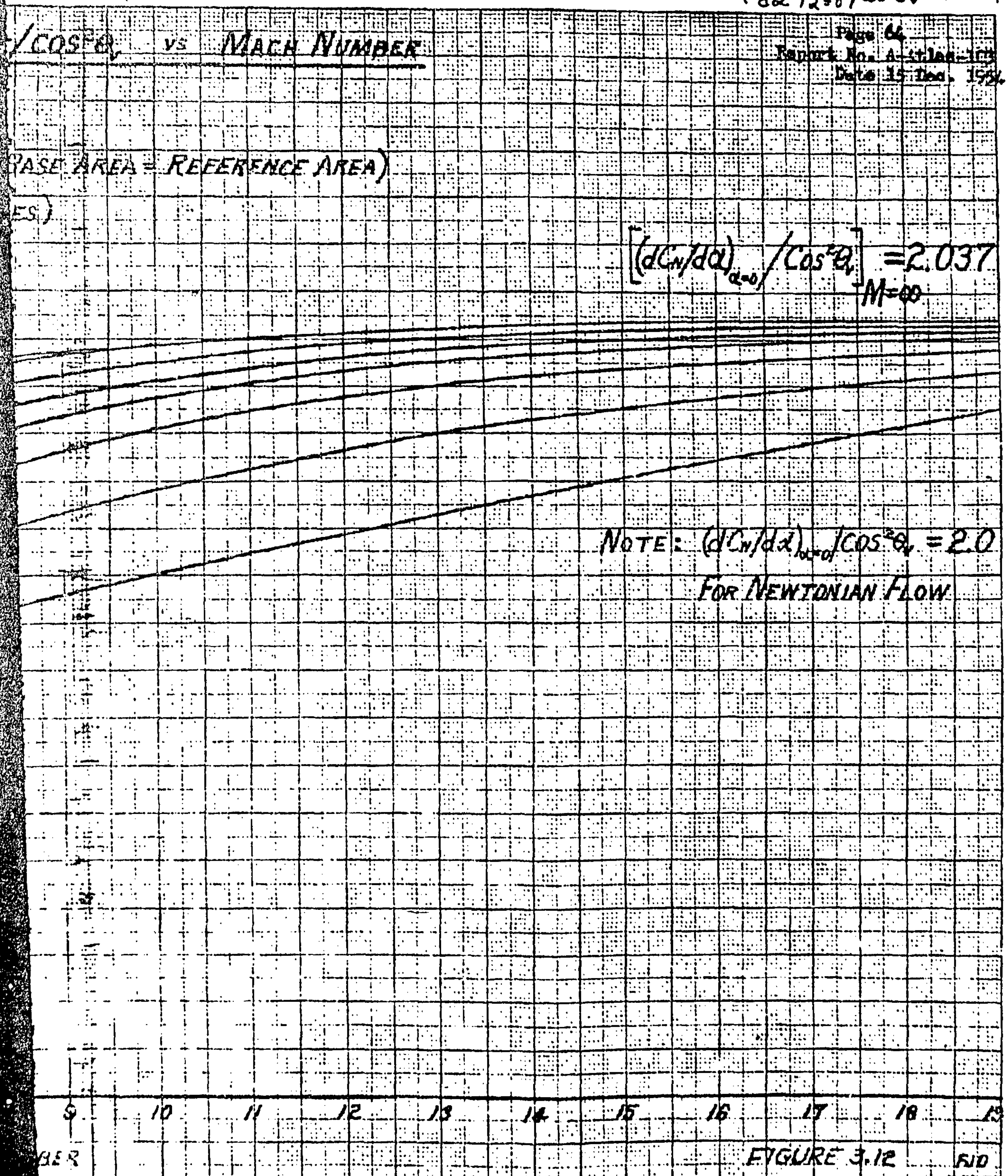

FIGURE 3.12

FJD
3-22-53

B

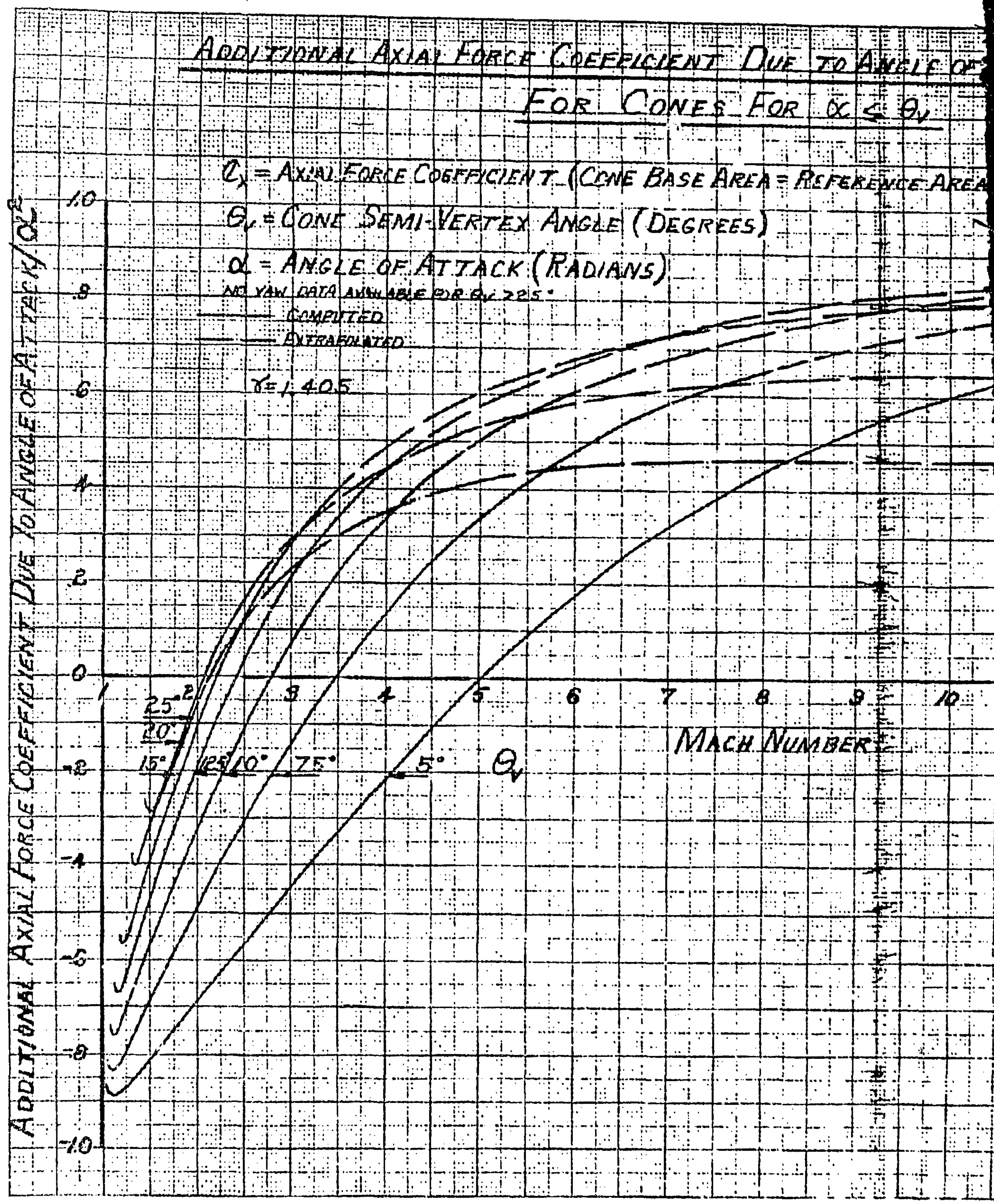
ADDITIONAL AXIAL FORCE COEFFICIENT DUE TO ANGLE OF
FOR CONES FOR α ≤ θv
Cx = AXIAL FORCE COEFFICIENT (CONE BASE AREA = REFERENCE AREA
θv = CONE SEMI-VERTEX ANGLE (DEGREES)
α = ANGLE OF ATTACK (RADIANS)
NO YAW DATA AVAILABLE FOR θv
COMPUTED
EXTRAPOLATED
γ = 1.405
ADDITIONAL AXIAL FORCE COEFFICIENT DUE TO ANGLE OF ATTACK/α²
1.0
.8
.6
.4
.2
0
-.2
-.4
-.6
-.8
-1.0
1
2
3
4
5
6
7
8
9
10
MACH NUMBER
25°
20°
15°
12.5°
10°
7.5°
5°
θv

$\Delta C_x / \alpha^2$ vs M_1

Page 65
Report No. A-[illegible]-103
Date 15 Dec. 1954

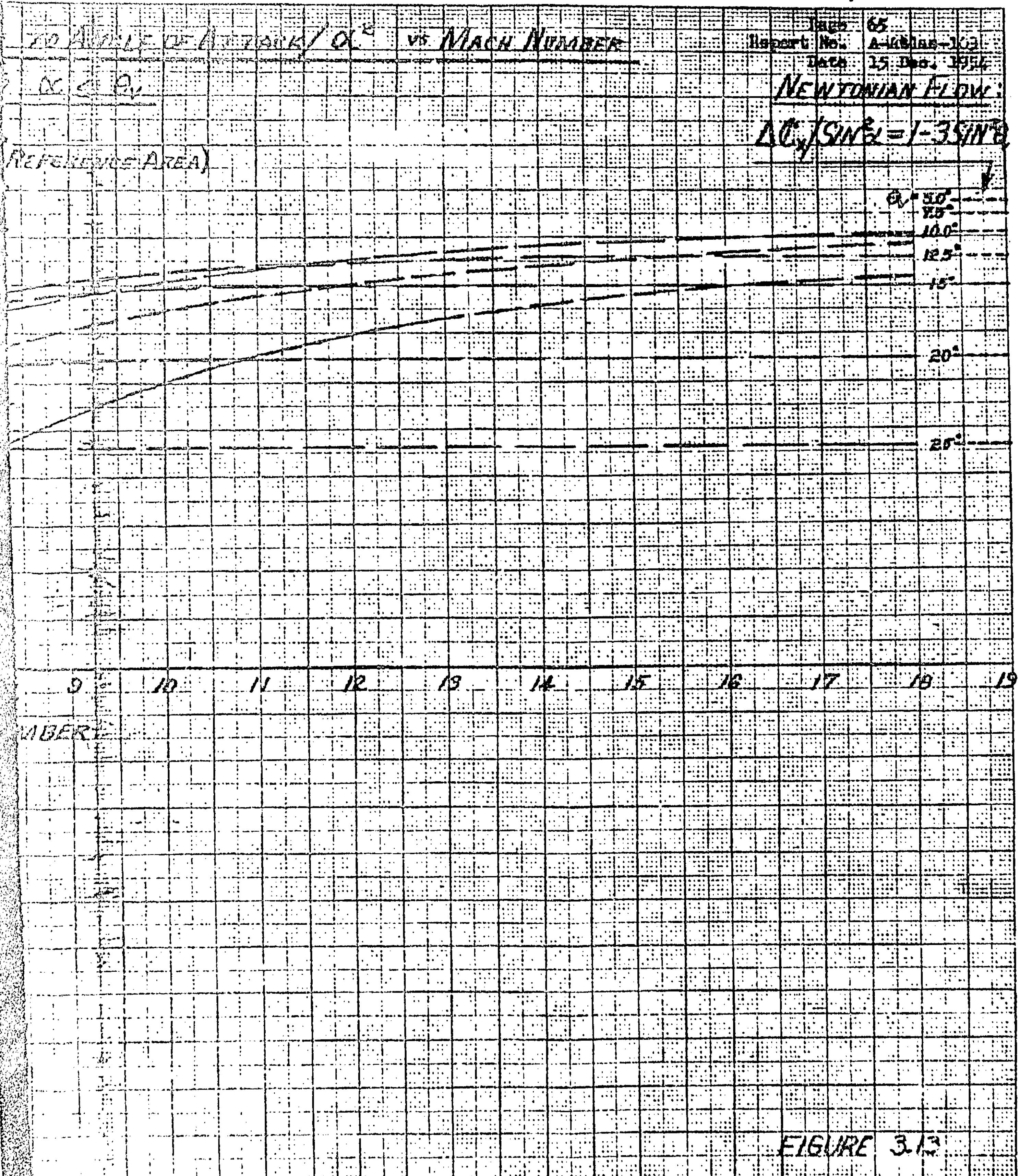

FIGURE 3.13

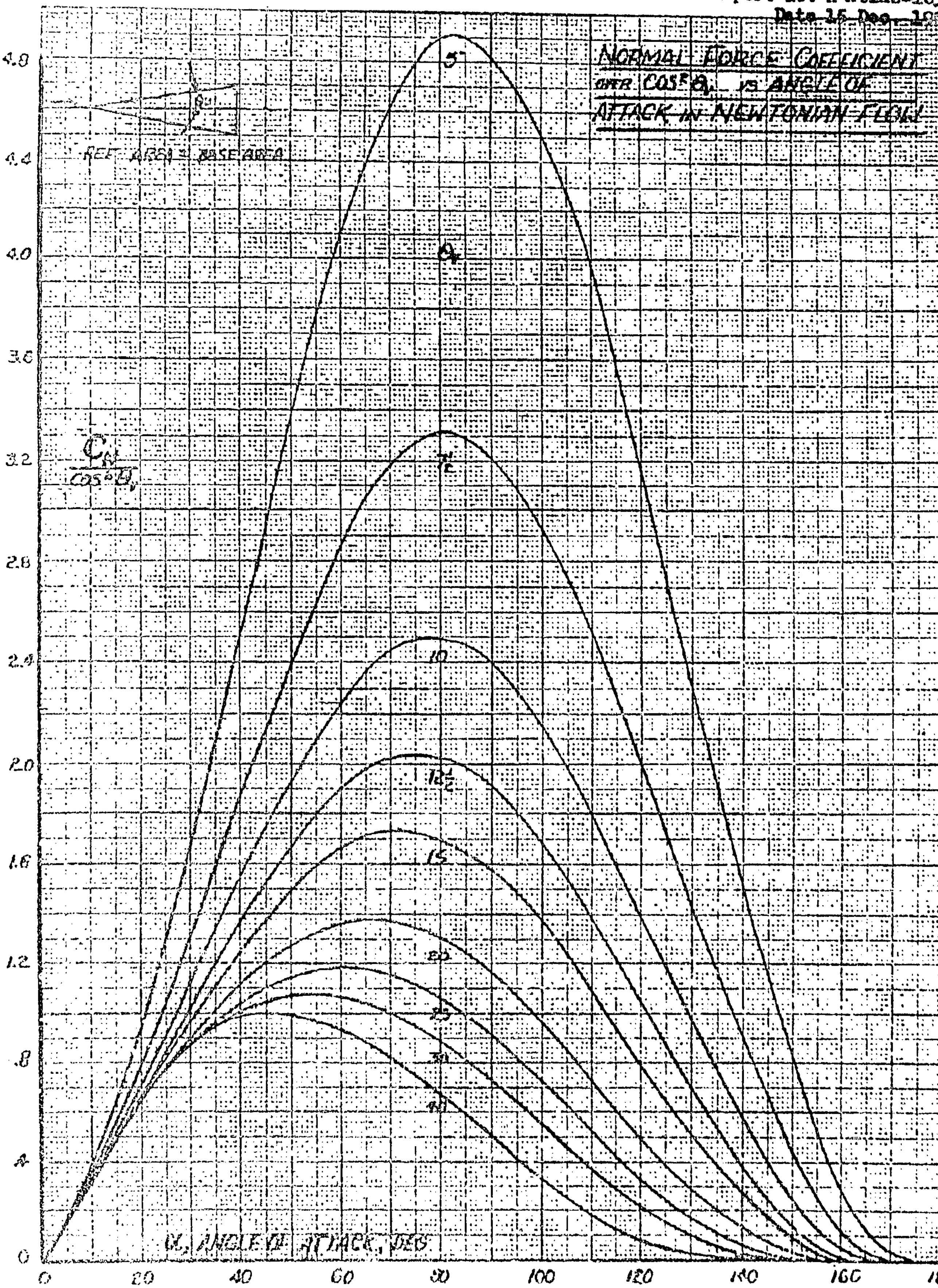
NORMAL FORCE COEFFICIENT OVER $\cos^2\theta_v$ VS ANGLE OF ATTACK IN NEWTONIAN FLOW
REF. AREA = BASE AREA
$\frac{C_N}{\cos^2\theta_v}$
θ_v
5
$7\frac{1}{2}$
10
$12\frac{1}{2}$
15
20
25
30
40
α, ANGLE OF ATTACK, DEG
4.8
4.4
4.0
3.6
3.2
2.8
2.4
2.0
1.6
1.2
.8
.4
0
0
20
40
60
80
100
120
140
160
180

FIGURE 3.14

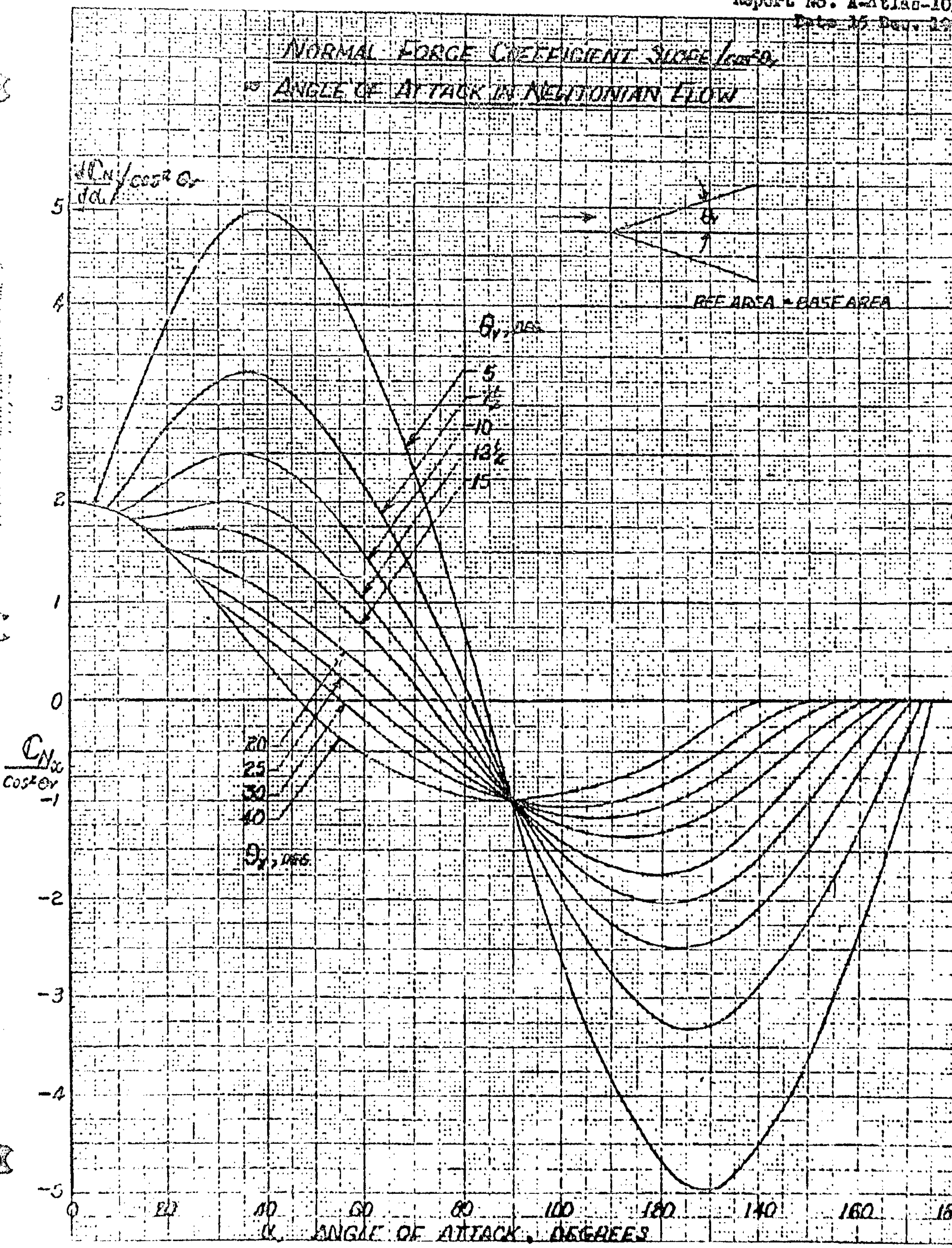
NORMAL FORCE COEFFICIENT SLOPE / $\cos^2\theta_v$
vs ANGLE OF ATTACK IN NEWTONIAN FLOW
$\frac{dC_N}{d\alpha}/\cos^2\theta_v$
$\frac{C_{N_\alpha}}{\cos^2\theta_v}$
θ_v
REF AREA = BASE AREA
θ_v, DEG.
5
7½
10
12½
15
20
25
30
40
θ_v, DEG.
5
4
3
2
1
0
-1
-2
-3
-4
-5
0
20
40
60
80
100
120
140
160
180
α, ANGLE OF ATTACK, DEGREES

FIGURE 3.15

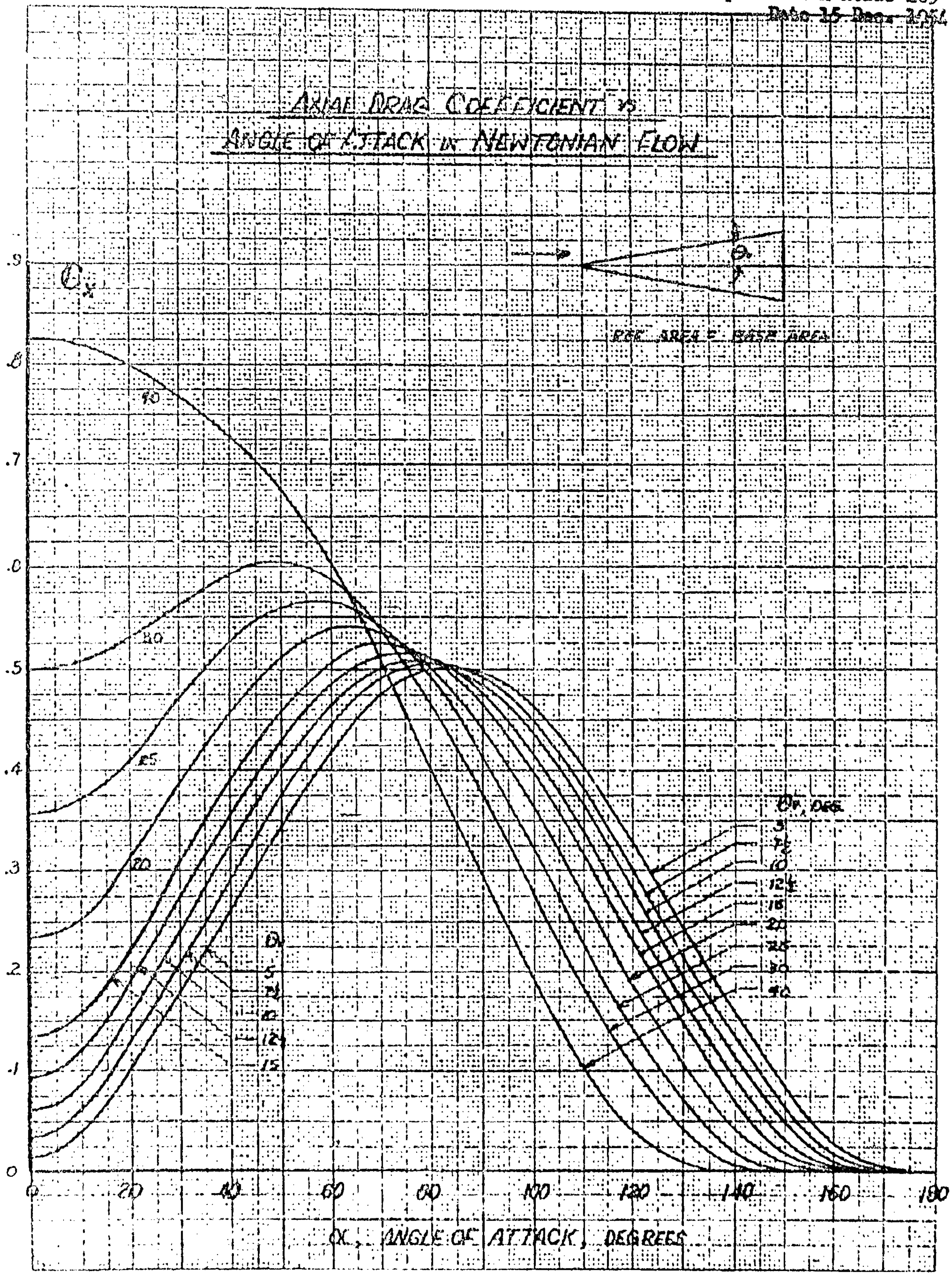
AXIAL DRAG COEFFICIENT vs ANGLE OF ATTACK IN NEWTONIAN FLOW
C_x
REF. AREA = BASE AREA
θ_v, DEG.
α, ANGLE OF ATTACK, DEGREES

FIGURE 3.16

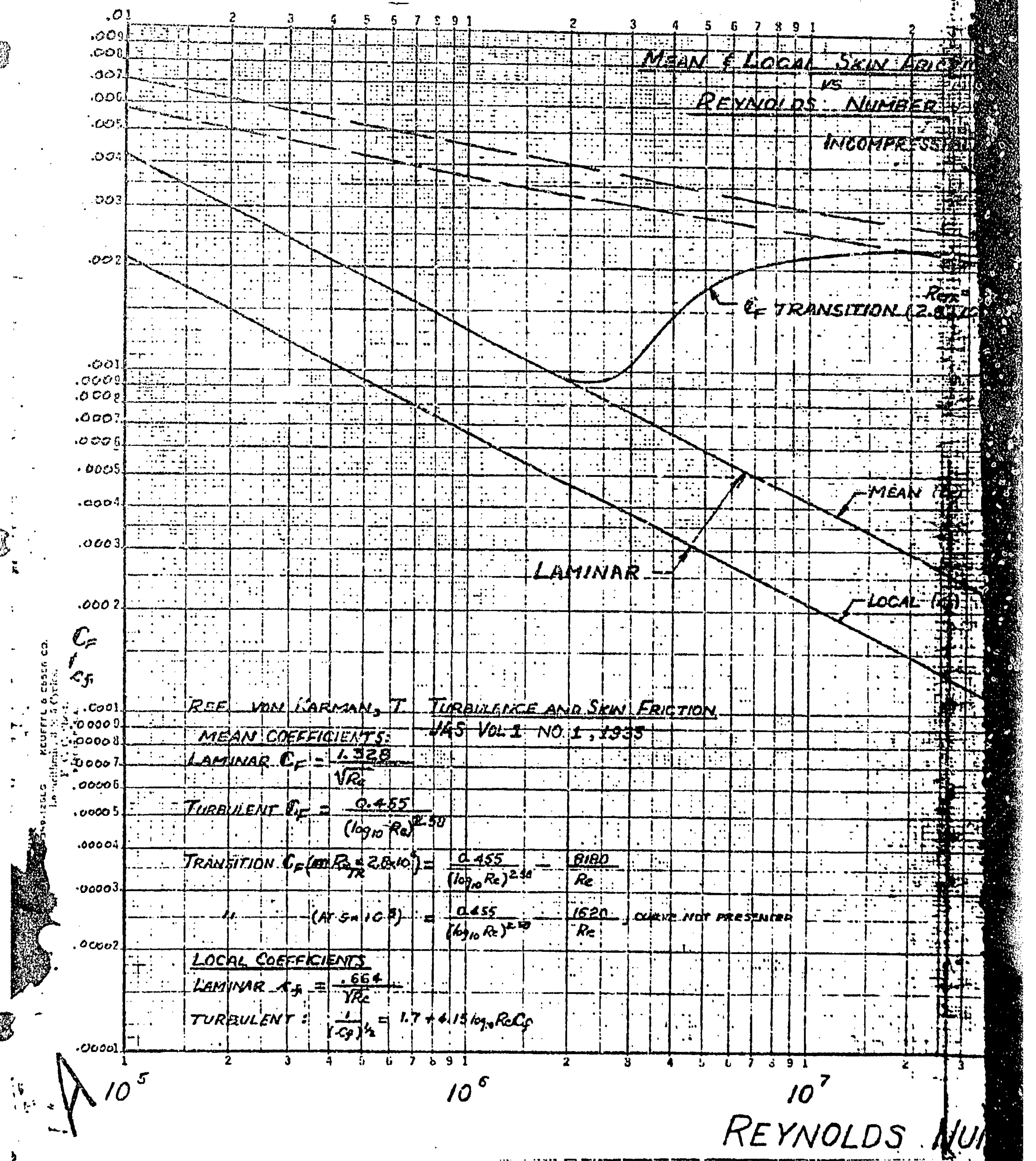
MEAN & LOCAL SKIN FRICTI
VS
REYNOLDS NUMBER
INCOMPRESSI
C_F TRANSITION (2.8×10
MEAN
LAMINAR
LOCAL
C_F
c_{f_i}
REF. VON KARMAN, T. TURBULENCE AND SKIN FRICTION
JAS VOL 1 NO. 1, 1935
MEAN COEFFICIENTS:
LAMINAR $C_F = \frac{1.328}{\sqrt{Re}}$
TURBULENT $C_F = \frac{0.455}{(\log_{10} Re)^{2.58}}$
TRANSITION $C_F (Re_{TR} = 2.8 \times 10^6) = \frac{0.455}{(\log_{10} Re)^{2.58}} - \frac{8180}{Re}$
" (AT 5×10^6) $= \frac{0.455}{(\log_{10} Re)^{2.58}} - \frac{1620}{Re}$ CURVE NOT PRESENTED
LOCAL COEFFICIENTS
LAMINAR $c_{f_i} = \frac{.664}{\sqrt{Re}}$
TURBULENT: $\frac{1}{(c_f)^{1/2}} = 1.7 + 4.15 \log_{10} Re\, c_f$
10^5
10^6
10^7
REYNOLDS NU

C_F & c_f vs R_e

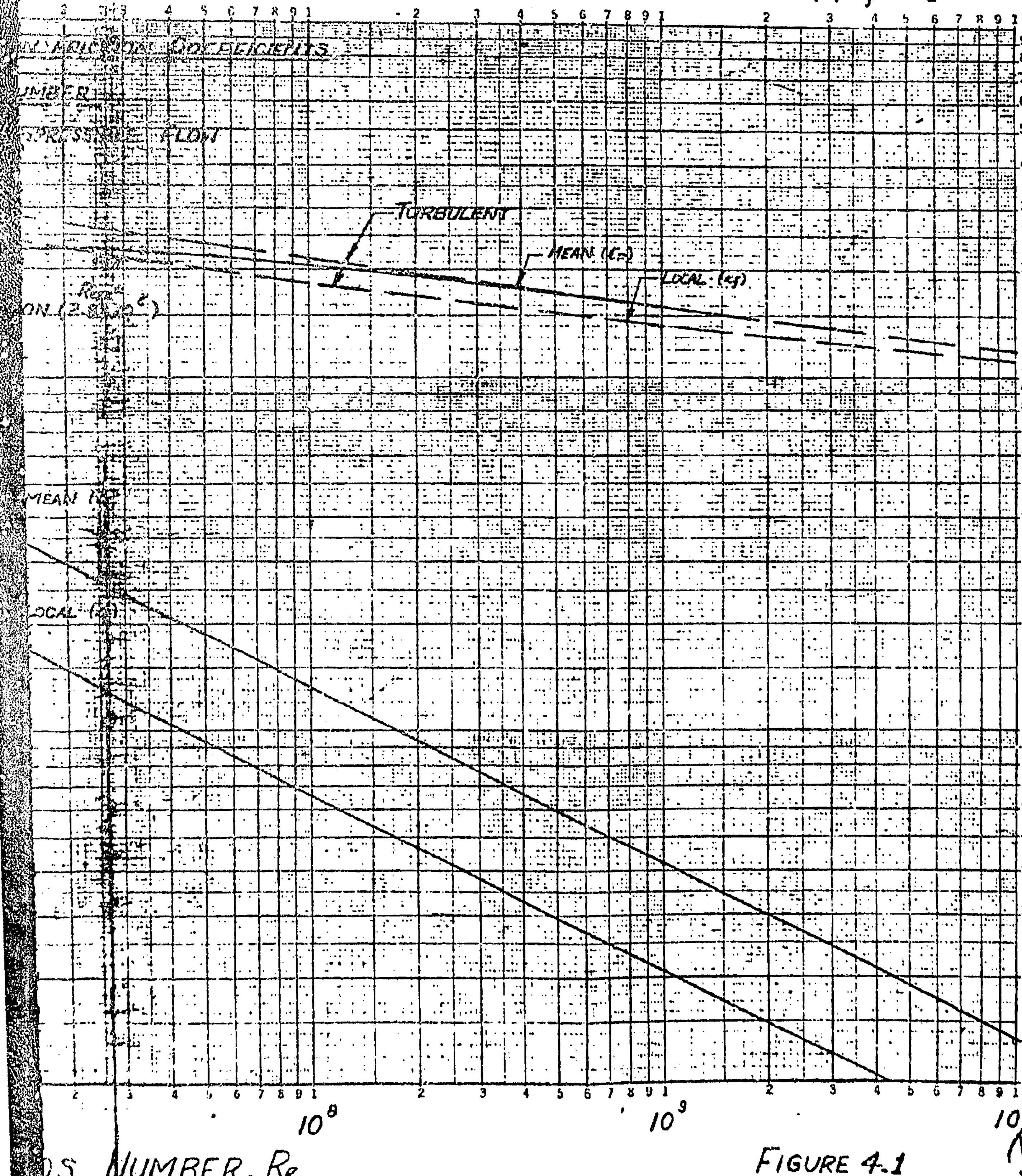

FIGURE 4.1

B

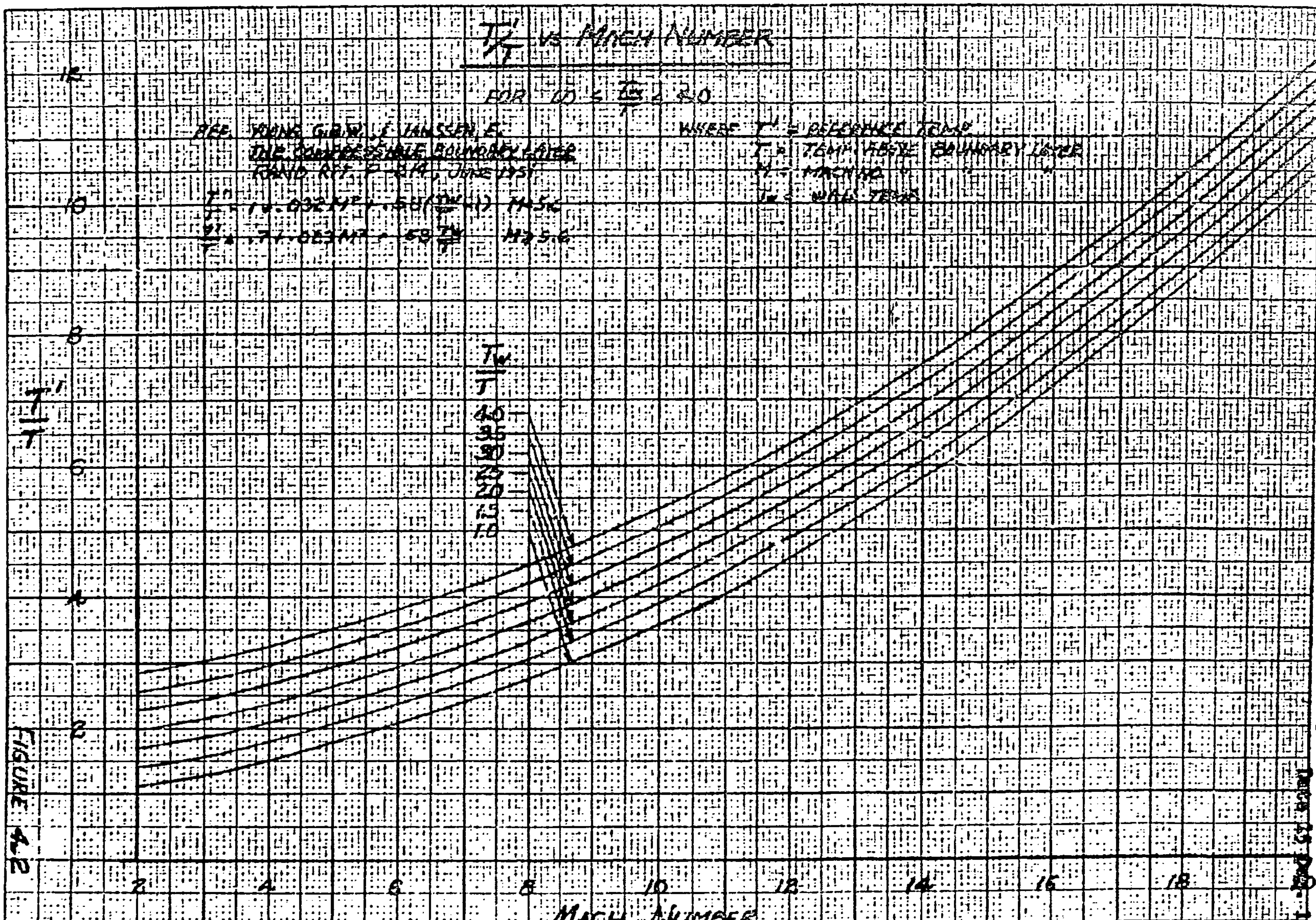
T'/T vs MACH NUMBER
FOR 1.0 ≤ Tw/T ≤ 4.0
REF. YOUNG, G.B.W. & JANSSEN, E.
THE COMPRESSIBLE BOUNDARY LAYER
RAND REP. P-214, JUNE 1951
T'/T = 1 + .032M² + .58(Tw/T − 1) M≤5.6
T'/T = .7 + .023M² + .58 Tw/T M≥5.6
WHERE T' = REFERENCE TEMP
T = TEMP ABOVE BOUNDARY LAYER
M = MACH NO.
Tw = WALL TEMP
Tw/T
4.0
3.5
3.0
2.5
2.0
1.5
1.0
T'/T
12
10
8
6
4
2
2
4
6
8
10
12
14
16
18
MACH NUMBER

FIGURE 4.2

TEMPERATURE, T

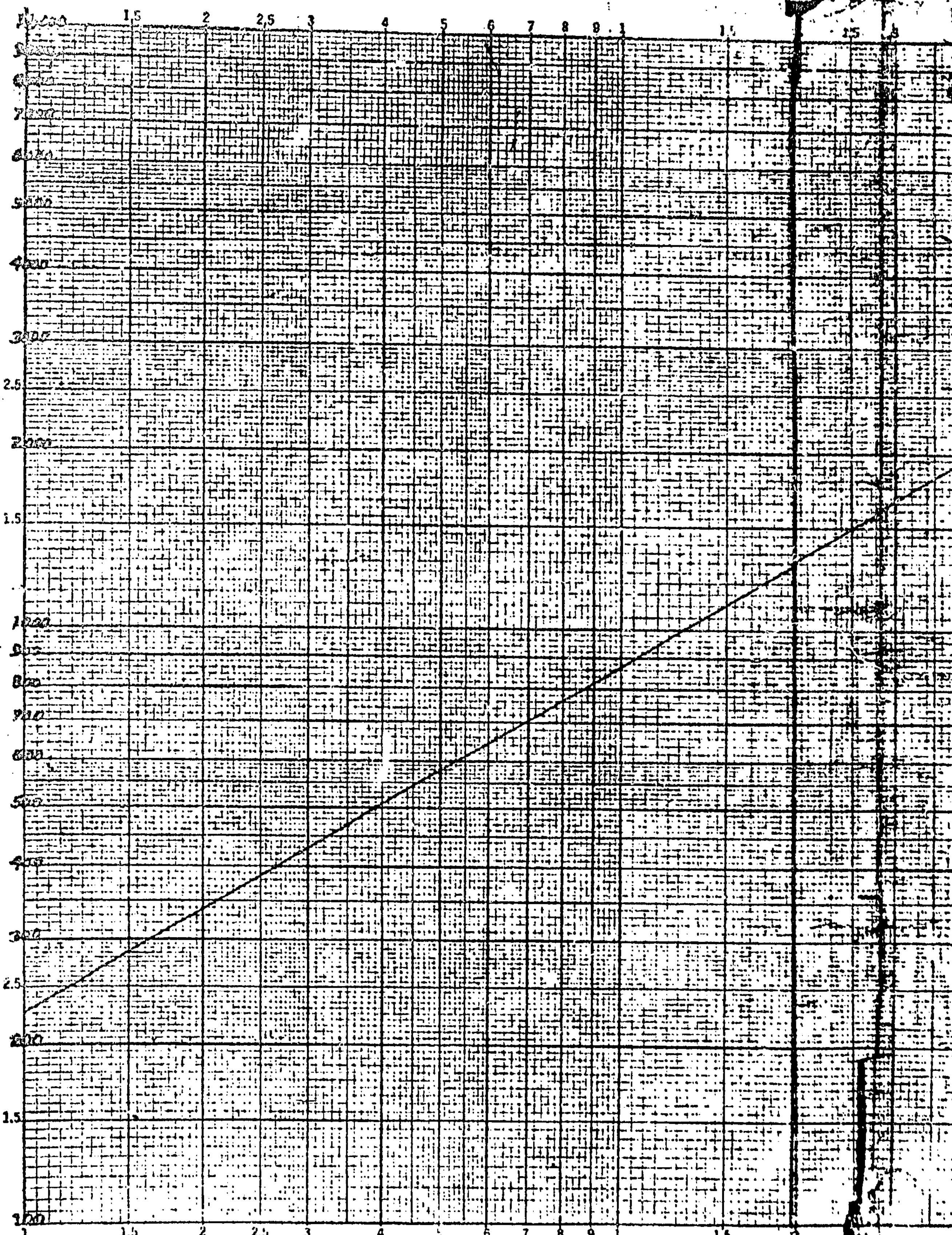

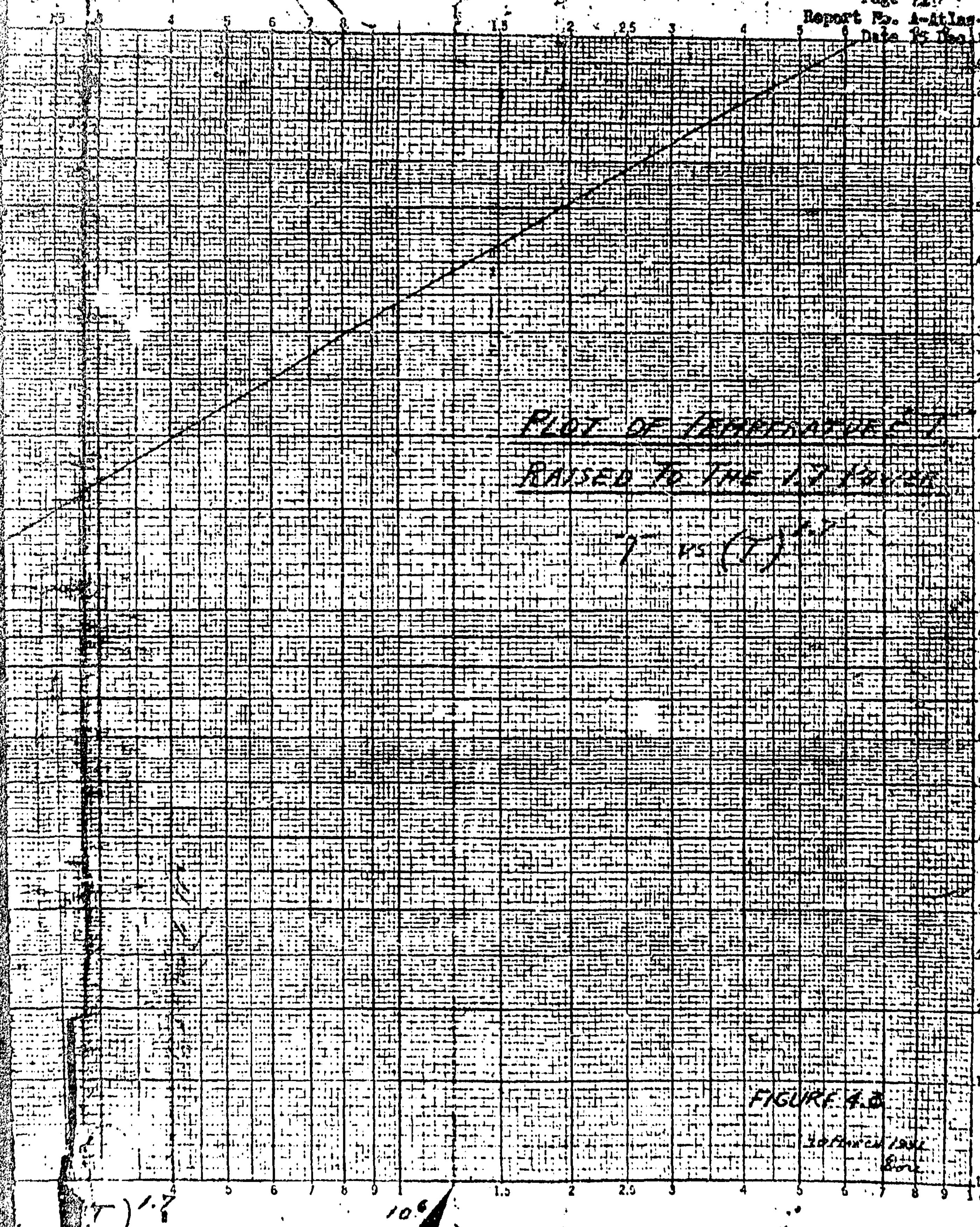
PLOT OF TEMPERATURE T
RAISED TO THE 1.7 POWER
T vs (T)^1.7
(T)^1.7
10^6
30 March 1954

FIGURE 4.8

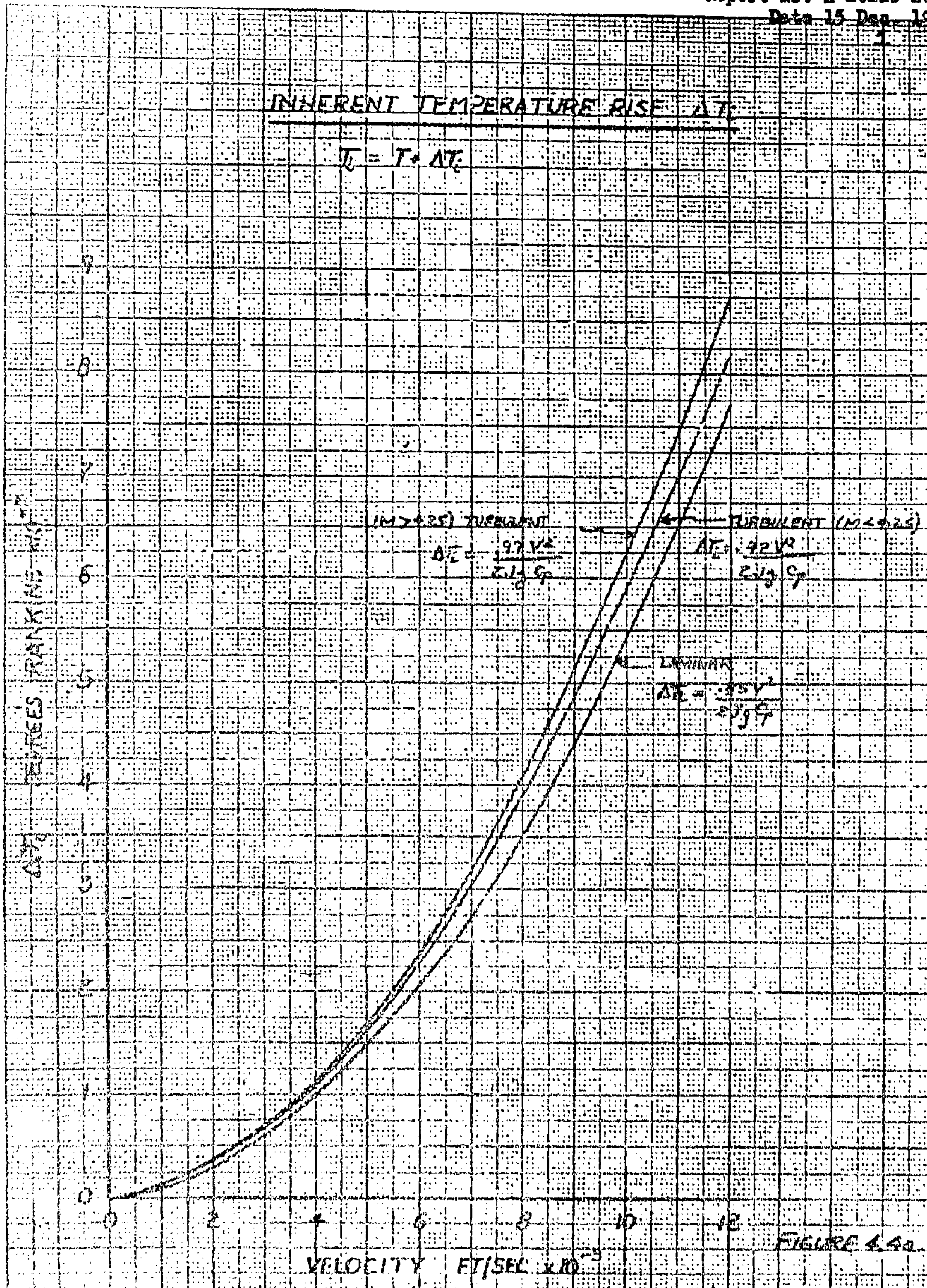
INHERENT TEMPERATURE RISE ΔTi
Ti = T + ΔTi
(M > .25) TURBULENT
TURBULENT (M < .25)
LAMINAR
ΔTi DEGREES RANKINE
VELOCITY FT/SEC x 10^-3
0
2
4
6
8
10
12

FIGURE 4.4a

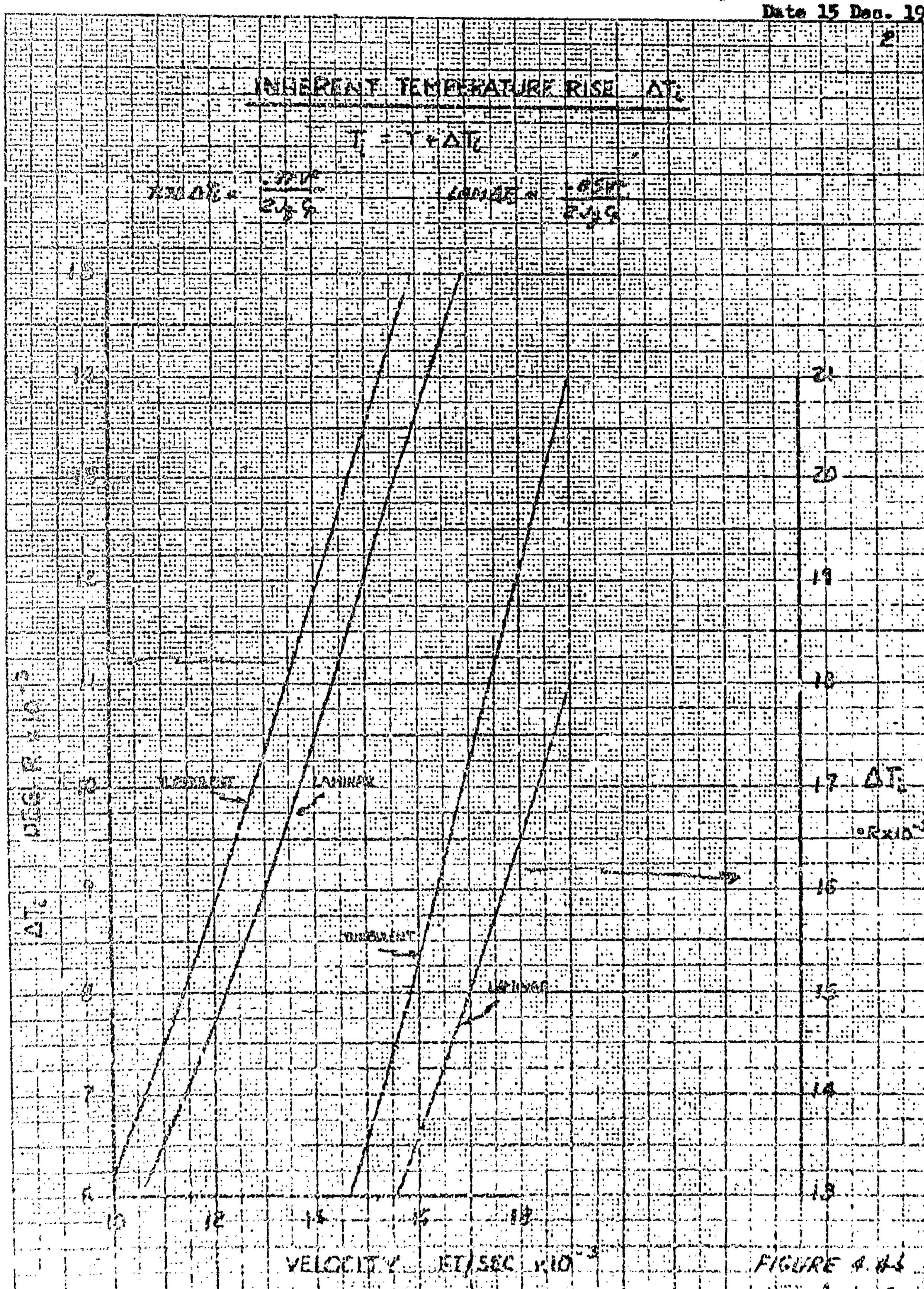
INHERENT TEMPERATURE RISE ΔT_i
$T_i = T + \Delta T_i$
TURBULENT
LAMINAR
TURBULENT
LAMINAR
ΔT_i
°R x 10^{-3}
VELOCITY FT/SEC x10^{-3}

FIGURE 4.4

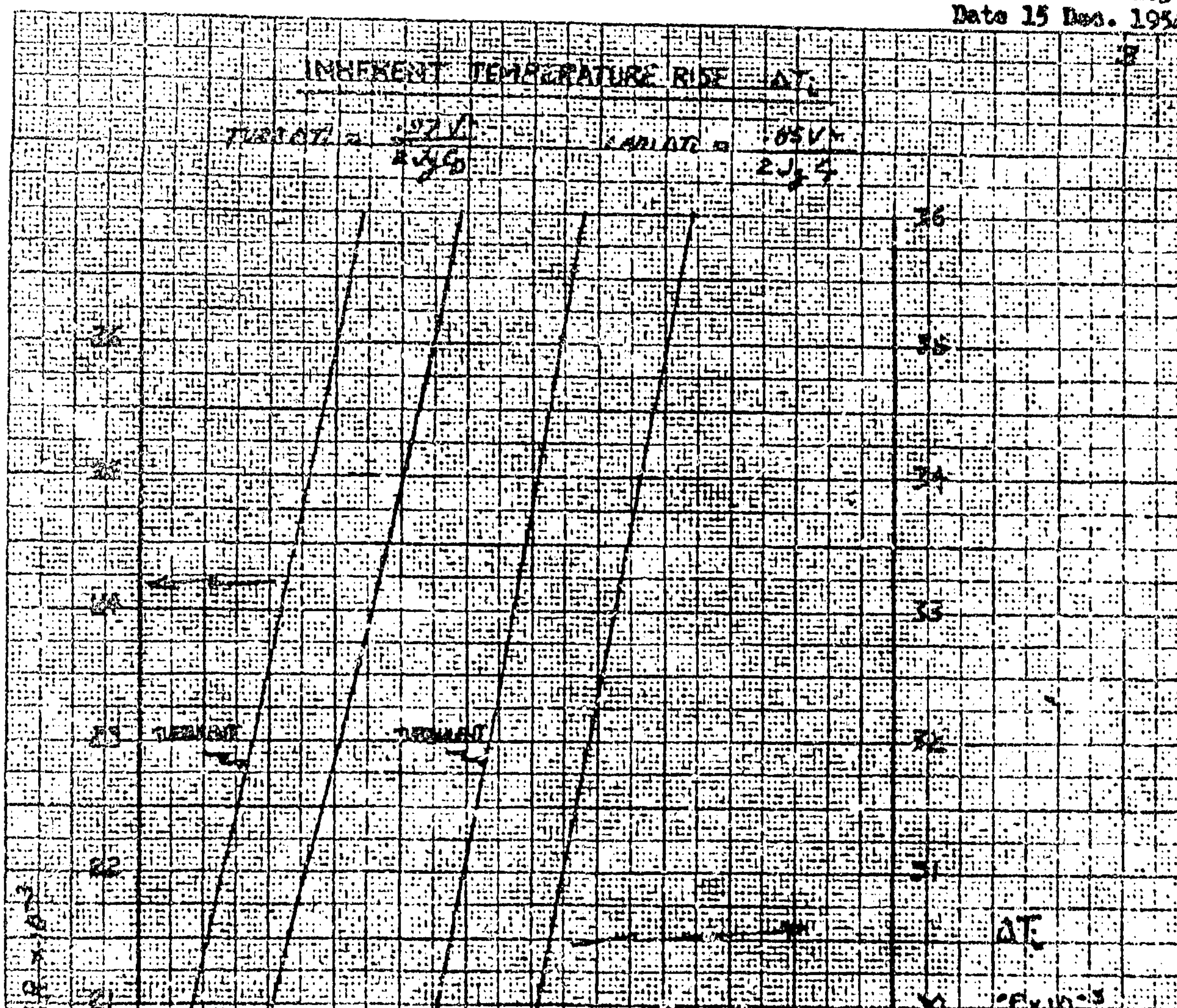
INHERENT TEMPERATURE RISE ΔT
TURBULENT
LAMINAR
VELOCITY FT/SEC x10^-3
FIGURE 4.4c

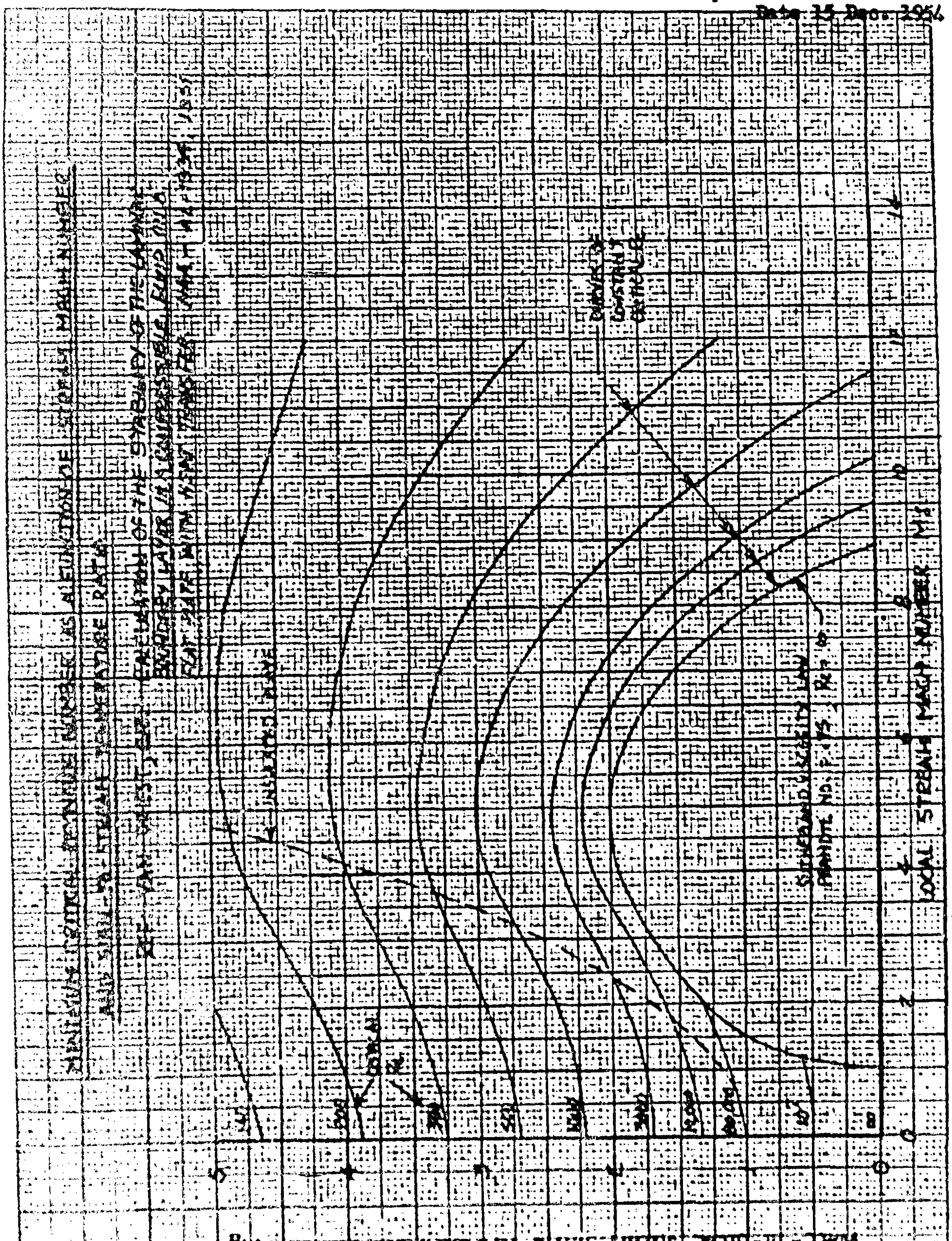

FIGURE [illegible].5

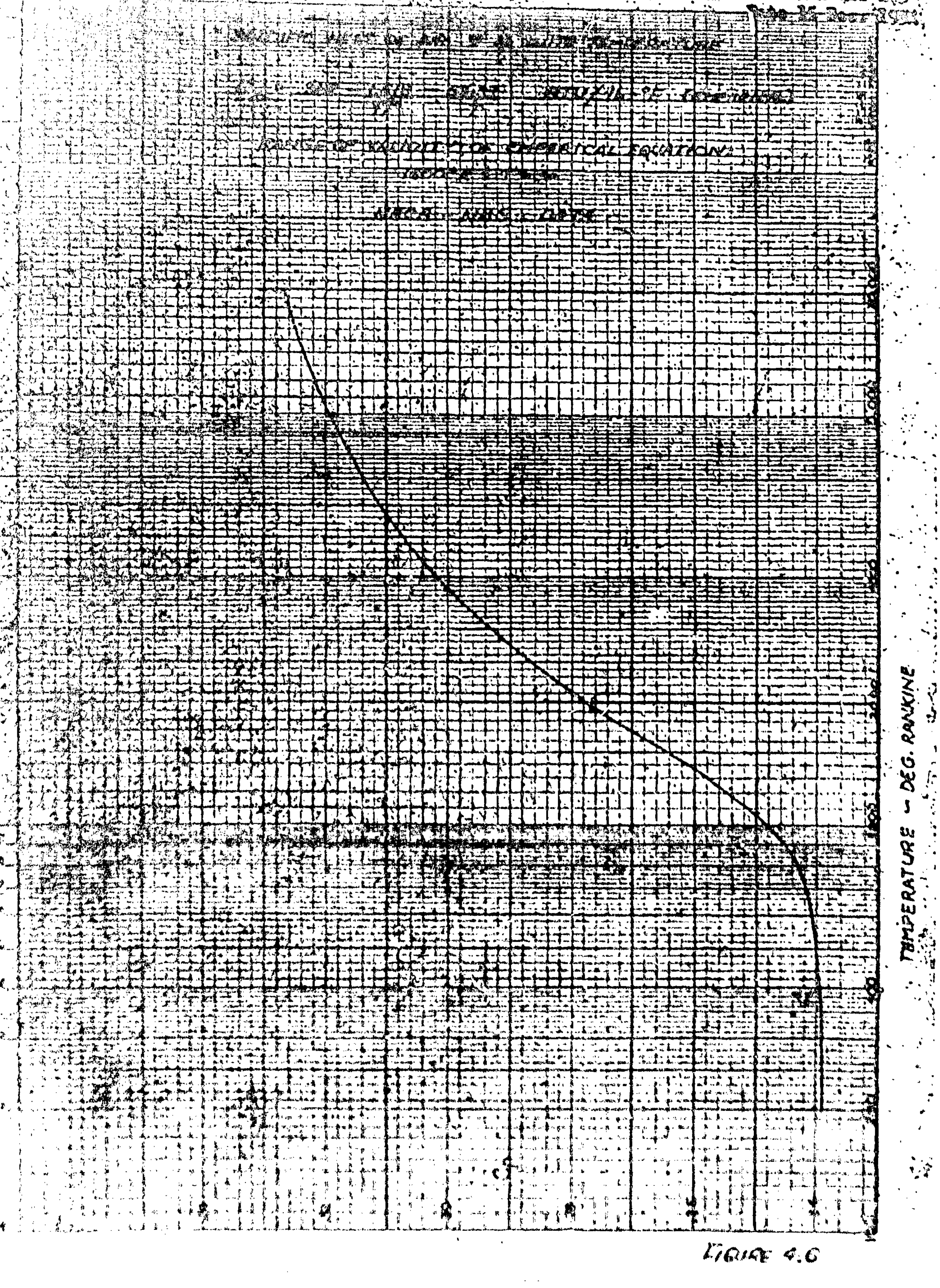
RANGE OF VALIDITY OF EMPIRICAL EQUATIONS
TEMPERATURE – DEG. RANKINE

FIGURE 4.6

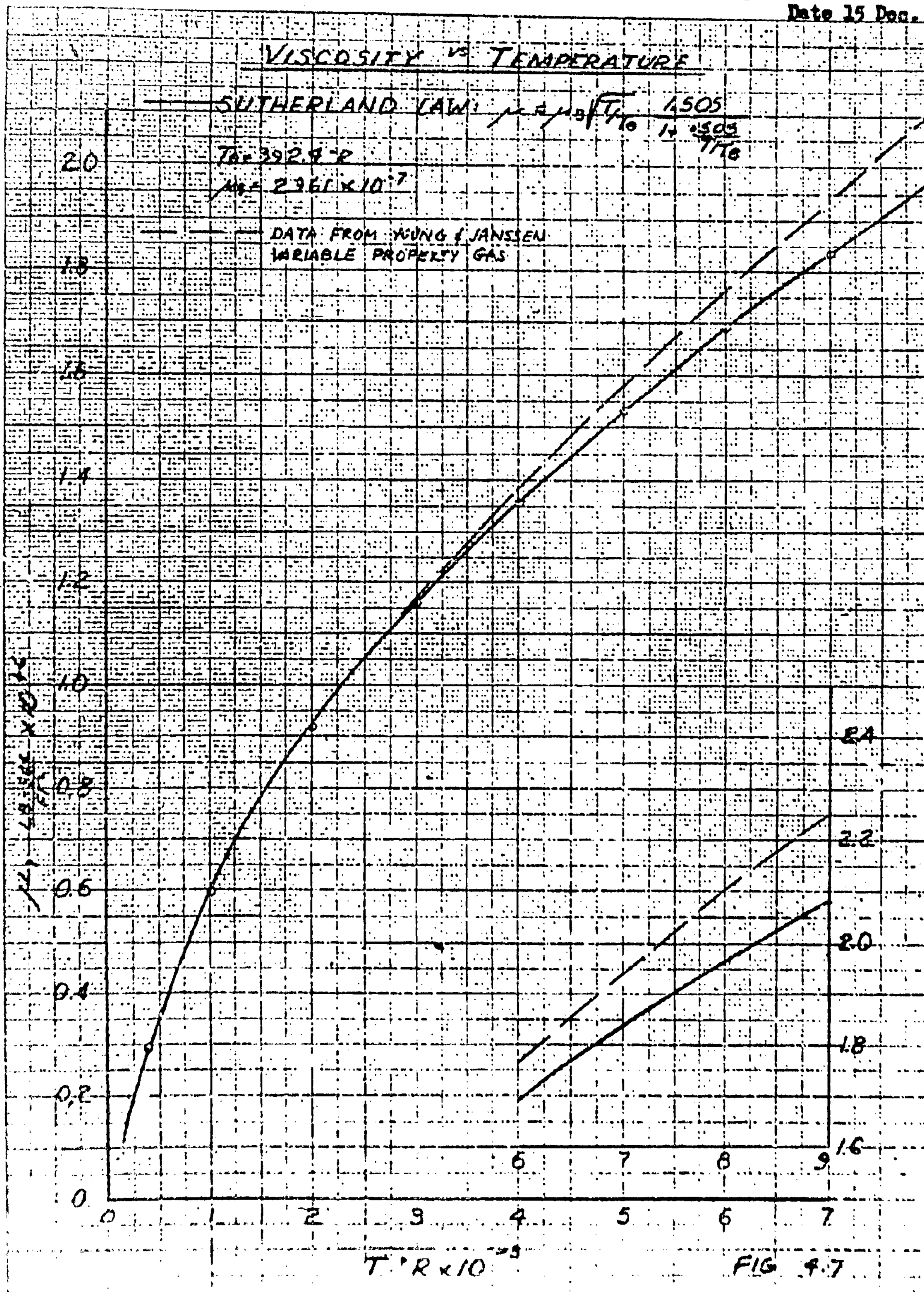
VISCOSITY vs TEMPERATURE
SUTHERLAND LAW
DATA FROM YOUNG & JANSSEN VARIABLE PROPERTY GAS
T °R × 10
FIG 4.7